Friedrich-Alexander-Universität
Erlangen-Nürnberg

Gamma-Ray Astronomy

I – Gamma-ray Production and Detection

Dr Alison Mitchell
Junior Research Group Leader,
FAU Erlangen-Nürnberg

Astroparticle School, Obertrubach-Bärnfels
9th October 2024

Emmy Noether-Programm
DFG Deutsche Forschungsgemeinschaft

Funded by
DFG Deutsche Forschungsgemeinschaft
German Research Foundation

Gamma-ray Astronomy

Non-thermal Astrophysics

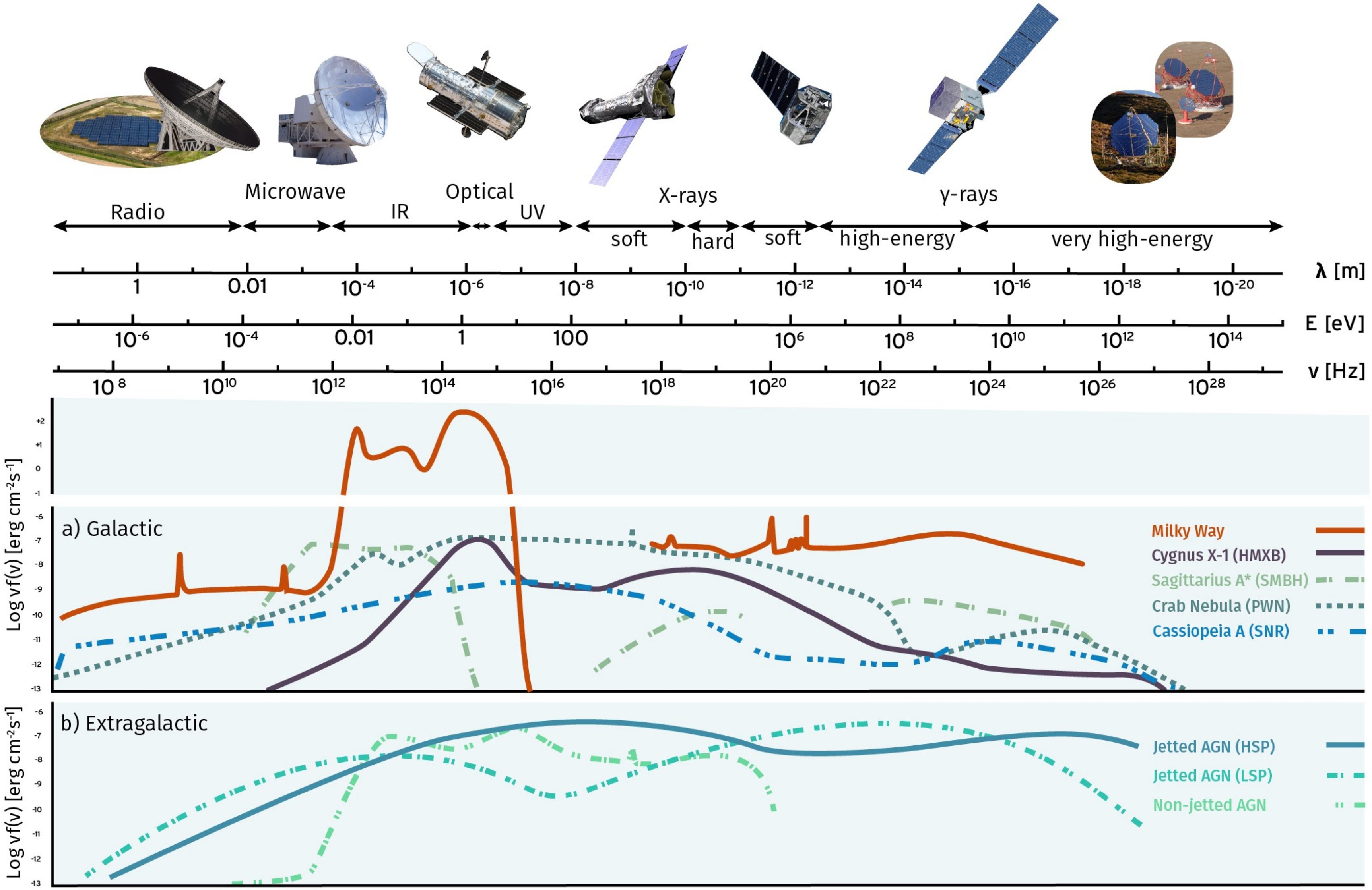

Credit: Annika Kreikenbohm, JMU Würzburg

Gamma-rays

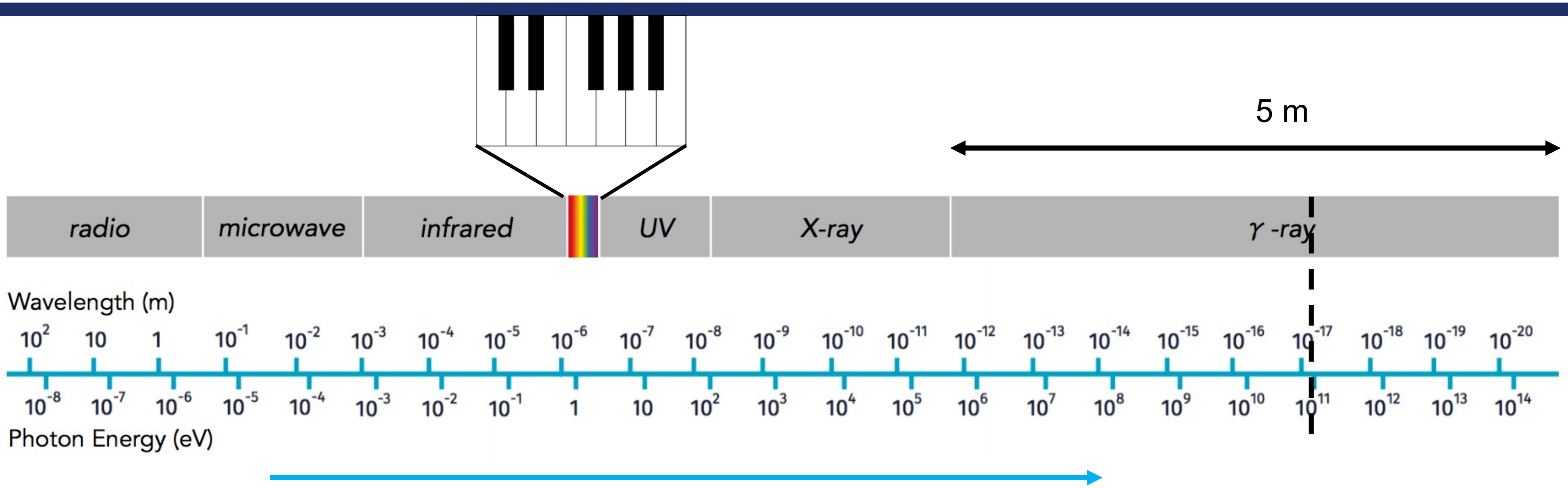

If visible light corresponds to one octave (16.5cm on a piano)

Each octave = double the energy

→ Then the entire electromagnetic spectrum is 12 m long

→ Gamma-rays are 19 octaves above visible light

→ Very high energy gamma-rays are 36 octaves higher

The entire gamma-ray range would be 5 m long

All-particle Cosmic Ray Spectrum

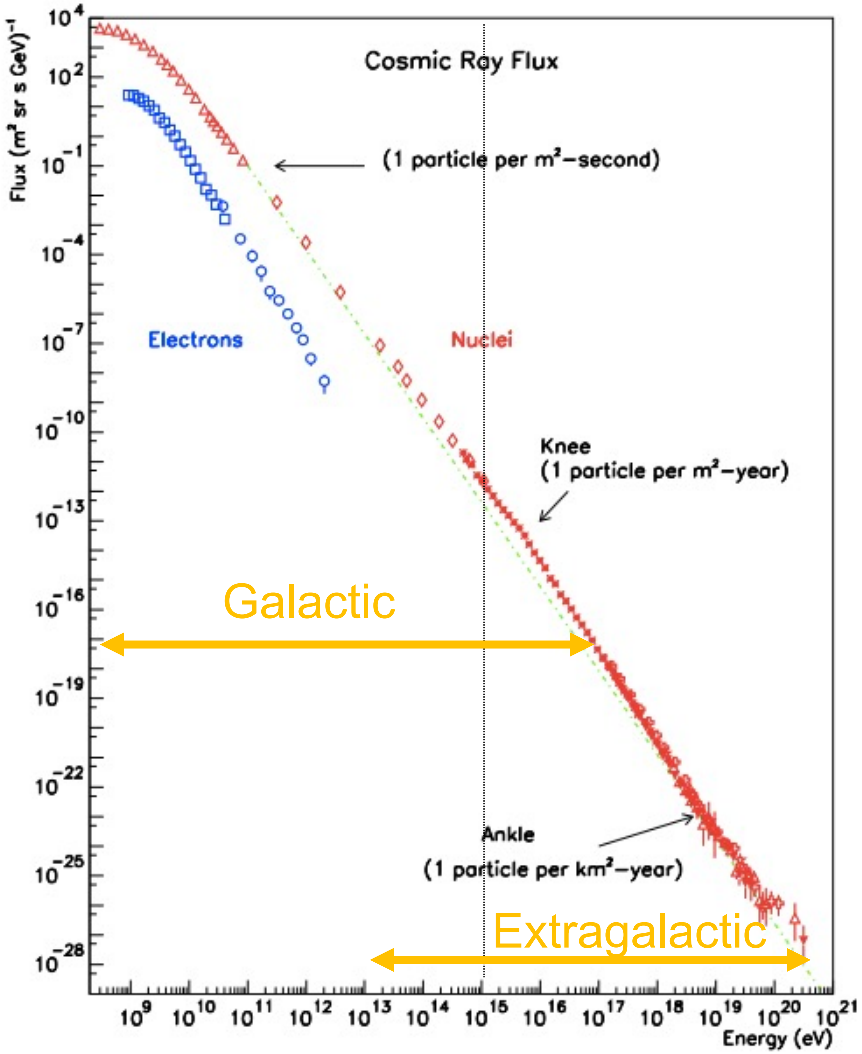

Cosmic Rays – highest energy particles in nature, up to 10^{20} eV

Approx. power law over many orders of magnitude:
~30 in flux
~10 in energy

Key features:

Solar modulation
Spectral breaks (“knee” and “ankle”)
GZK effect → high energy cut-off

Energy density $\varepsilon_{CR} \sim 1 \text{eV/cm}^3$, comparable to magnetic field, IR etc. in our galaxy

The Galactic –Extragalactic Transition

A natural transition between power law source components is ankle-like

Knee can form from propagation / confinement effects

Implication → particles with higher energies freely escape the accelerator

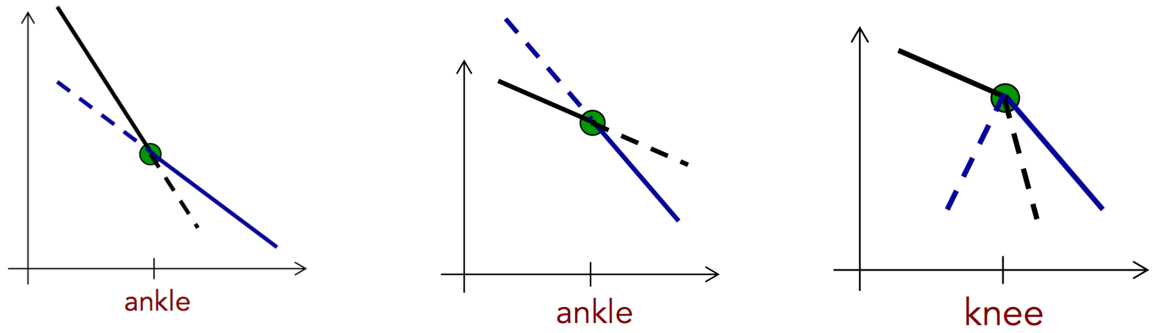

E. Parizot

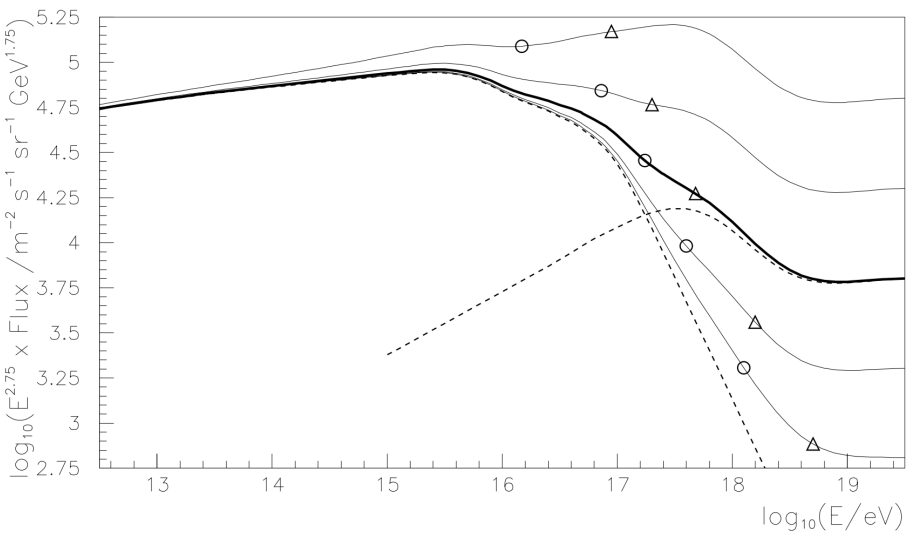

Hillas, conf. proc. (arXiv:0607109)

An invisible transition between components is also possible

e.g. for changing component fractions, the transition is still essentially smooth
(circle = 50% extragalactic, triangle = 80% extragalactic)

Hillas Limit

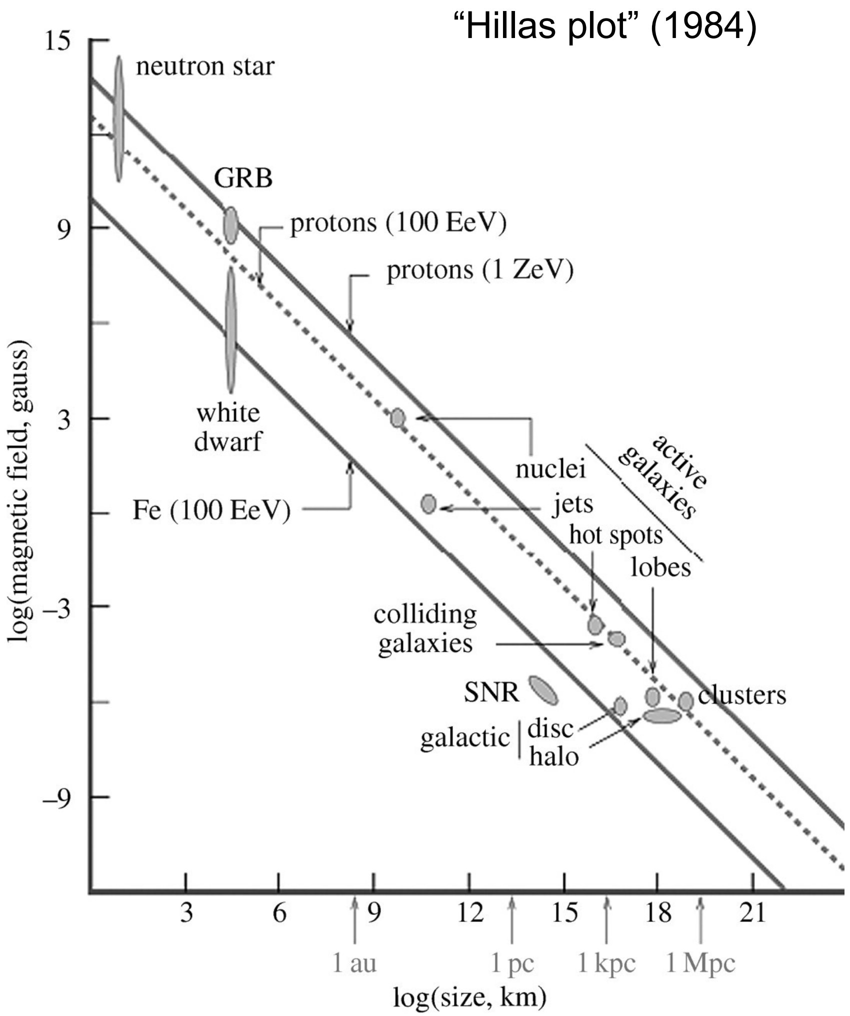

Maximum energy that can be obtained whilst a particle remains in the accelerating region

$$E_{\max} = Ze\beta cBL$$

Corresponds to a minimum size → Larmor radius L in a magnetic field B

“PeVatrons” = accelerators of particles to energies ≥ 10^{15} eV

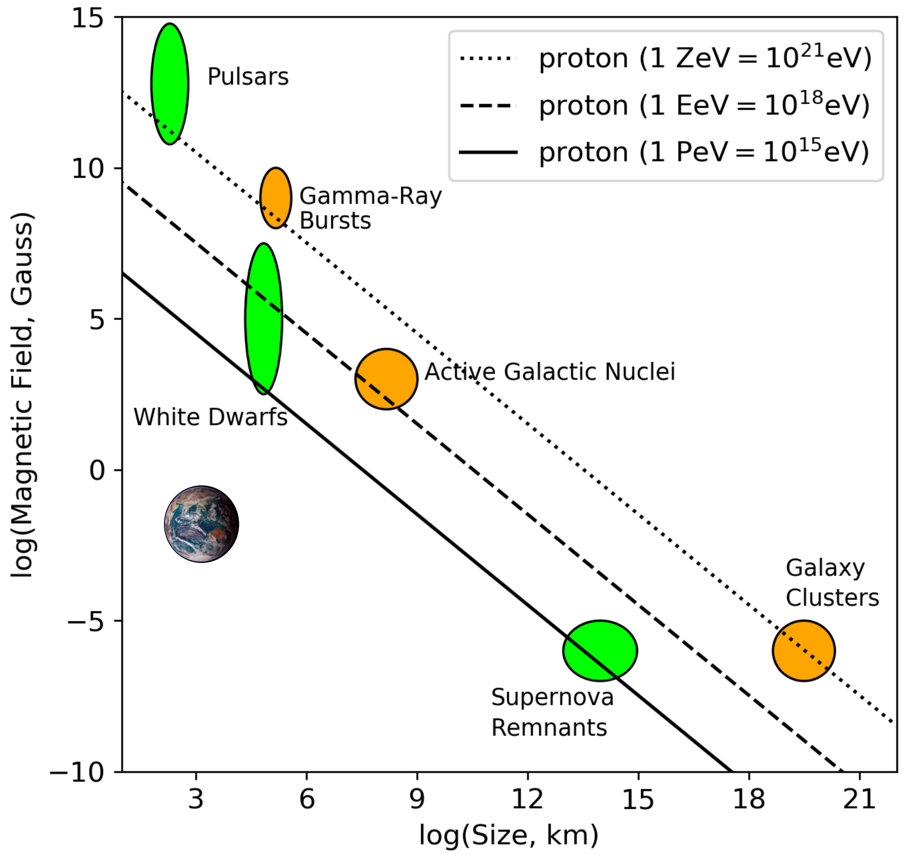

Particle Acceleration – Shocks

Where are cosmic rays accelerated? Need to reach ~10^{21} eV and explain power-law behaviour over many orders of magnitude in energy, Γ~ 2-3

$$\frac{dN}{dE} \propto E^{-\Gamma}$$

Shock – supersonic motion of material. Ahead of the shock, matter is not “aware” of the shock approaching.

At a shock front, mass, momentum and energy are conserved.
This provides us with the Rankine – Hugoniot conditions

$$\rho_1 u_1 = \rho_2 u_2 \qquad \text{(1) Mass}$$

$$\rho_1 u_1^2 + p_1 = \rho_2 u_2^2 + p_2 \qquad \text{(2) Momentum}$$

$$\frac{u_1^2}{2} + w_1 = \frac{u_2^2}{2} + w_2 \qquad \text{(3) Energy}$$

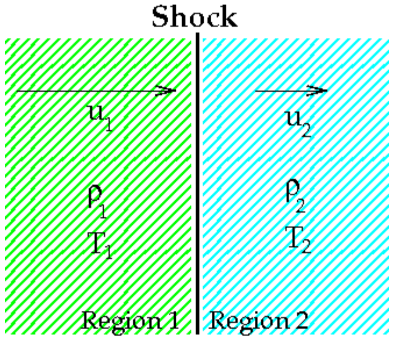

Particle Acceleration – Shocks

It can be shown that the compression ratio between material upstream and downstream of the shock is: $\frac{\rho_2}{\rho_1} = \frac{U_1}{U_2} = \frac{\gamma+1}{\gamma-1} \approx 4$

$$\frac{p_2}{p_1} = \frac{2\gamma M^2 - (\gamma - 1)}{\gamma + 1}$$

For a monatomic gas γ=5/3 (e.g. fully ionised plasma in astrophysics)

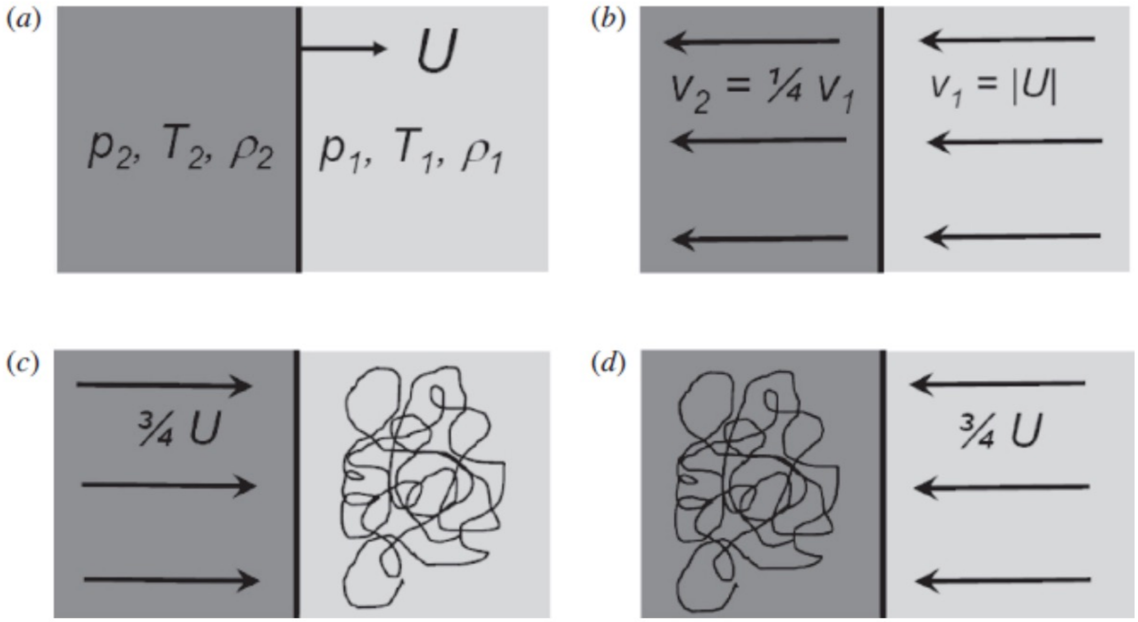

(a) Observer’s frame
(b) Shock reference frame
(c) Upstream frame
(d) Downstream frame

Particle always sees plasma moving towards it with speed ¾ U

First Order Fermi Acceleration

Particles scatter across shock front and get isotropised

Energy gain on each shock crossing: $E = E_0\beta^n$

Probability of remaining in the vicinity of the shock: $N = N_0 p^k$

Shock crossing requires Lorentz transformation with change in energy

→ $\frac{\Delta \mathrm{E}}{\mathrm{E}} = \frac{v}{c}\cos\theta$ and on average

$$\left\langle \frac{\Delta E}{E} \right\rangle = \frac{2}{3}\frac{v}{c}$$

Average energy gain is proportional to the velocity.
"First-order" = first order in velocity

Power law result:

$$N(E)dE \propto E^{-2}dE$$

Which is a universal result, not too dissimilar from the -2.7 spectral index seen in the cosmic ray spectrum.

In the strong shock regime,
Mach number M>>1

Where $M \equiv \frac{v_1}{c_1}$ and the sound speed

$$c_1 = \left(\frac{\gamma p_1}{\rho_1}\right)^{\frac{1}{2}}$$

Particle Acceleration – second order Fermi

Second order Fermi acceleration arises from interactions with randomly moving magnetic mirrors

Particles interacting with clouds → assume these are unaffected by the particle scattering

Then one can show that (!) the average gain in energy per interaction is: $\left\langle \frac{\Delta E}{E} \right\rangle = \frac{8}{3}\frac{v^2}{c^2}$

Energy can increase or decrease, but increases on average because head-on collisions are more probable.

“Second-order” = second order in velocity.

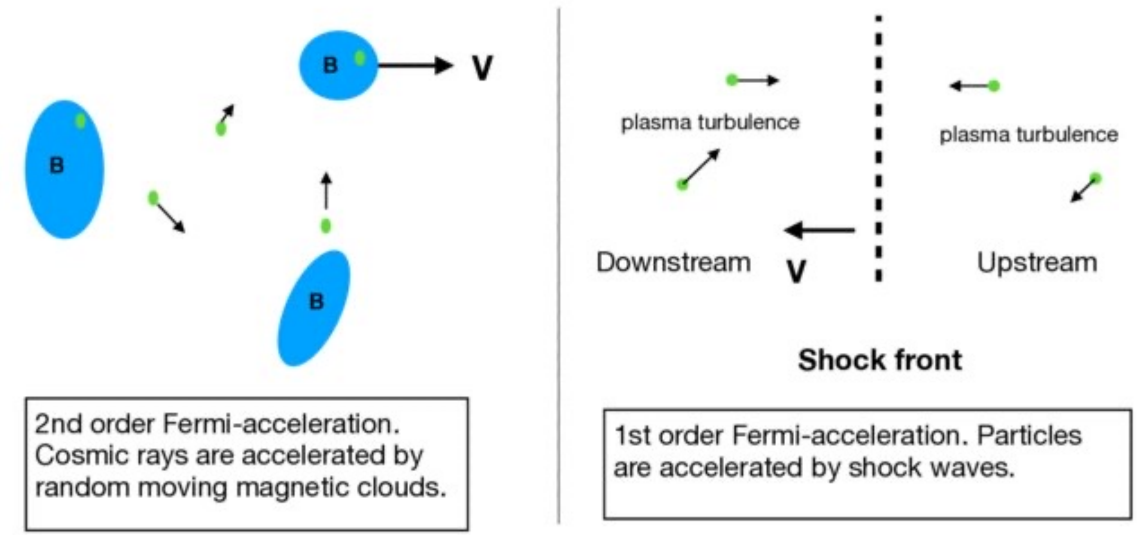

Che & Zank (2019)

Gamma-ray emission mechanisms

Searching for the origins of hadronic cosmic rays

→ Constrain hadronic vs leptonic emission scenarios

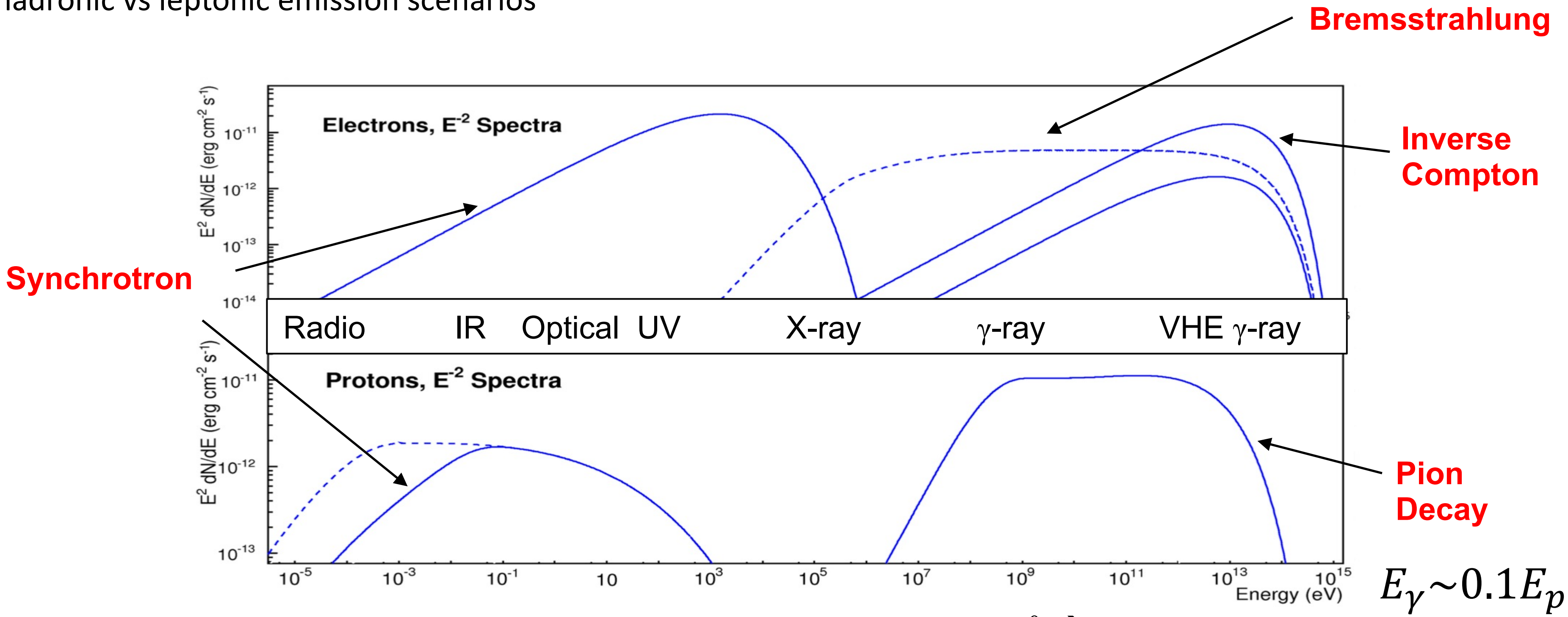

$E_\gamma \sim 0.1 E_p$

$\pi^0 \rightarrow \gamma + \gamma$

Bremsstrahlung or "braking radiation" – from deceleration of a charged particle in the vicinity of another charged particle.

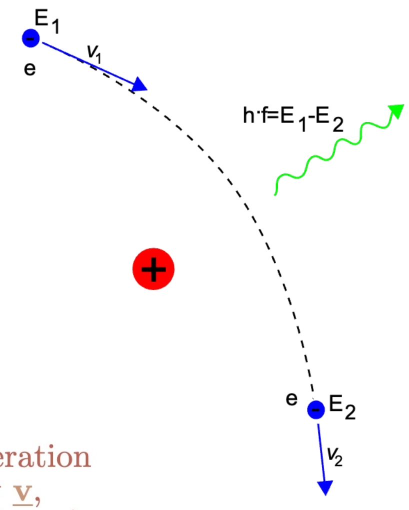

Synchrotron radiation – relativistic case

From a charged particle gyrating in a magnetic field B with energy density U_m

Radiated Power:

$$P_{synch} = \frac{4}{3} c \left(\frac{v}{c}\right)^2 \gamma^2 \sigma_T U_m$$

Energy loss timescale:

$$\tau_c \approx \frac{1}{\gamma} \left(\frac{\mathrm{B}}{1nT}\right)^{-2} 1.6\times10^{11} \text{ yrs}$$

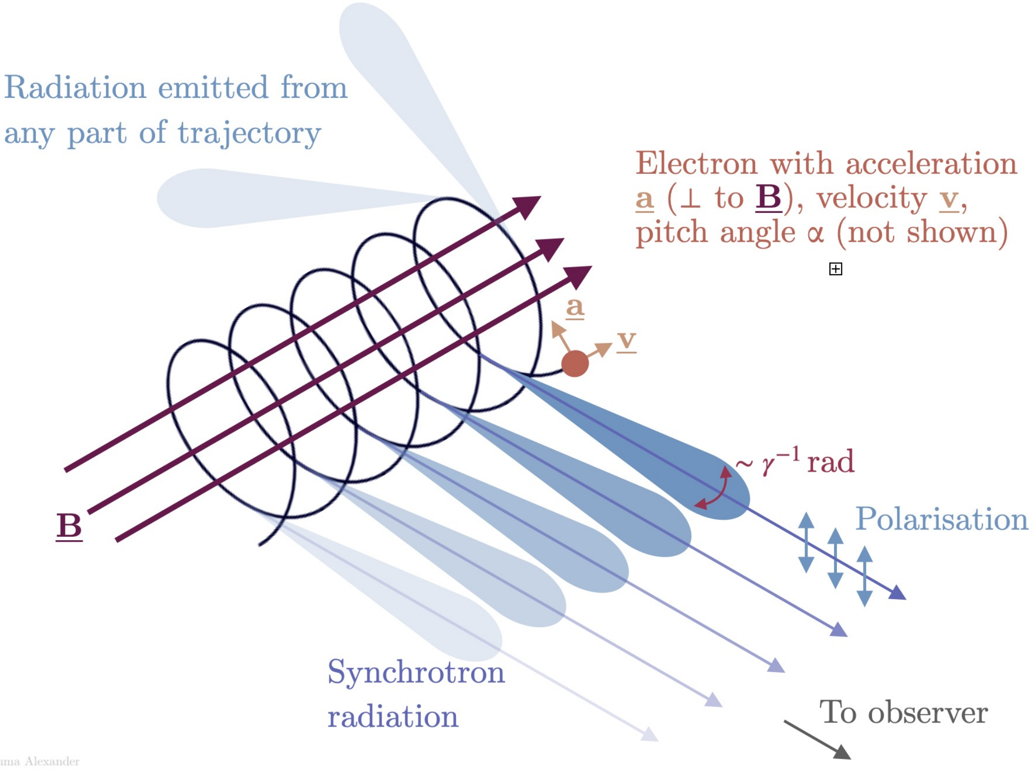

Inverse Compton Scattering

Transfer of energy from an energetic electron to a photon – boosting photon to gamma-ray energies

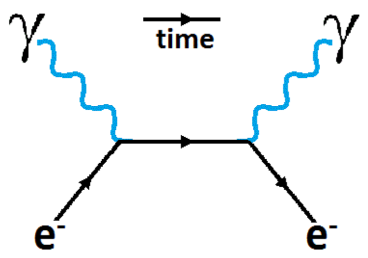

Scattering off background radiation fields, energy density U_{rad}

CMB, FIR, NIR, Vis… i.e. ambient radiation and starlight.

Radiated Power:

$$P_{IC} = \frac{4}{3} c \left(\frac{v}{c}\right)^2 \gamma^2 \sigma_T U_{rad}$$

c.f. Synchrotron – same relation, energy loss rate depends only on the electric field

$\tau_{CMB} \approx \frac{1}{\gamma} 3\times10^{12}$ yrs

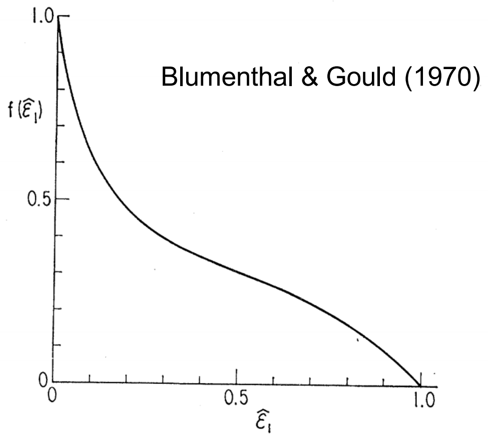

FIG. 3. Scattered photon distribution function in the Thomson limit.

gamma-ray energy factor
~1/9 on average

Pion Decay

Proton energy loss timescale via p-p interactions:

$\tau_{pp} \approx \frac{1}{n} 6 \times 10^7$ yrs (n = target material density, cm^{-3})

Charged pion decay: $\pi^+ \rightarrow \mu^+ + \nu_\mu$ and $\pi^- \rightarrow \mu^- + \overline{\nu_\mu}$

Decay ~ 10^{-8} s

Neutral pion decay: $\pi^0 \rightarrow \gamma + \gamma$

Decay ~ 10^{-16} s

Gamma-ray cut-off corresponding to particle production threshold

Gamma-rays have equal energy in rest frame of the pion.

$E^*_\gamma = \frac{1}{2} m_{\pi^0} c^2 \approx 67.5$ MeV

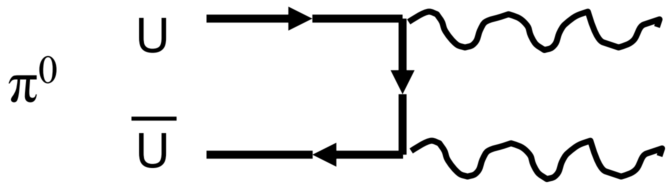

"Pion-bump" – spectral signature of hadronic cosmic ray acceleration

(Neutrinos – "smoking gun" signature)

Interaction Cross-sections

Proton-proton cross-section parameterised based on experimental data, e.g. from the LHC and other facilities.

Total cross-section is relevant for p-p interactions producing pions at source

Careful converting lab frame (fixed-target) to centre-of-mass frame $\sqrt{s}$

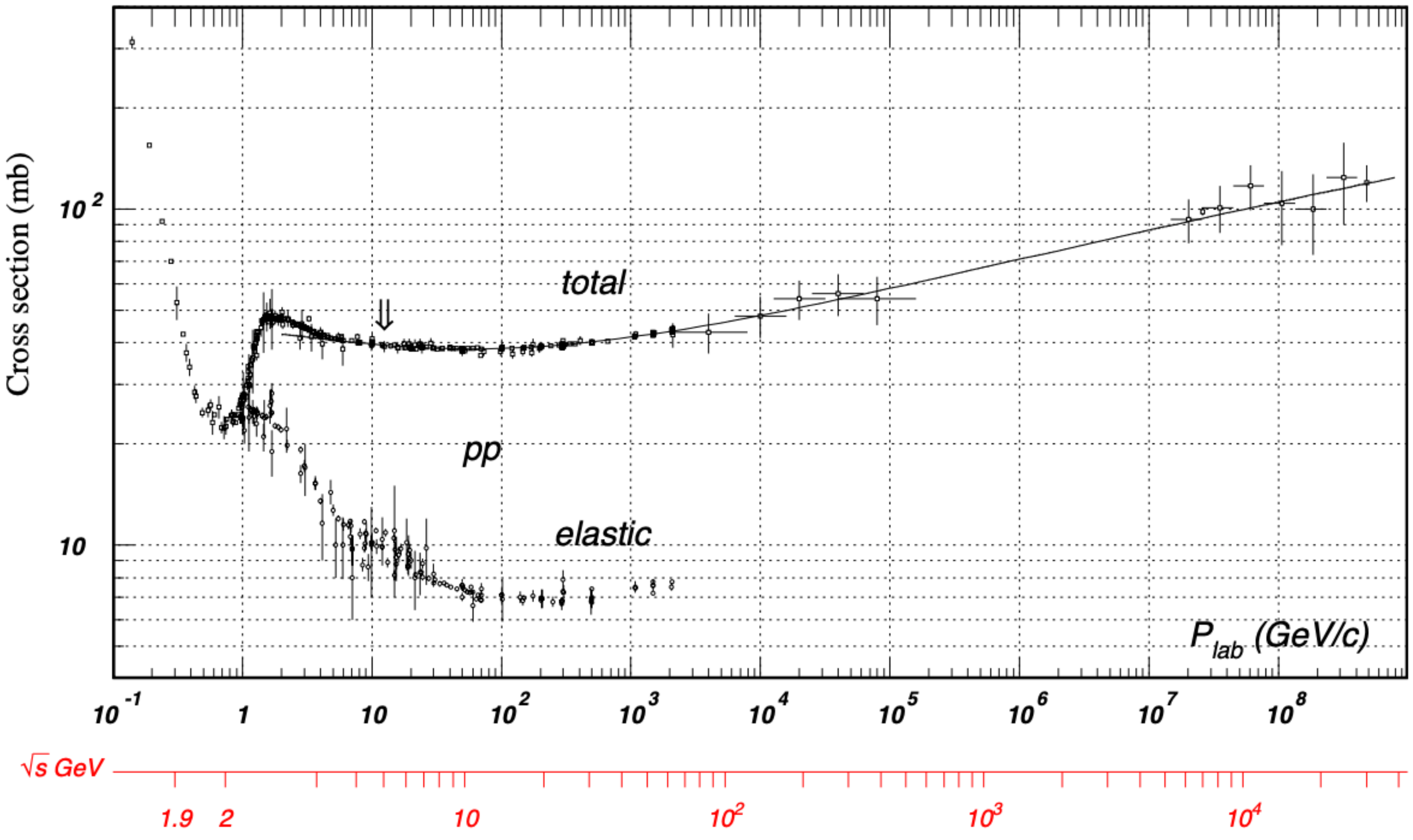

Particle Data Group, Beringer et al. PRD **86** 010001 (2012)

The sky in different wavelengths

Visible light

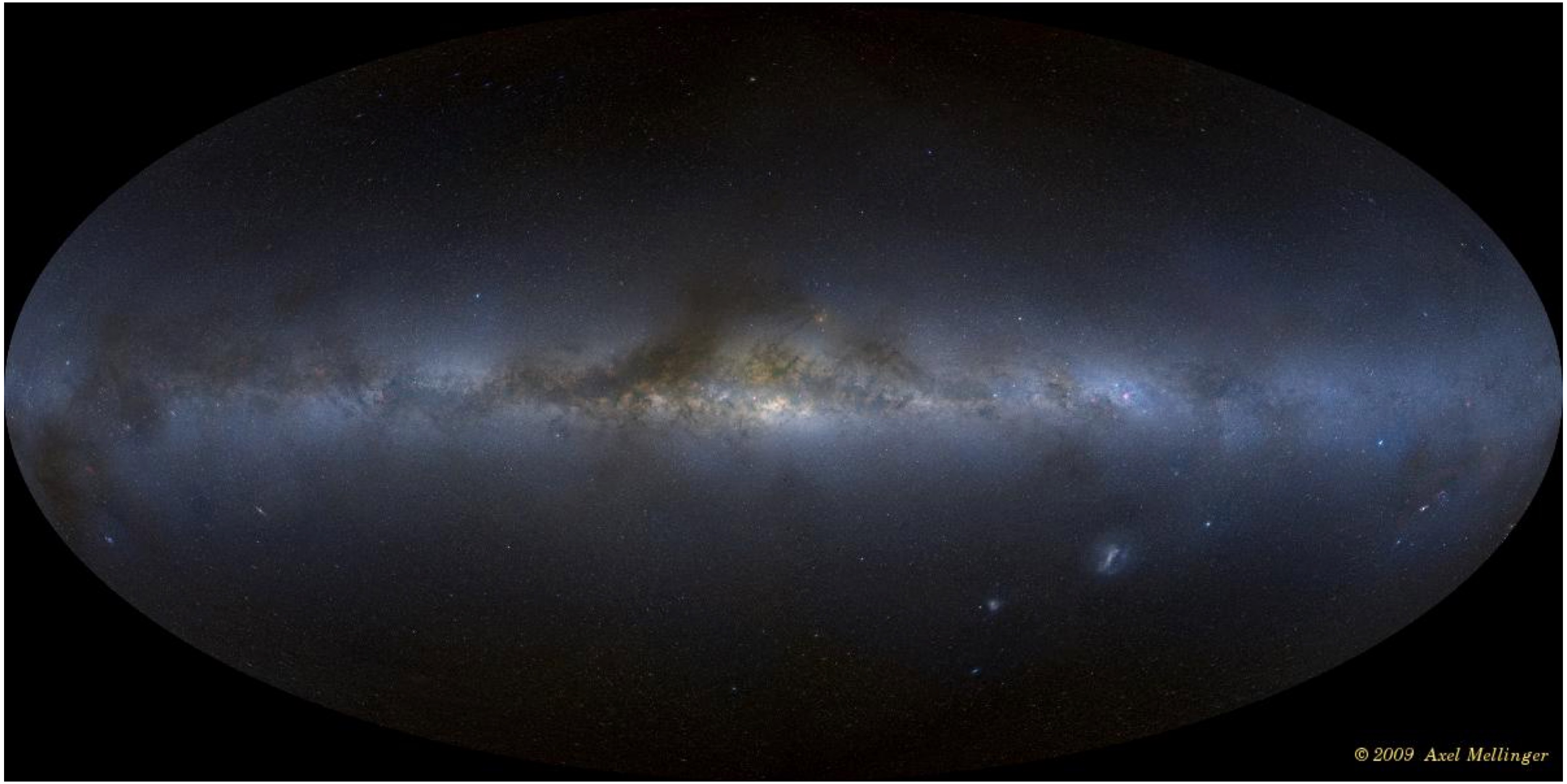

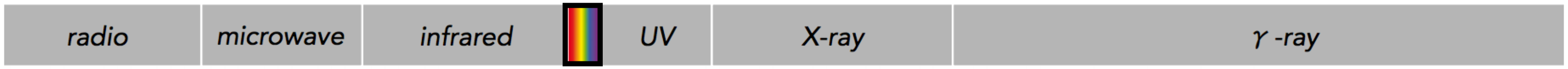

The sky in different wavelengths

Infrared radiation

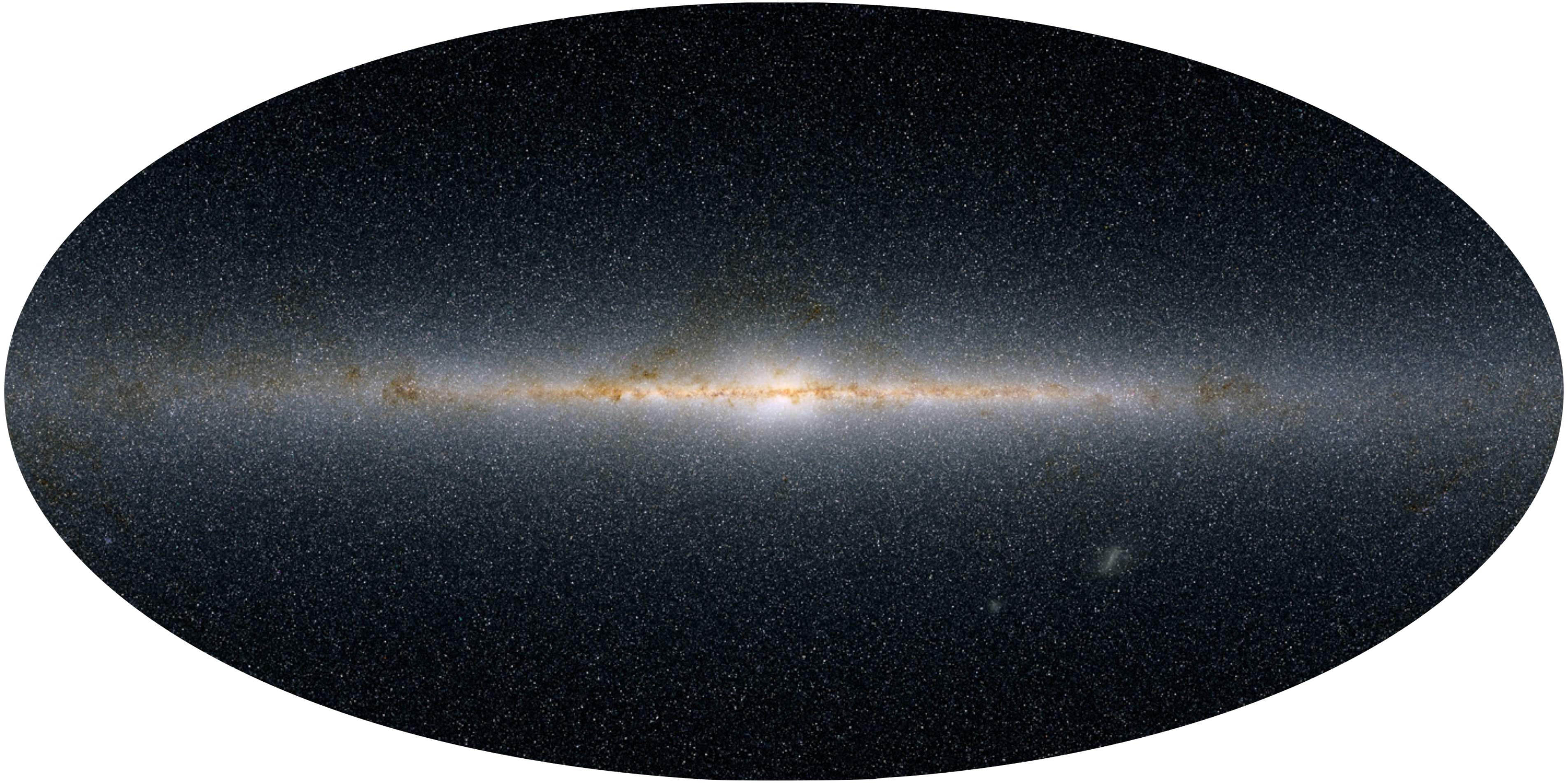

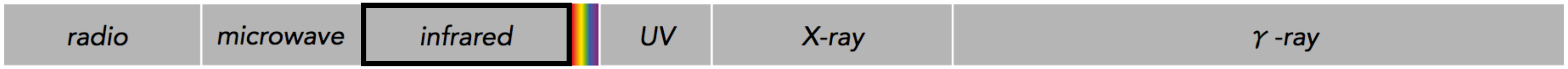

The sky in different wavelengths

X-ray

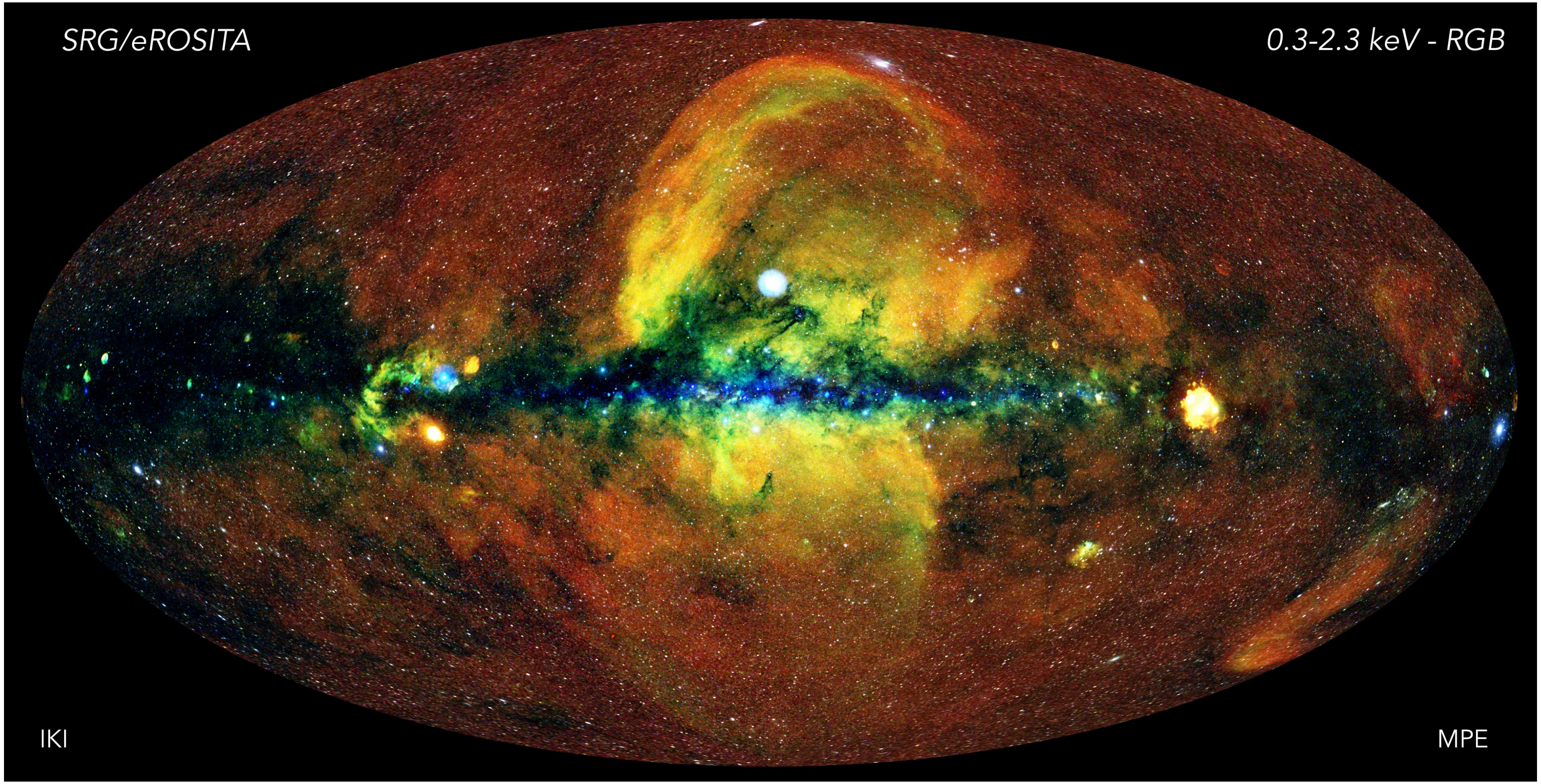

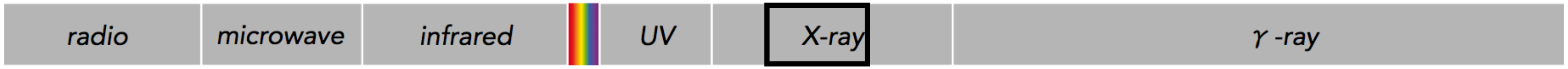

The sky in different wavelengths

Gamma-ray

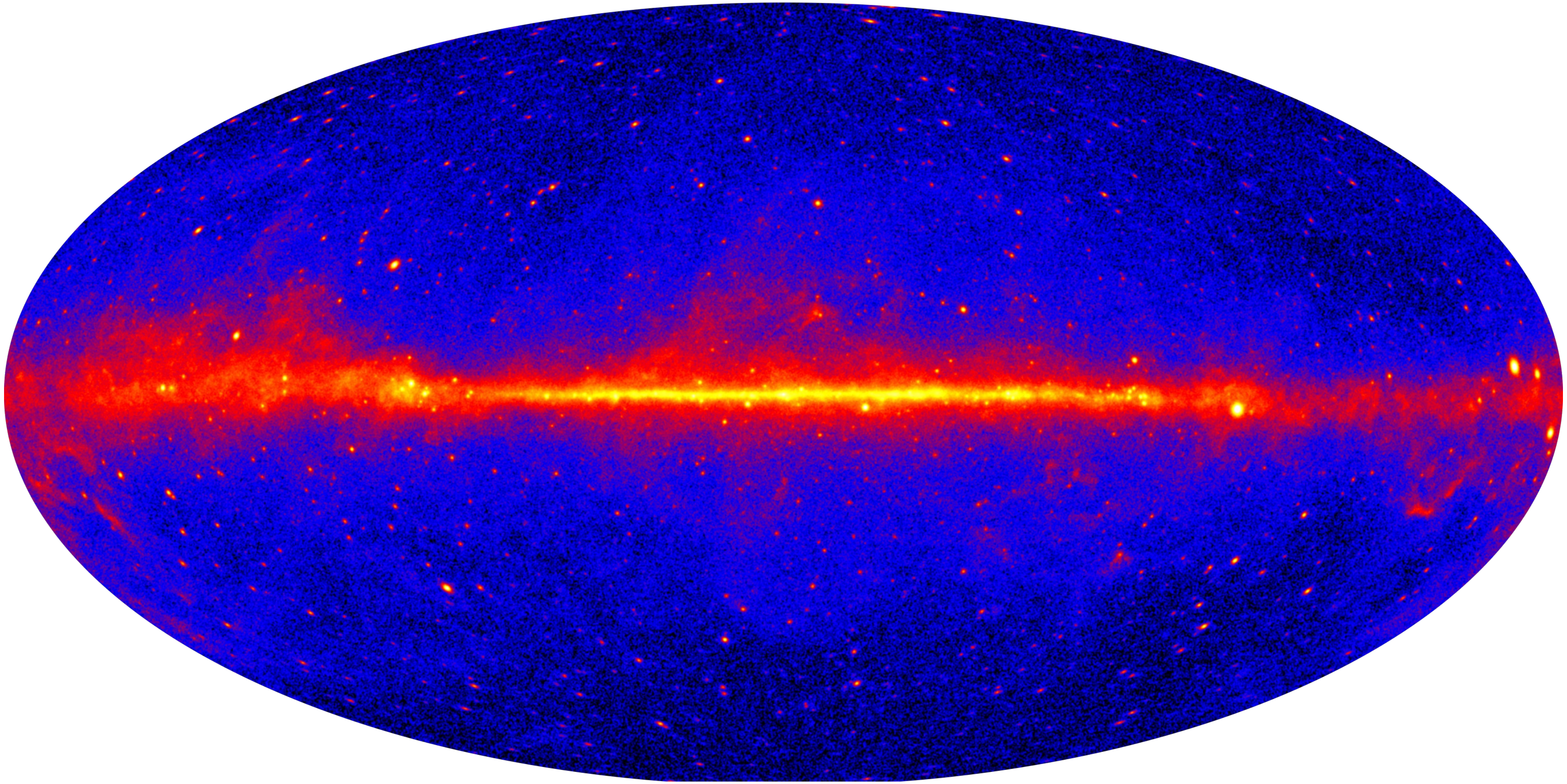

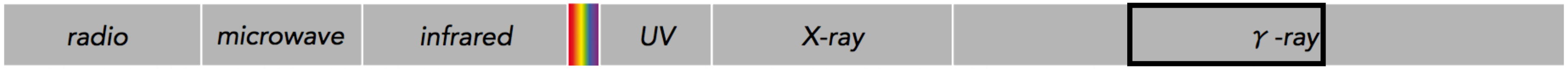

Astrophysical Observations with wavelength

Atmospheric transparency

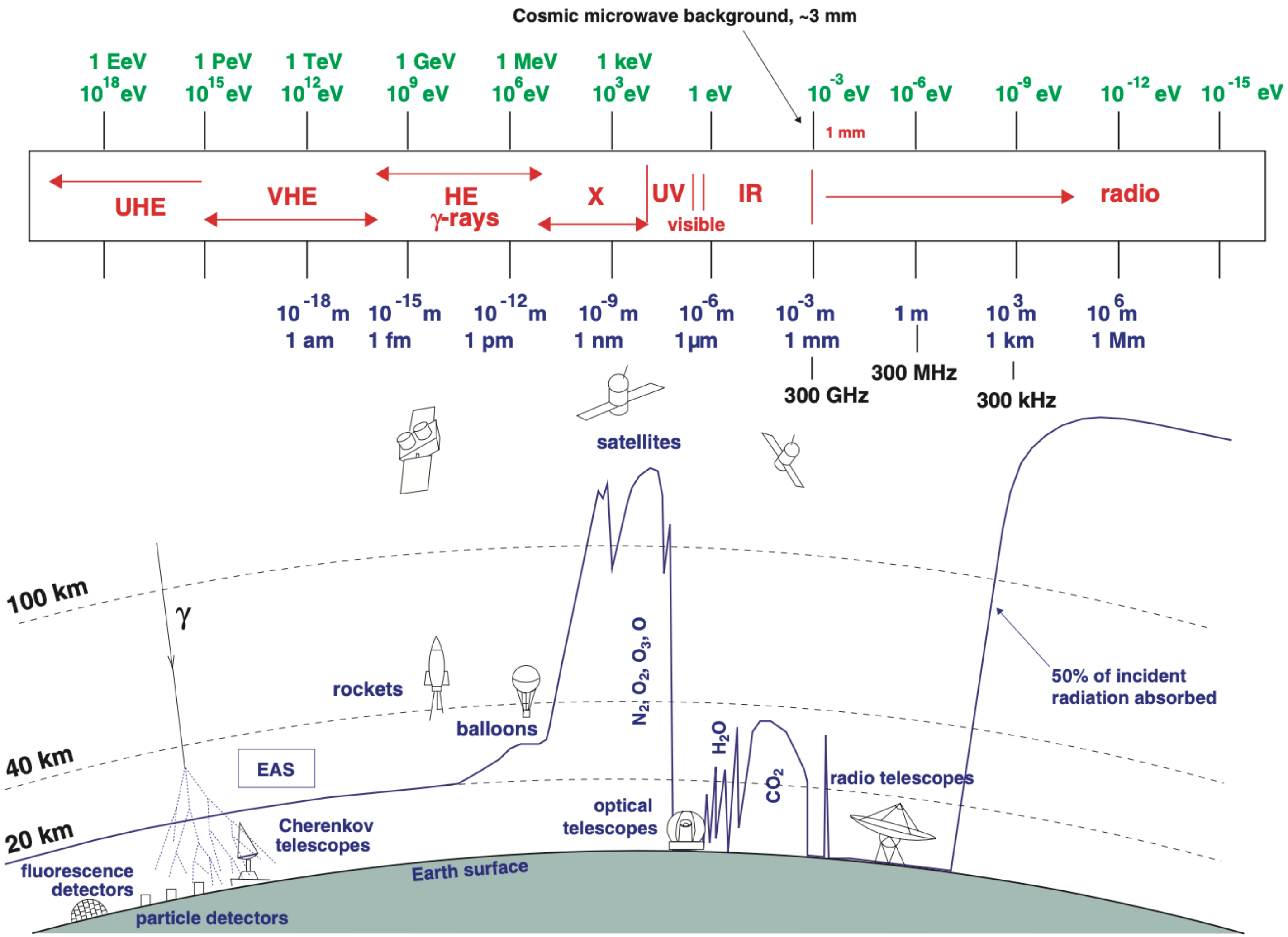

Gamma-ray Detection by Satellites

The MeV Gap

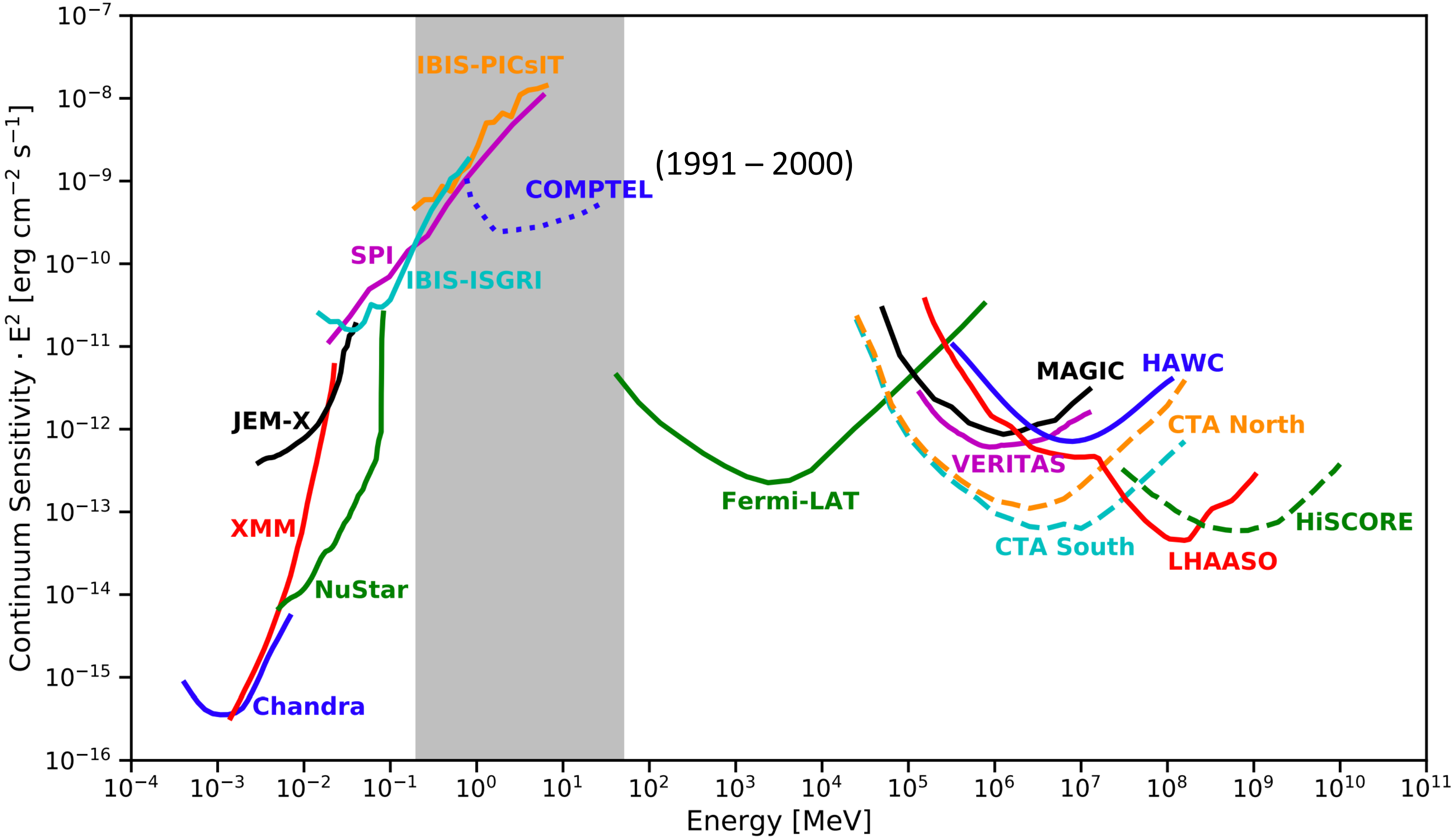

Lucchetta et al. JCAP08 (2022) 013

Gamma-ray Detection by Satellites

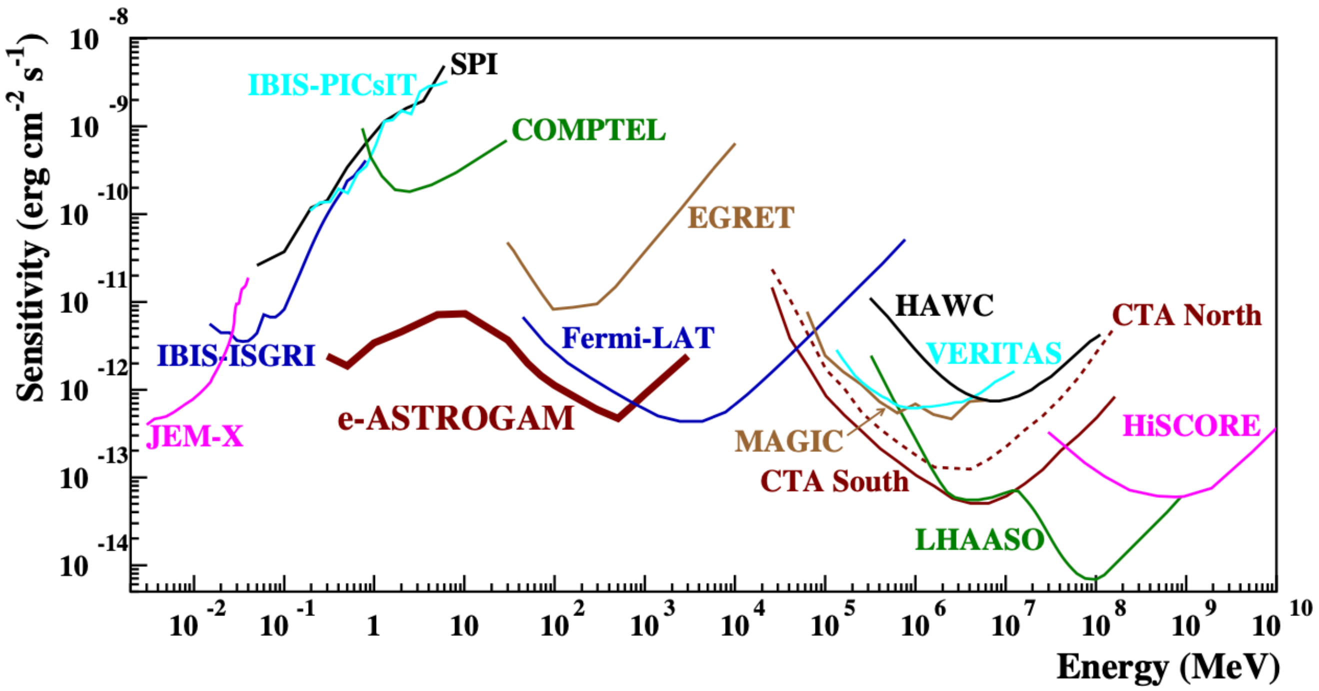

e-ASTROGAM collaboration, Exp. Astr. **44**, 25-82 (2017)

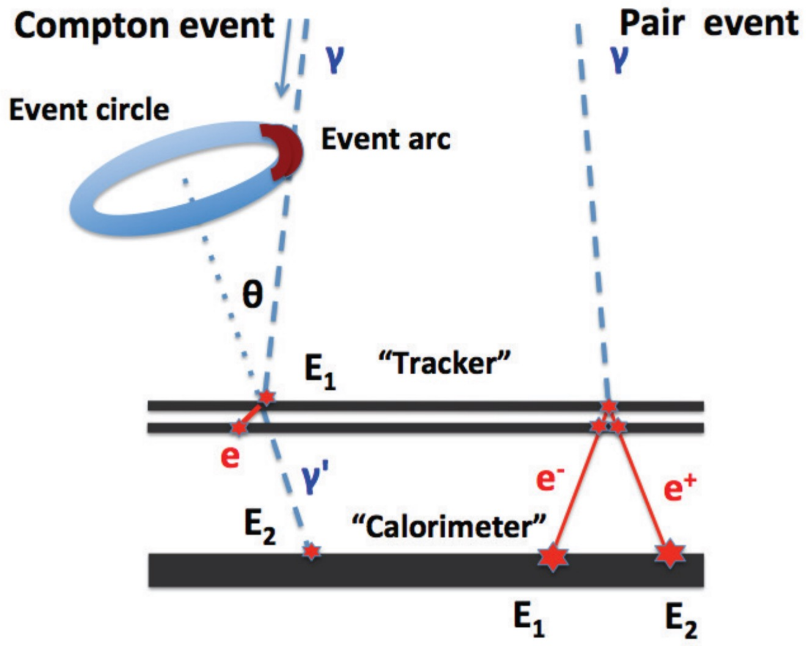

Moiseev et al., arXiv:1508.07349

Compton scattering events
Pair-production events

Fermi-LAT (Large Area Telescope)

Pair-conversion Technique

Gamma-rays from MeV to ~2 TeV

Large number of sources and variety of source classes detected.

Launched in 2008, ~16 years of operation

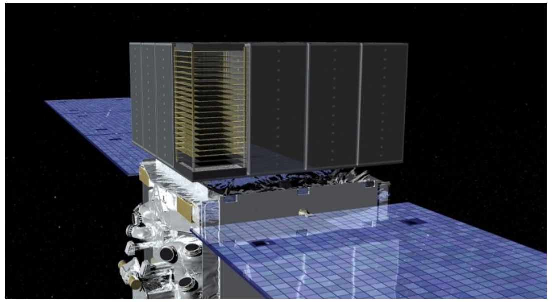

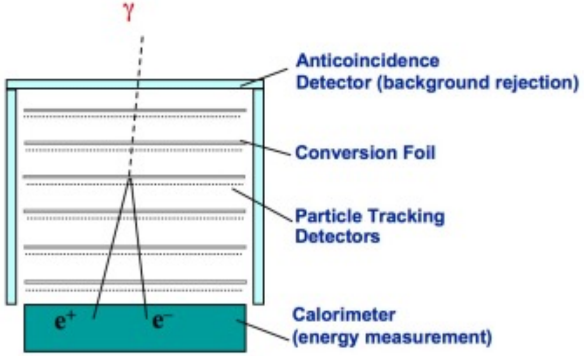

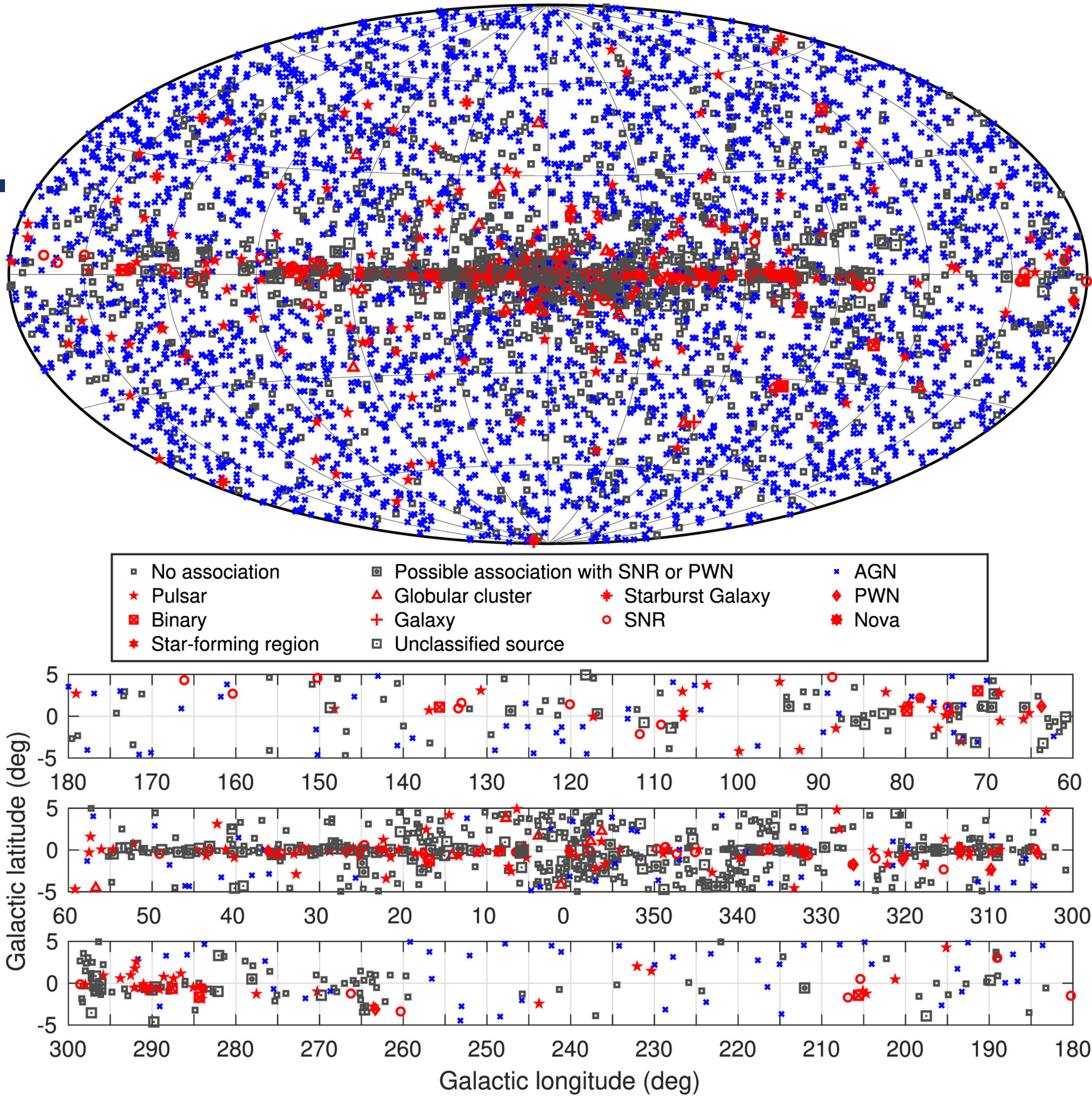

Fermi-LAT All Sky 12 year 1 GeV – 2 TeV

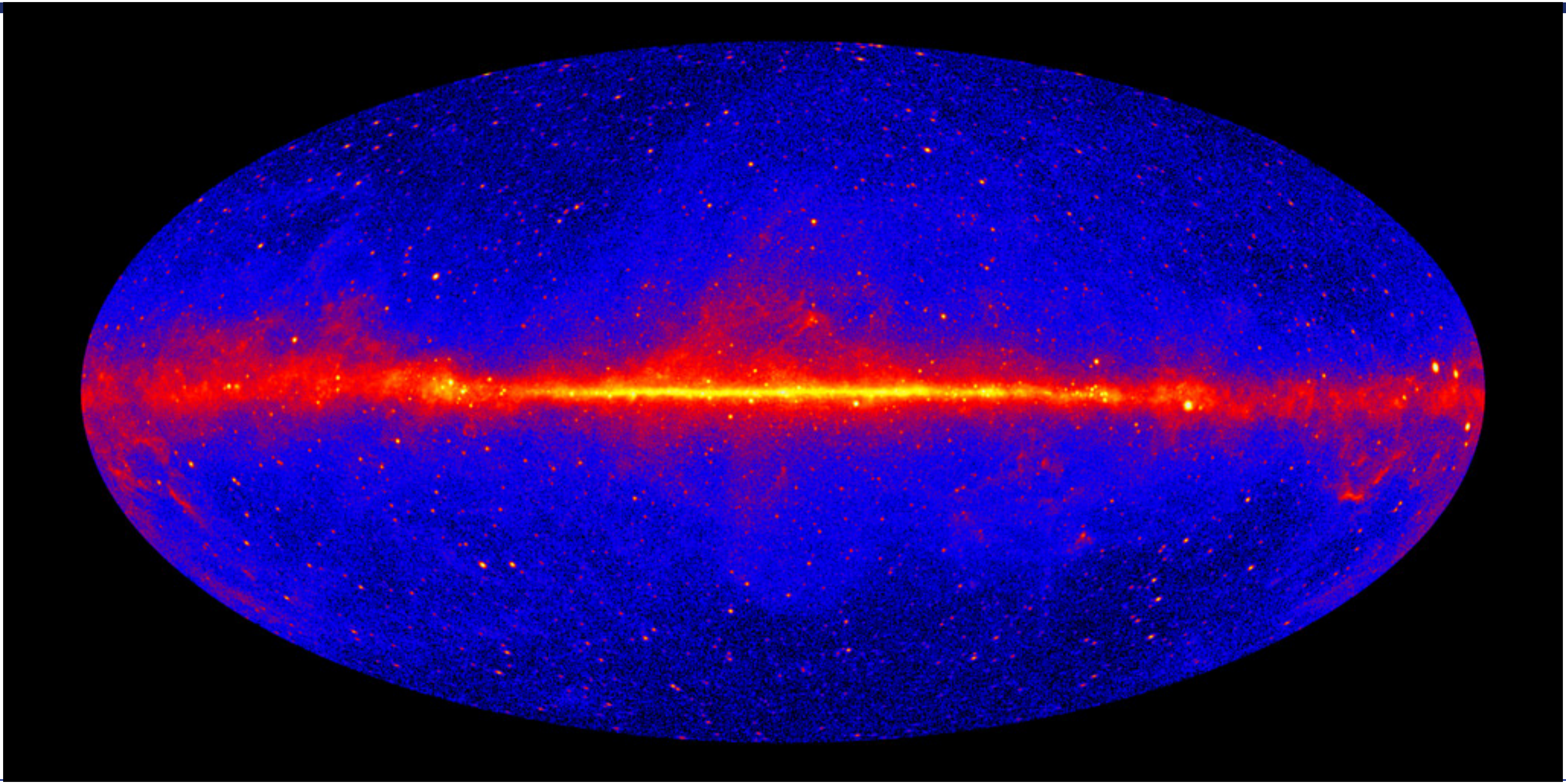

NASA/DOE/Fermi LAT Collaboration

Extensive Air Showers – Simulations & Observables

Rely on simulations to describe EAS; assume more energetic EAS can be described as a superposition of less energetic showers.

Observable properties:

1. Particles at ground
2. Cherenkov radiation
3. Fluorescence emission
4. Radio emission

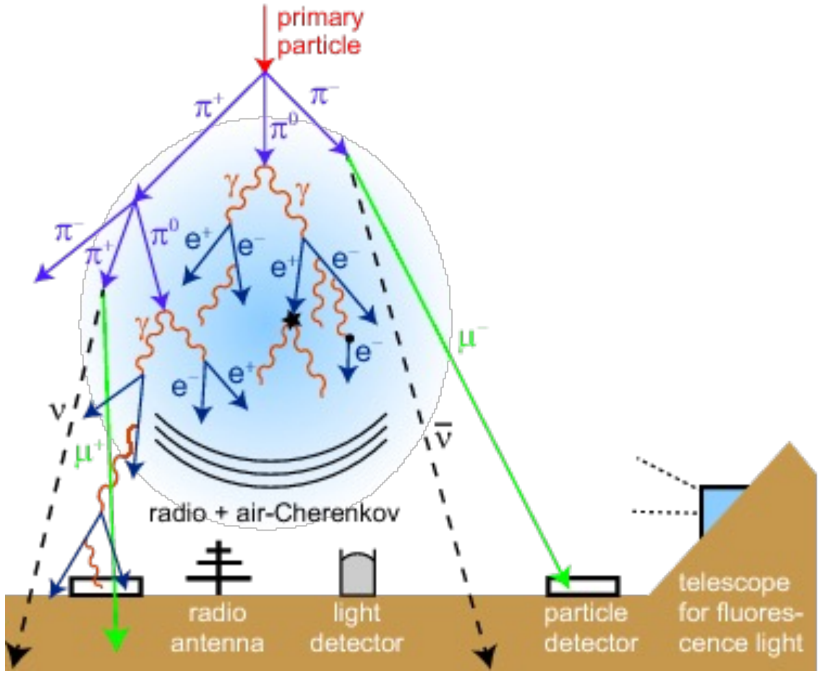

High energies – CR and gamma-rays would pass through satellite or miss it altogether (key is detection area)

→ Observe EAS = use atmosphere as part of detector

Extensive Air Showers: Heitler model of particle cascades

EAS development in the atmosphere

Key interaction processes occur once per radiation length
e.g. whilst passing in vicinity of nucleus

Radiation length X_0: energy loss by 1/e due to Bremsstrahlung

Shower size increases until average energy is critical energy, reaching “shower maximum”, after which ionisation losses dominate over radiation.

Atmospheric depth:

$$X = \frac{1}{\cos\theta}\int \rho dh$$

Scale height $\rho = \rho_0 e^{-h/h_s}$ where $h_s \sim 8$km.

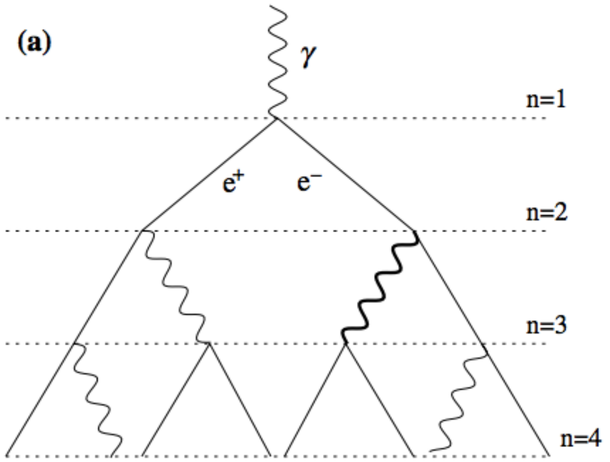

Matthews, Astropart. Phys. 22 (2005) 387-397

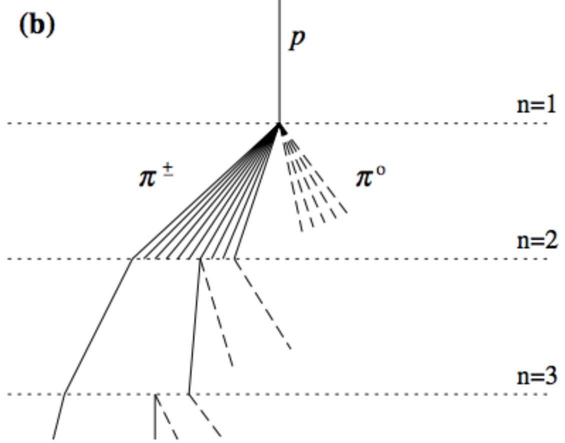

Leptonic EAS: bremsstrahlung, pair production

Key processes:
Bremsstrahlung $e^{\pm} \rightarrow e^{\pm} + \gamma$
Pair production $\gamma \rightarrow e^{+} + e^{-}$

Energy split evenly after each radiation length X_{em},
$X_{1/2} = X_{em} \ln 2$ until $E_c = 85$ MeV

$X_{em} \sim 37$ g/cm^2 for bremsstrahlung, and 9/7 X_{em} for pair production

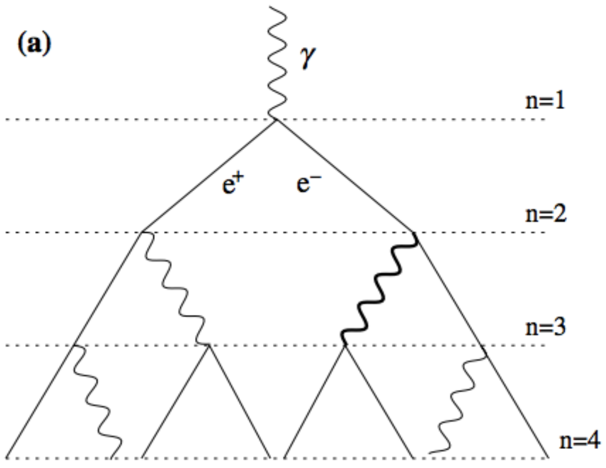

After n radiation lengths: (or distance x)
→ N particles = $2^n = 2^{x/X_0}$, E(x) = $E_0 2^{-x/X_0}$

→ $N_{max} = E_0/E_c = 2^n$

→ $X_{max} = X_0 + n_{max} X_{1/2}$

Total atmosphere ~ 25 radiation lengths

Hadronic EAS: production of muons

Heitler model considers production of pions only (dominant)
approx. ~15 new particles per interaction

- 2/3 $\pi^{\pm}$, 1/3 π^{0}
- $\pi^0 \rightarrow \gamma + \gamma$ decays in 10^{-16} s, generating EM cascade
- $\pi^+ \rightarrow \mu^+ + \nu_\mu$ form muonic component, decay in 10^{-8} s
- E_c ~ 20 GeV
- Energy transfer to EM component
  $E_{em} = 1 - (2/3)^n$ → 90% after n~6
- X_{had} ~ 120 g/cm^2

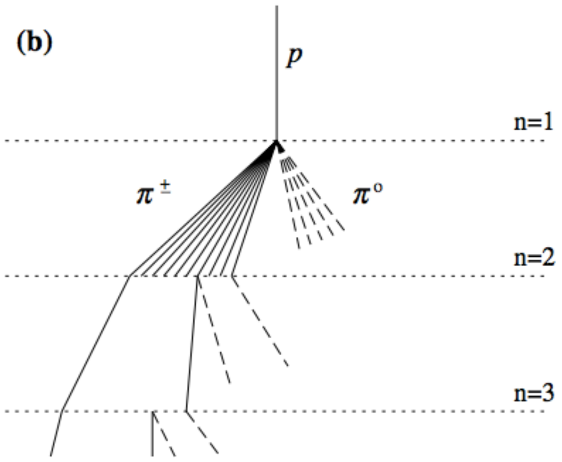

Total atmosphere ~ 11 radiation lengths

Cherenkov radiation

Cherenkov radiation is produced when charged particles travel faster than the local speed of light
$v > c_m = c/n$

For air: n =1.0003, for water: n = 1.333

This induces a dipole field in the local medium

As the medium relaxes, dipole transitions release radiation

Note: $\mathrm{n(h)} = 1 + n_0 e^{-h/h_0}$

https://www.mpi-hd.mpg.de/hfm/CosmicRay/ChLight/ChLat.html

Cherenkov cone opening angle:

$$\cos\theta_c = \frac{c}{vn}$$

Number of photons produced per unit length is proportional to Z^2

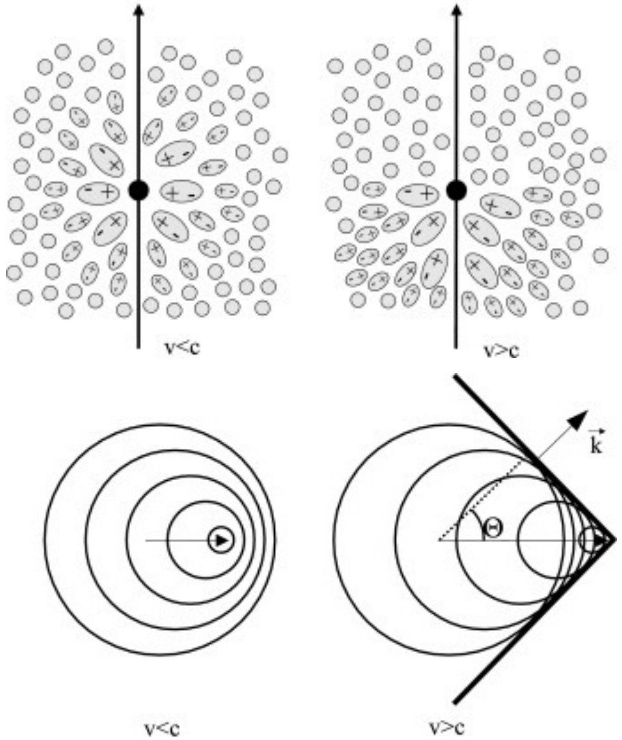

Longitudinal and Lateral shower profiles

Cherenkov light profile

Peaks in characteristic ring – Cherenkov pool radius ~125 m

Note – light emitted earlier arrives later

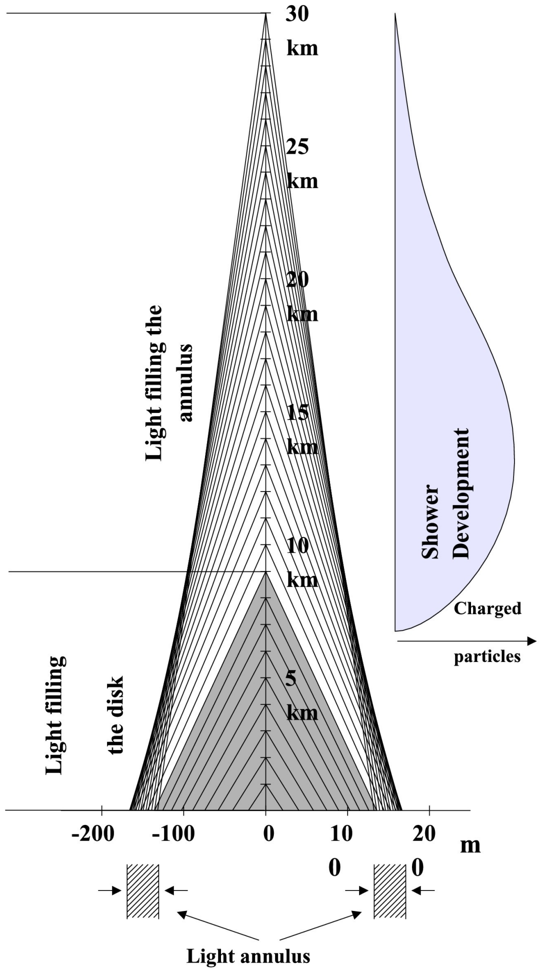

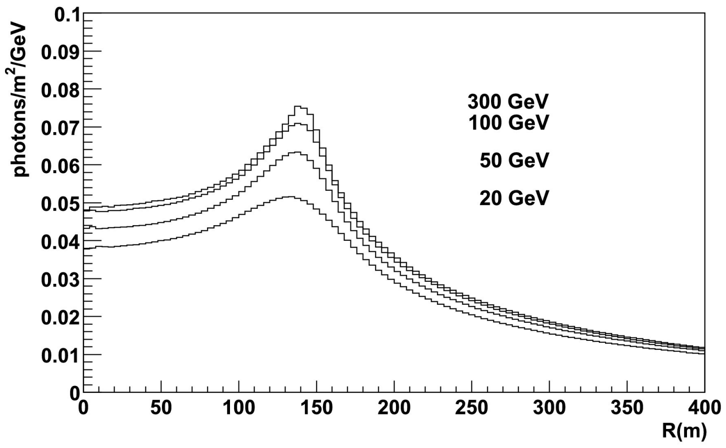

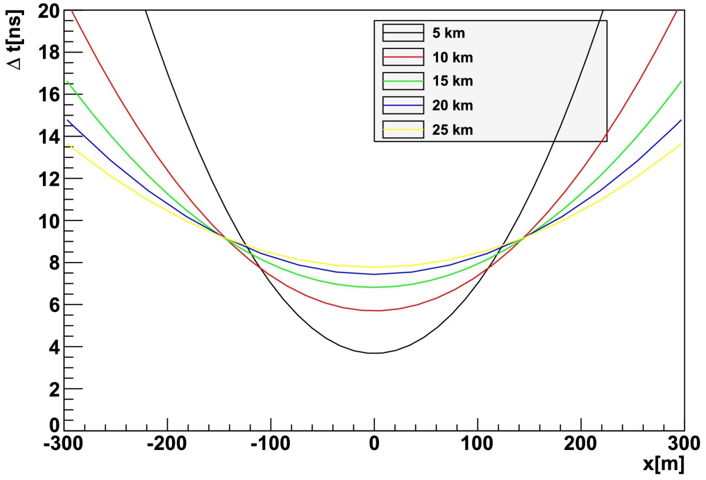

Detection Techniques for Very-High-Energy gamma-rays

Two main detection methods:

- **Particle detector arrays:**
  - Water Cherenkov Detectors (WCDs)
  - Up to 24/7
- **Imaging Atmospheric Cherenkov Telescopes (IACTs)**
  - Night only, low moonlight

Energy deposit in atmosphere
→ Earth's atmosphere acts as a calorimeter

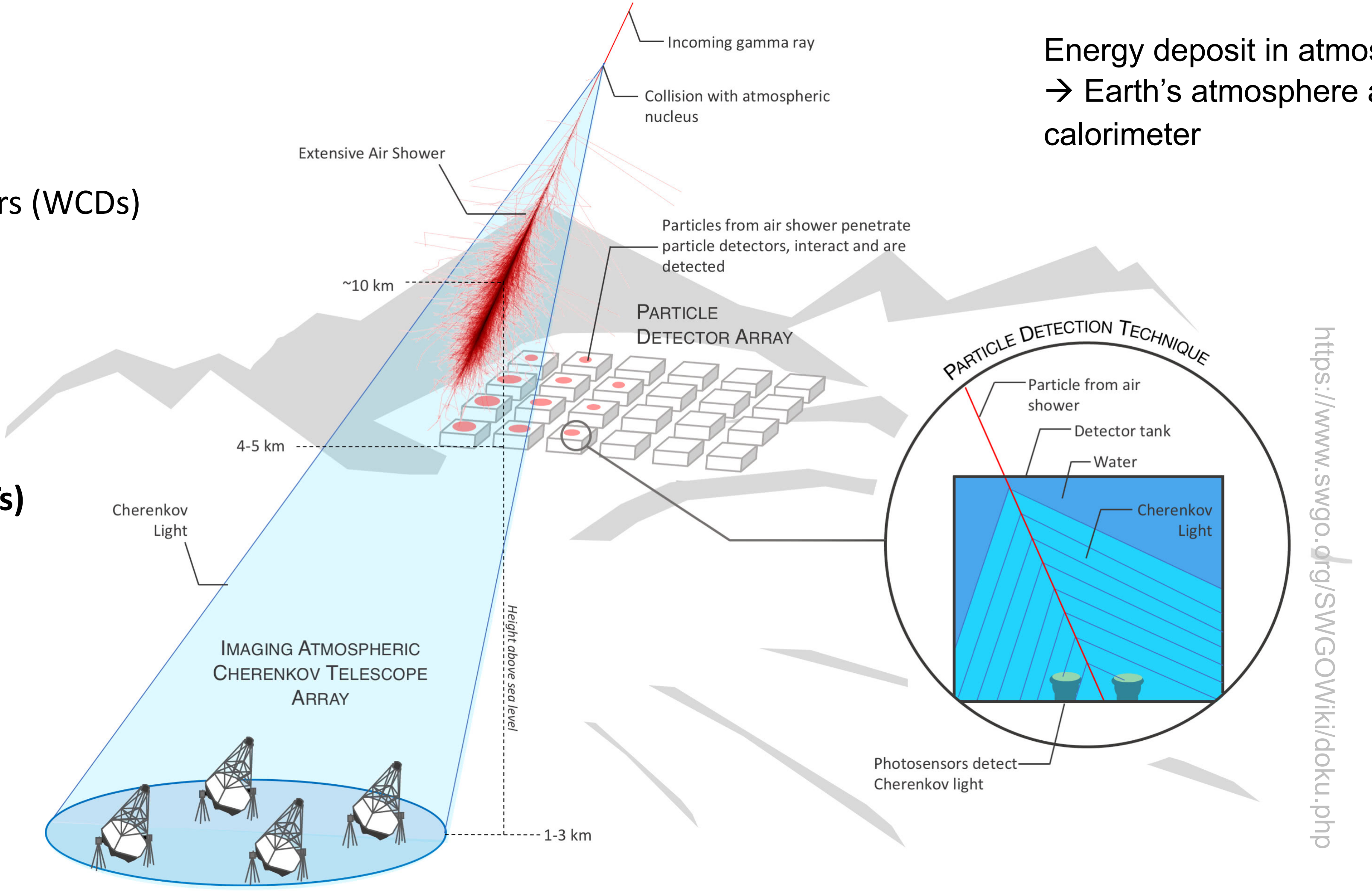

Shower image, 100 GeV γ-ray adapted from: F. Schmidt, J. Knapp, "CORSIKA Shower Images", 2005, https://www-zeuthen.desy.de/~jknapp/fs/showerimages.html

Not to scale

IACT timeline

- **1981 - 2011**: Whipple Observatory (Arizona, USA) – 10m, detection of the Crab nebula in 1989
- **1987 - 2002**: HEGRA (La Palma, Spain) – 5 IACTs "High-Energy Gamma-Ray Astronomy"
- **1991 – 2011***: CANGAROO (Woomera, Australia) *several phases
  "Collaboration of Australia and Nippon for a Gamma Ray Observatory in the Outback"
- **1996 - 2003**: CAT (Themis, France) – "Cherenkov Array at Themis" 4m
- **2002 - now**: H.E.S.S. (Khomas Highlands, Namibia)
  "High Energy Stereoscopic System" 4x12m & 1x28m
- **2004 - now**: MAGIC (La Palma, Spain) – "Major Atmospheric Gamma Imaging Cherenkov" 2x17m
- **2007 - now**: VERITAS (Arizona, USA)
  "Very Energetic Radiation Imaging Telescope Array System" 4x12m
- **2008 – now:** HAGAR (Hanle, Ladakh, India) "High Altitude GAmma Ray telescope" 7x 4.4m2
- **2011 - now**: FACT (Spain) – "First G-APD Cherenkov Telescope"
- **2020 – now:** MACE (Hanle, Ladakh, India) "Major Atmospheric Cherenkov Experiment" 21m
- **2021 - now**: CTA (La Palma, Spain and Chile, construction ongoing) – "Cherenkov Telescope Array"

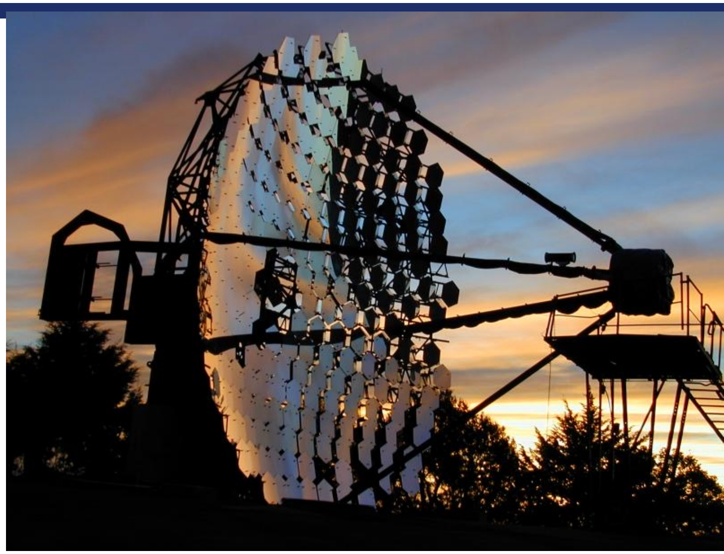

https://veritas.sao.arizona.edu/whipple

WCD / particle detector Timeline

- **1986 - 1999**: CYGNUS Experiment (Los Alamos, New Mexico, USA)
  "Cosmic Gamma-ray Neutron Uncluttered Spectrum" – water tanks
- **1990 - now**: Tibet ASγ (Yangbajing, Tibet, China) — still operational
  "Tibet Air Shower Gamma Experiment"
- **1990 – 1998:** CASA-MIA (Dugway, Utah, USA) "Chicago Air Shower Array - Michigan Muon Array"
- **1999 - 2008**: Milagro (New Mexico, USA) – water pond with PMTs
- **2000 - 2013**: ARGO-YBJ (Yangbajing, Tibet, China) – RPCs (resistive Plate Chambers)
  "Astrophysical Radiation with Ground-based Observatory at YangBaJing"
- **2000 - now**: GRAPES-3 (Ooty, India) — still operational
  "Gamma Ray Astronomy PeV Energies Phase-3" – scintillator & muon detectors
- **2015 - now**: HAWC (Sierra Negra, Mexico) — still operational
  "High-Altitude Water Cherenkov Observatory" – water tanks
- **2021 - now**: LHAASO (Daocheng, Sichuan Province, China) — still operational
  "Large High Altitude Air Shower Observatory" – WCDs, scintillation, muon detectors

Also:

ALPACA / ALPAQUITA
planned for Bolivia
and
SWGO planned for Chile

Imaging Atmospheric Cherenkov Telescopes

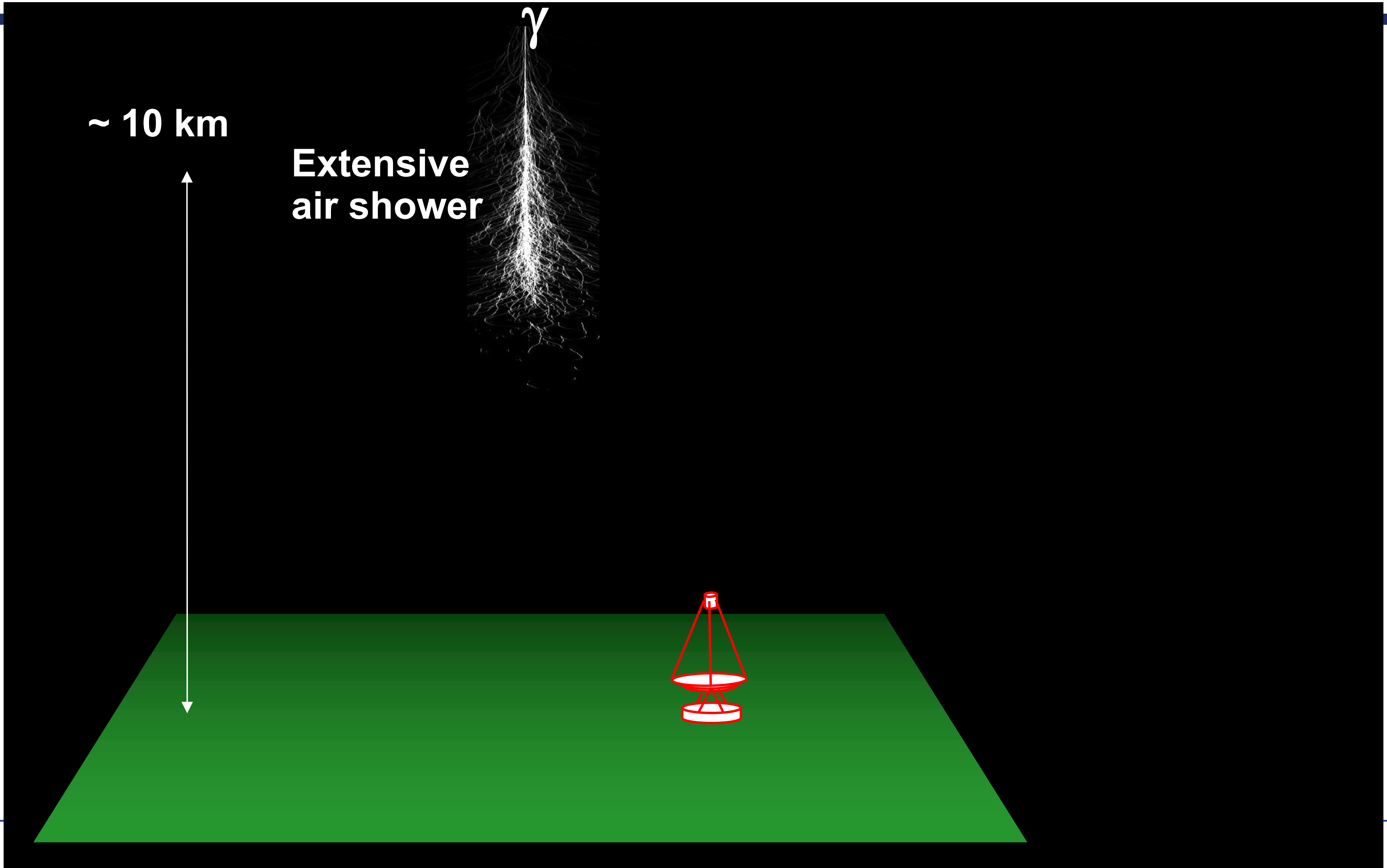

Imaging Atmospheric Cherenkov Telescopes

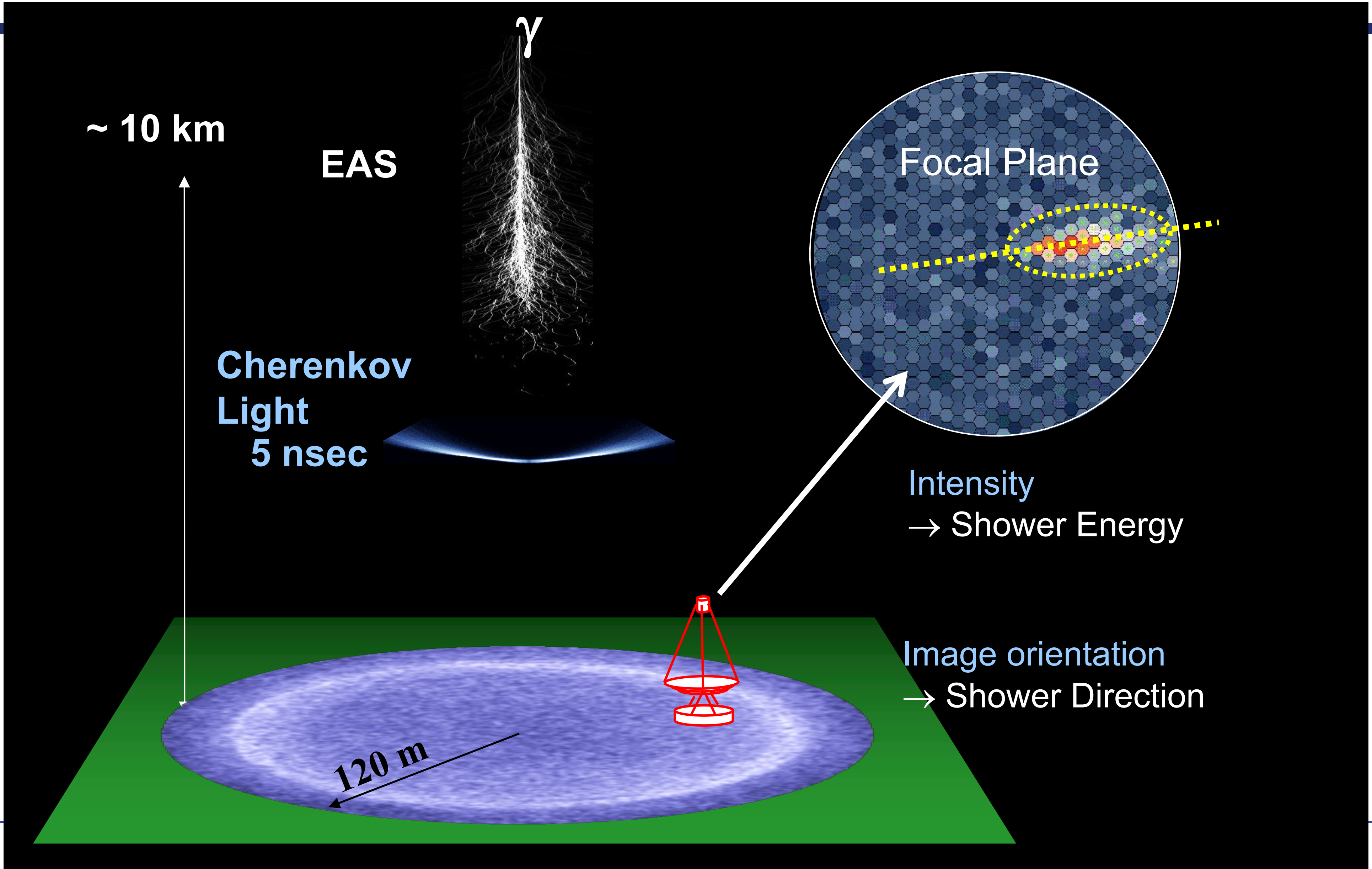

IACTs: Stereoscopic Observations

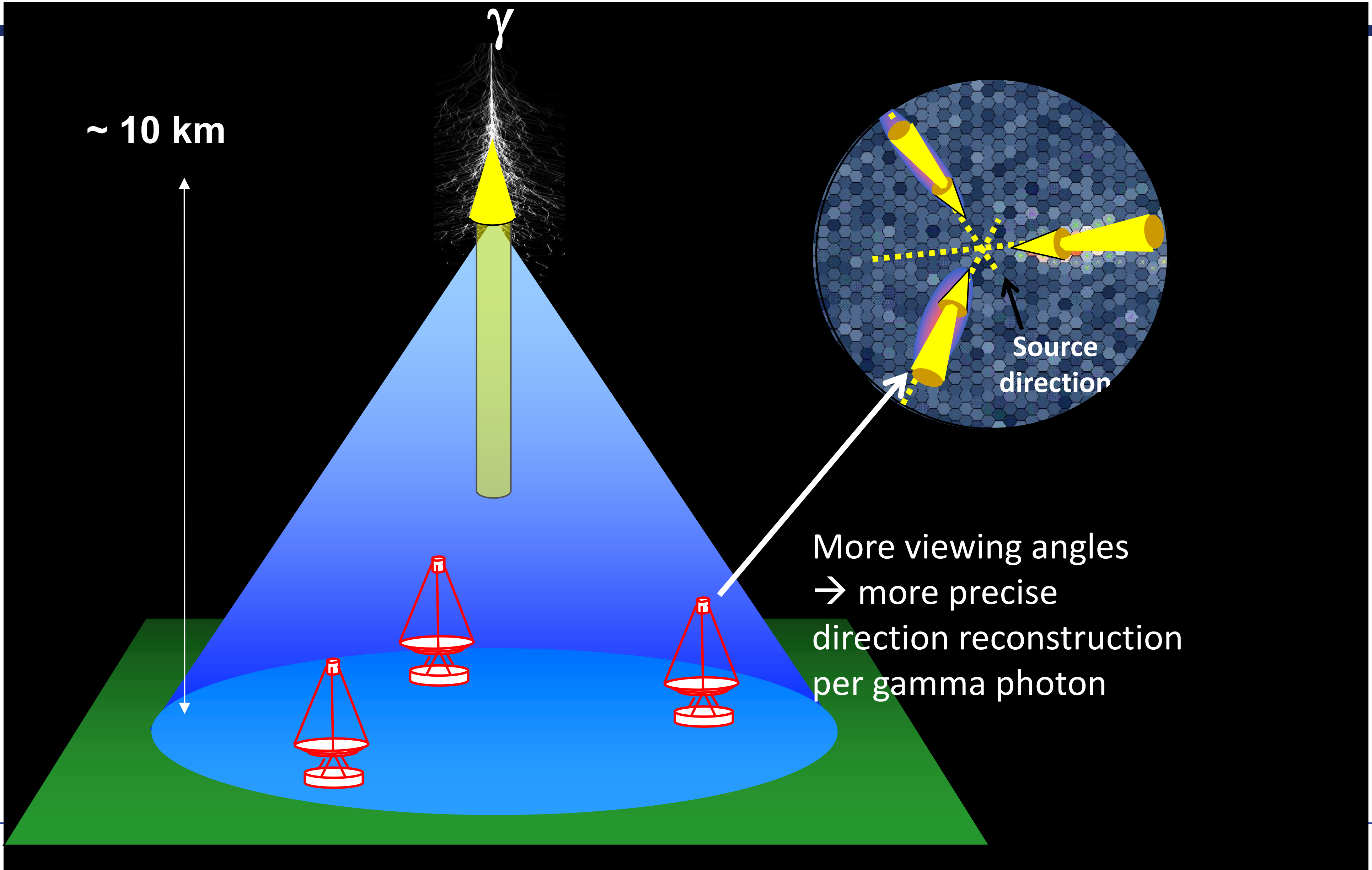

Imaging Atmospheric Cherenkov Technique

Extensive Air Shower detection

Key: ability to distinguish gamma-ray initiated EAS from hadronic EAS background

Camera image parameterisation via Hillas Parameters

Data analysis is heavily based on Monte Carlo – simulations of extensive air shower development in the atmosphere, Cherenkov radiation production and subsequent detector response.

Event reconstruction – involves comparing real data to expectations based on simulations to find the most likely true energy and direction

e.g. via lookup tables (filled histograms) or likelihood-based template fitting

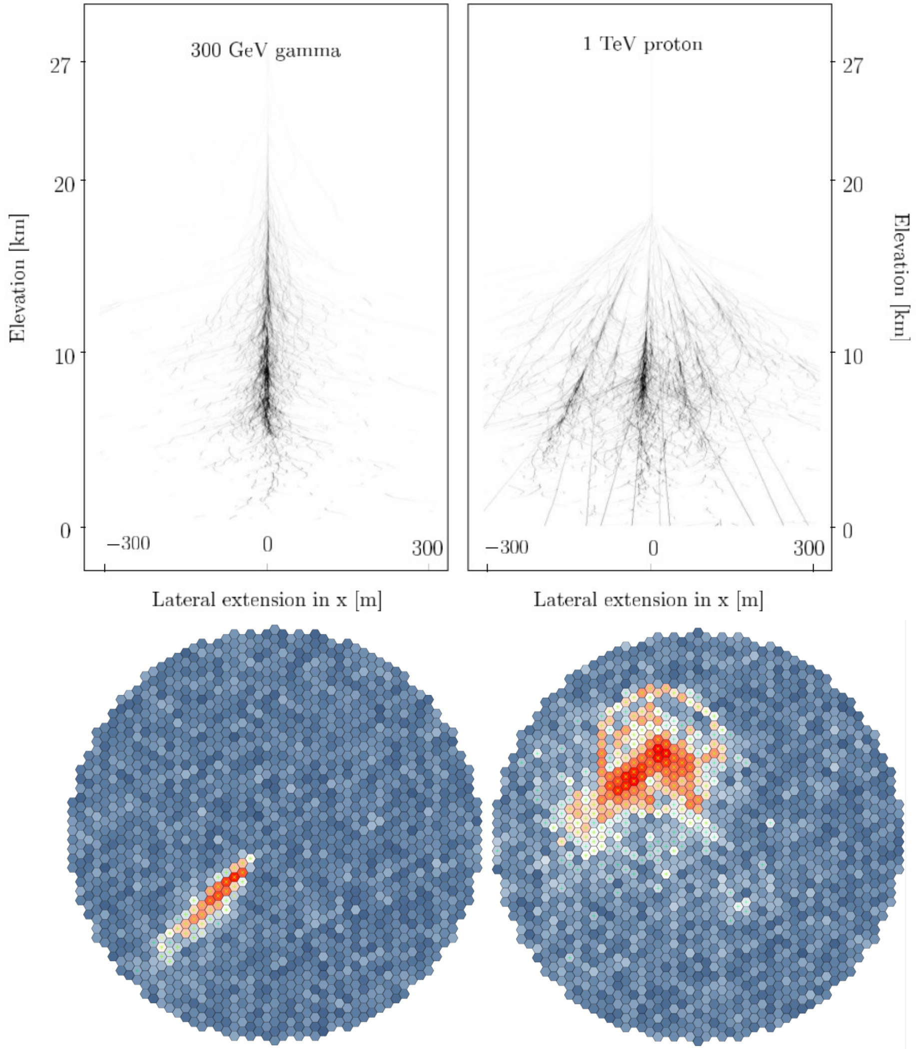

Correspondence to Shower development in Atmosphere

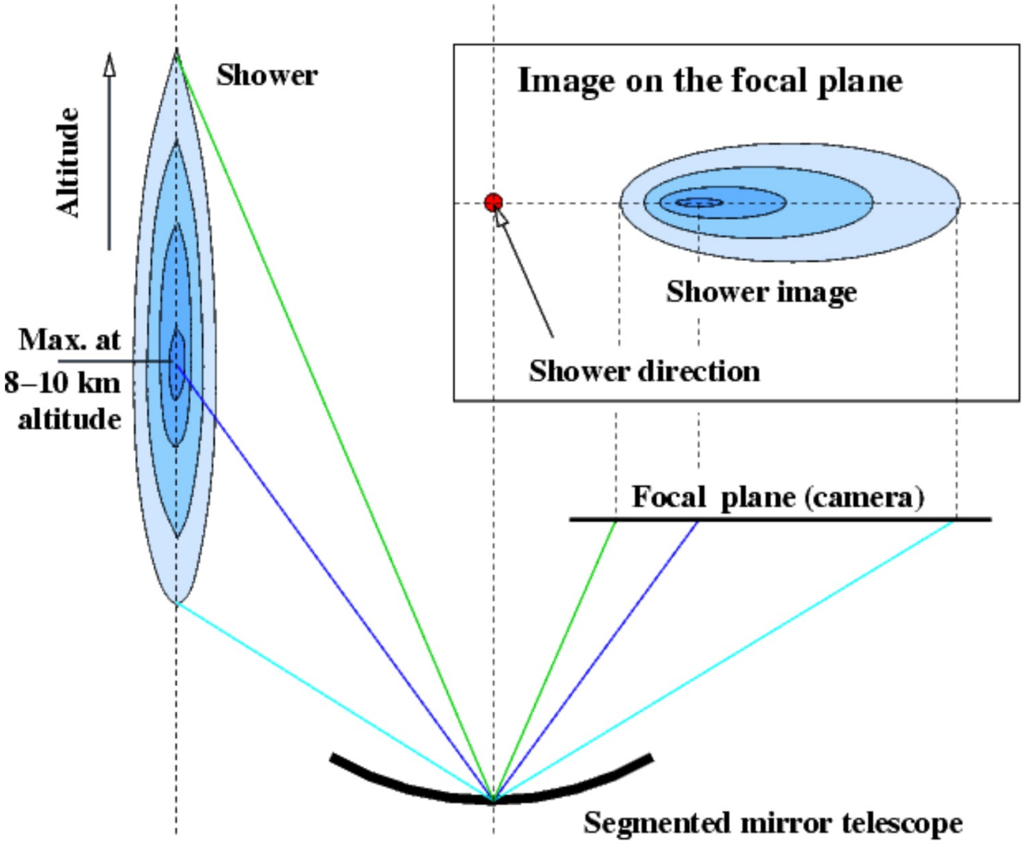

IACTs are angular imaging.

Length of shower corresponds to length of shower development

Cherenkov shower opening angle in air ~1º

Conditions of atmosphere affect Cherenkov light production and shower development.

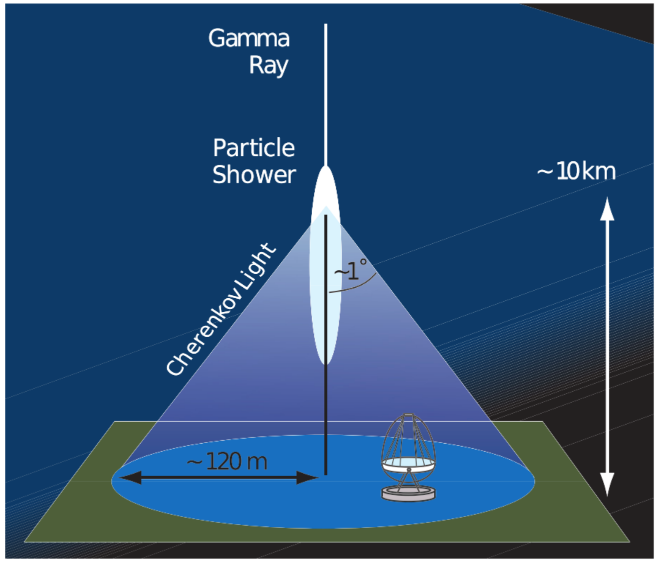

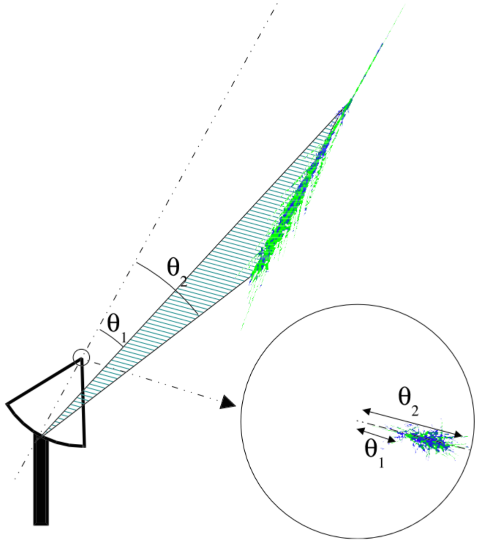

Bernlöhr, Corsika school (2014)
De Naurois & Mazin, C.R. Physique **16**, 610-627 (2015)

Hillas Parameters

Simple geometric parameterisation of camera images can be used to distinguish gamma-ray from hadronic events.

Ellipse fitting to camera images per telescope and compare to lookup tables based on simulations.

The mean reduced scaled width (MRSW) = $\frac{1}{N_{tel}}\sum_{i}^{N_{tel}}\frac{w_i-\langle w\rangle_i}{\sigma_i}$ similarly MRSL combine information over multiple telescopes.

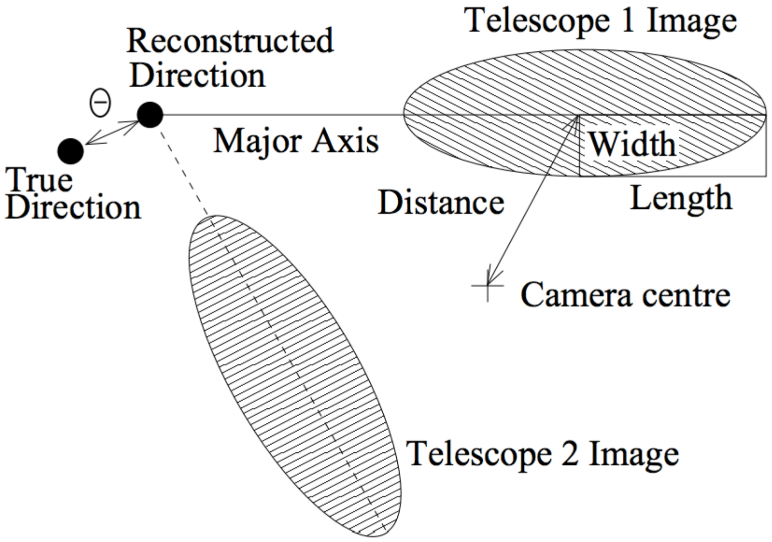

H.E.S.S. collaboration A&A **457**, 899-915 (2006)

MRSW from simulations compared
a) to OFF data and
b) to Crab data after selection cuts

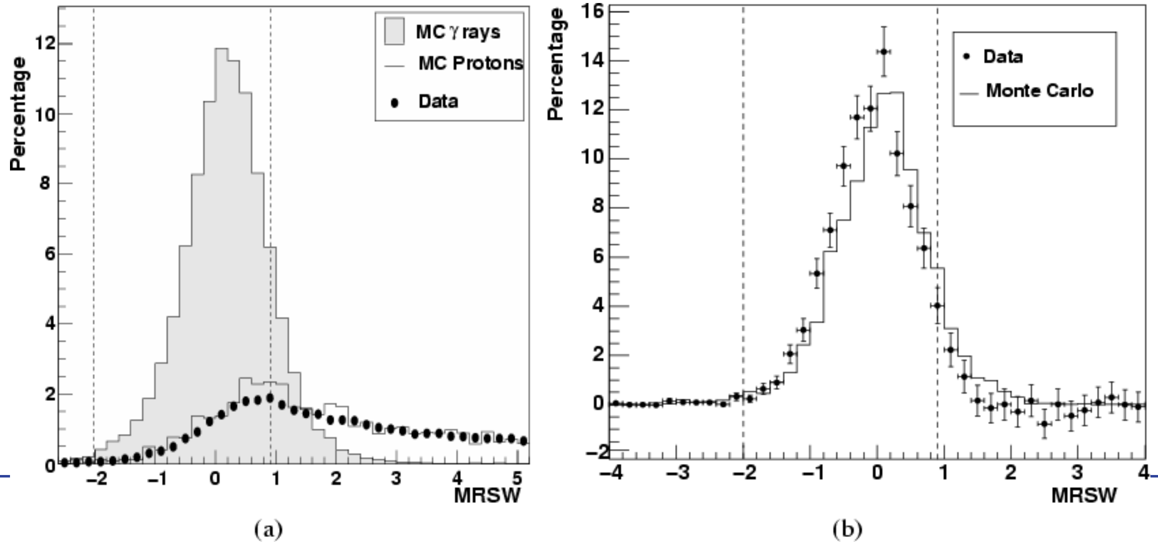

(a) (b)

Boosted Decision Trees

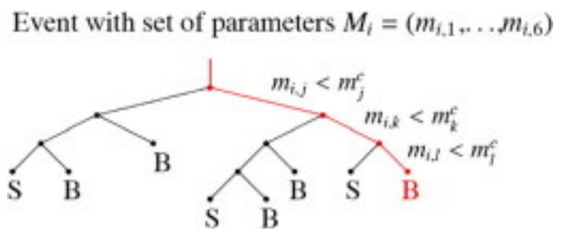

Combine several variables into a boosted decision tree (BDT) for enhanced gamma-hadron separation power

Training done using Monte Carlo and/or OFF data

Grey = gamma, red = proton

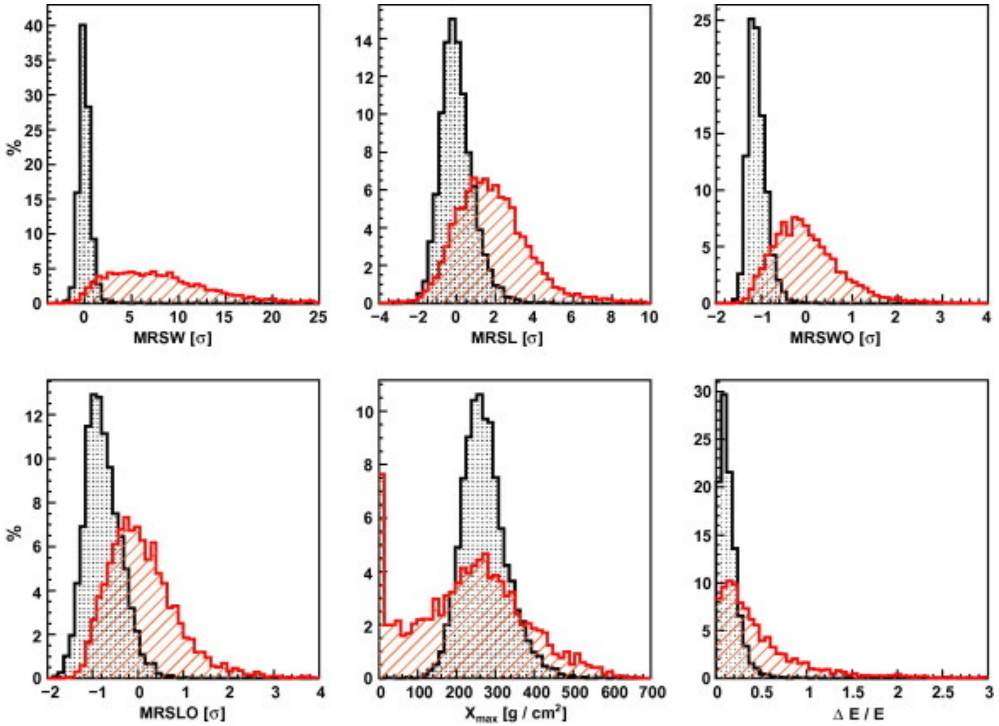

End result: much more powerful separation encoded into a single variable, ζ

Note – this needs to be trained for a specific energy range and zenith angle band

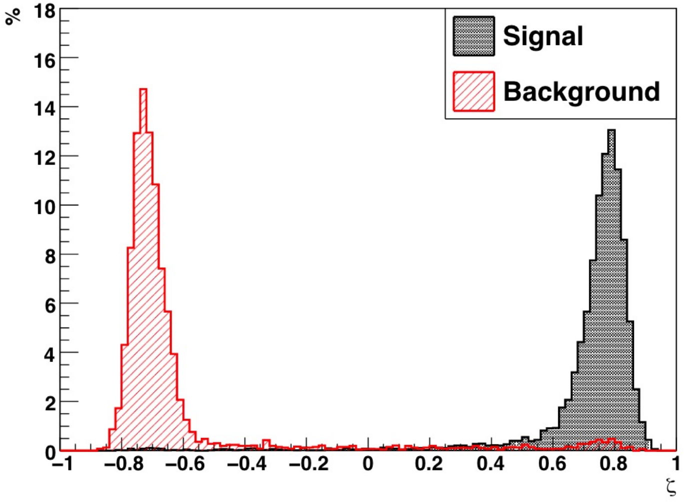

Ohm et al. Astropart. Phys. **31**, 383-391 (2009)

Image Cleaning, likelihood fitting & image templates

First step is always image cleaning → removing "noisy" pixels / those likely due to background optical light

e.g. so-called "tail-cuts" or dual-threshold cleaning:
All pixels with a charge above a high threshold are kept, along with neighbouring pixels above a lower threshold.
Typically: 10 / 5 p.e. or 7 / 4 p.e.

Likelihood-fitting → construct a pixel-wise likelihood function and evaluate the log-likelihood (ln L) compared to either an analytical shower model, or a database of simulated image templates.

Probability density P for a given pixel value s with expectation value μ, photoelectron number n, pedestal width σ_p and single p.e. resolution σ_γ

$$P(s|\mu,\sigma_p,\sigma_\gamma) = \sum_n \frac{\mu^n e^{-\mu}}{n!\sqrt{2\pi\left(\sigma_p^2 + n\sigma_\gamma^2\right)}} \exp\left(-\frac{(s-n)^2}{2\left(\sigma_p^2 + n\sigma_\gamma^2\right)}\right)$$

$$\ln\ L = -2 \times \ln\ P(s|\mu,\sigma_p,\sigma_\gamma)$$

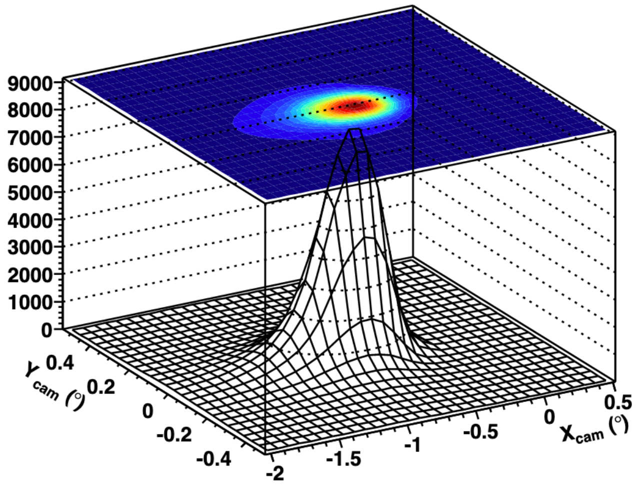

Deep Neural Networks

Potentially powerful gain in gamma-hadron separation or reconstruction

CNNs – limited by sparsity following cartesian transformation

GNNs (or GCNN) –more flexible, treating pixels as nodes

<u>Limitations:</u>
Neural network highly sensitive to environmental conditions (e.g. NSB, atmosphere...)

→ computationally expensive re-training?

hadronic interaction model uncertainties → see CR

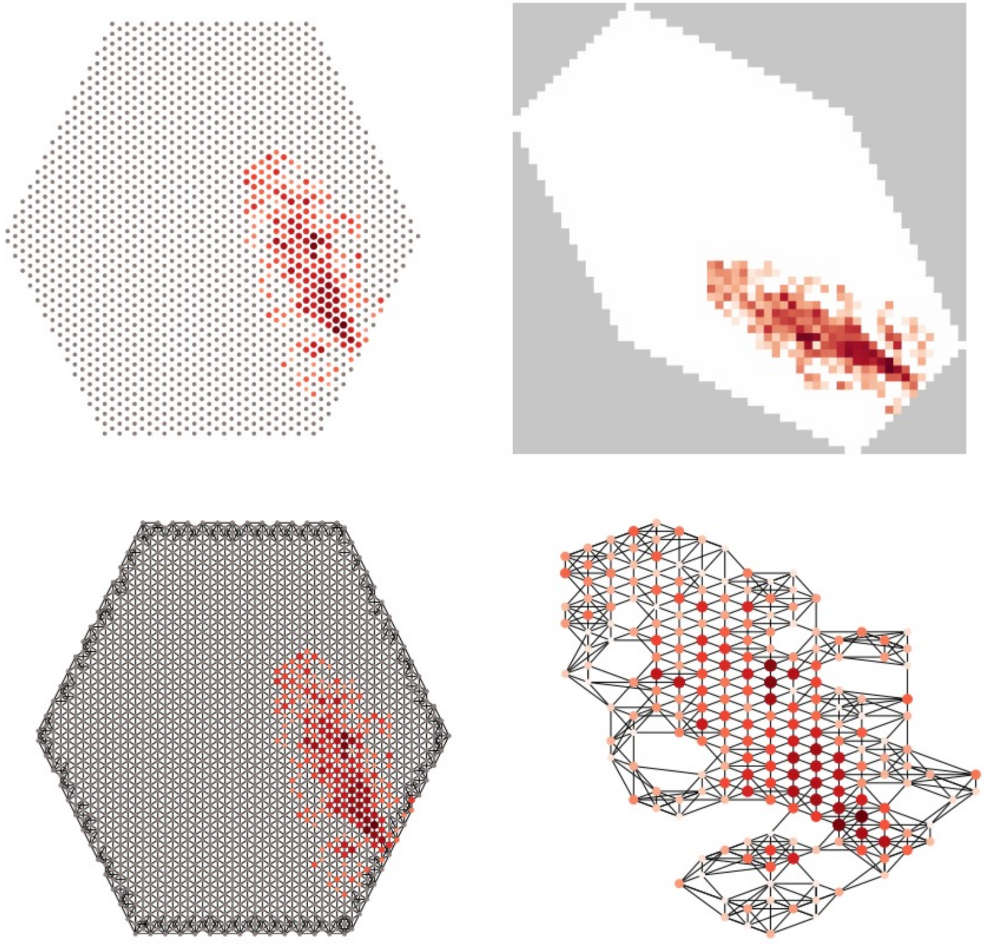

J. Glombitza et al JCAP11(2023)008

Instrument components

Each IACT has:

Mirror dish (segmented)

Optical camera -- fast imaging

Rotation / tracking capability

<u>Optical configuration:</u>

<u>Davies-Cotton</u>: mirror panels of 2f focal length on a sphere with f
→ low aberrations

<u>Parabolic</u>: maintains isochronous photon arrival times

<u>Schwarzschild-Couder</u>: dual mirror, reduced camera size, increased threshold, yet larger field-of-view

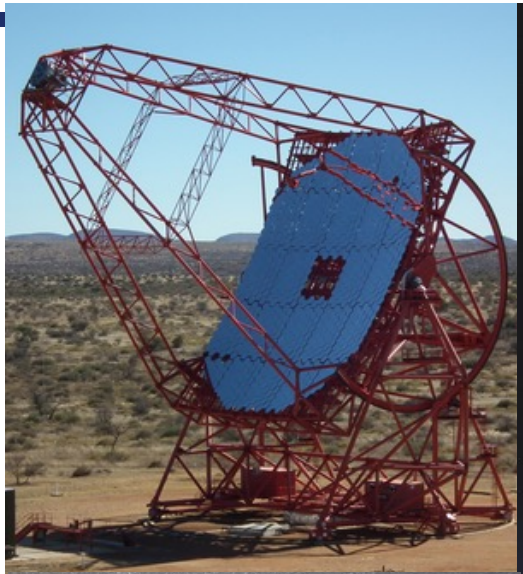

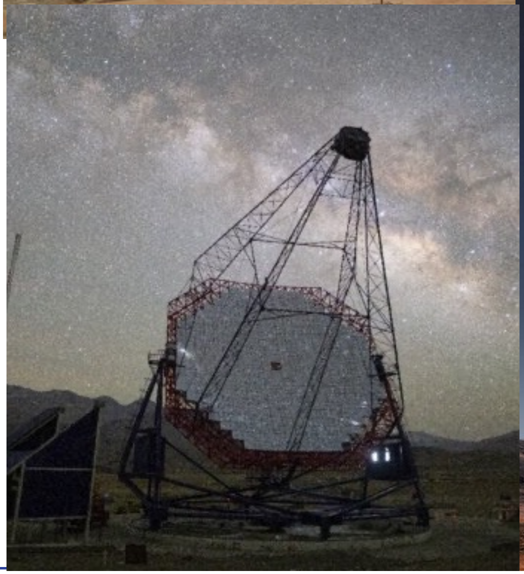

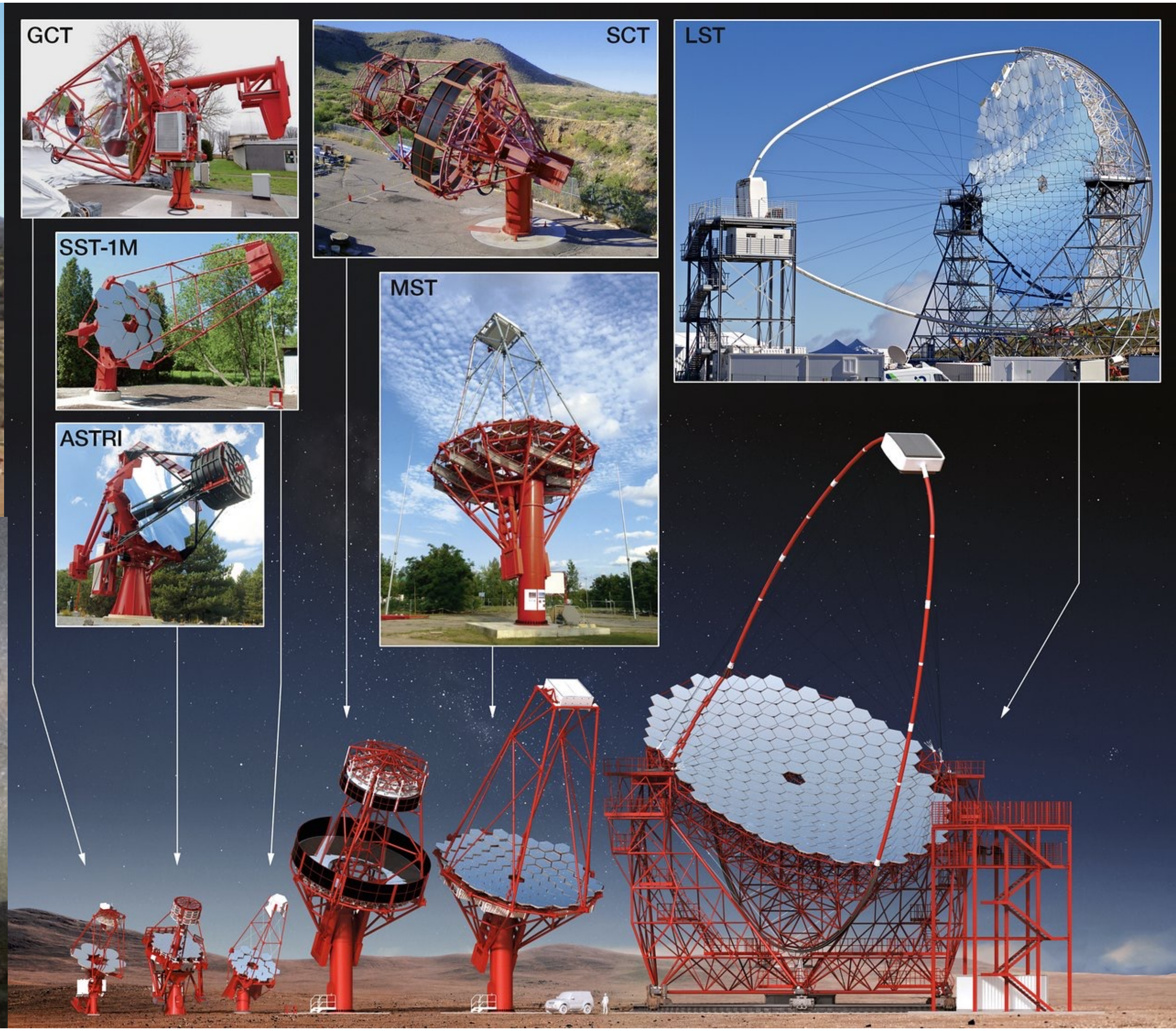

Water Cherenkov Detectors (WCDs)

As an example: HAWC detector located in Mexico

Array of 300 WCDs at 4100m above sea level.

Air shower events trigger across array – can operate during day and night.

Gamma-ray vs Cosmic Ray ?

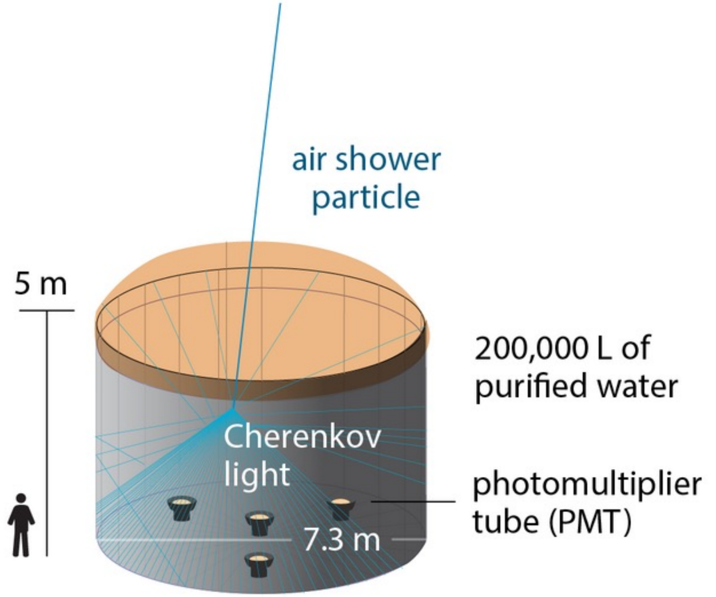

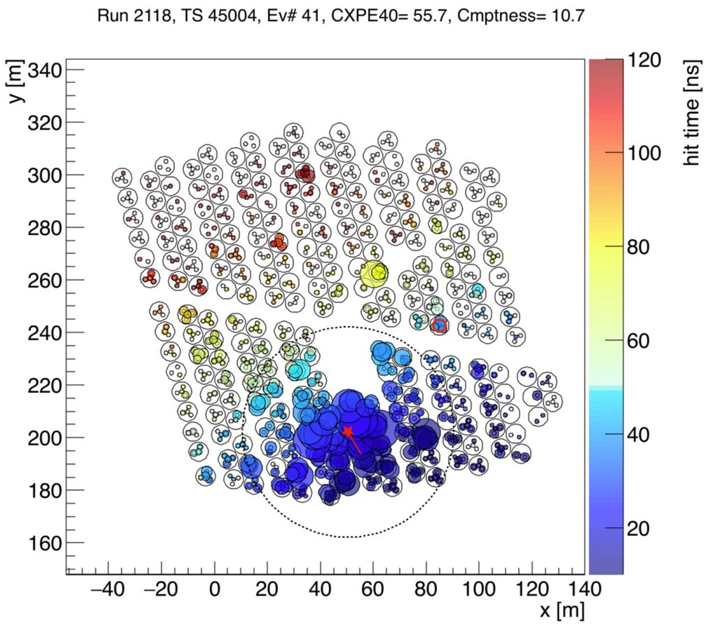

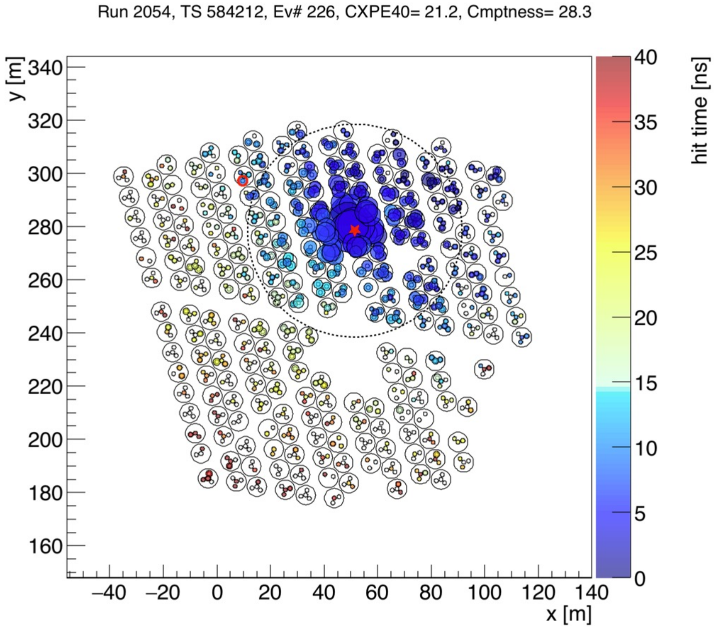

Photomultiplier Tubes & Silicon Photomultipliers

PMTs & SiPMs

Each photon releases a number of electrons from the photocathode

High Voltage supply directs the electron(s) towards a dynode

Dynodes multiply the signal

Final signal readout at the Anode

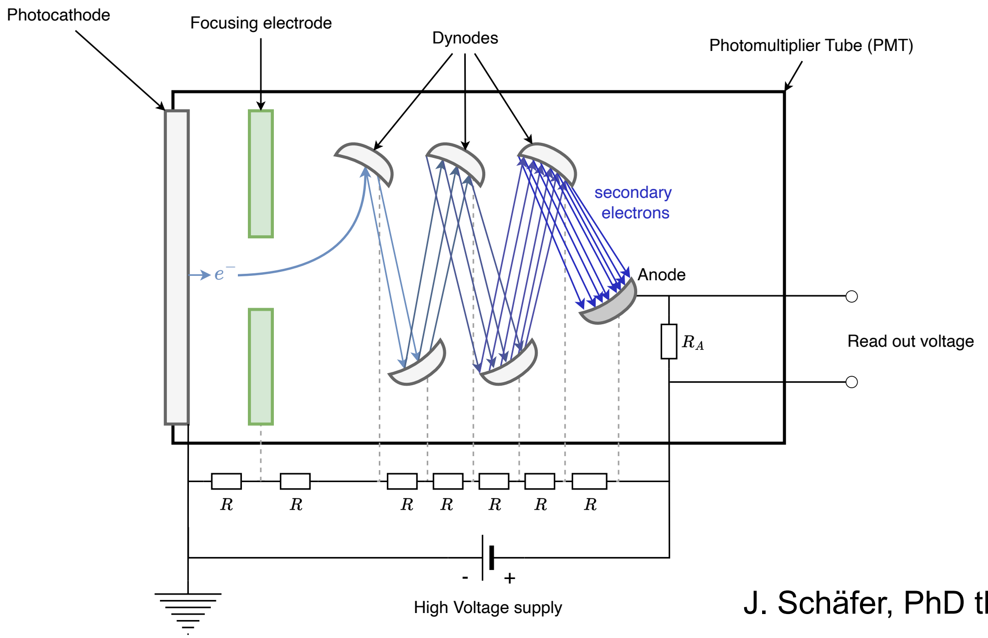

J. Schäfer, PhD thesis

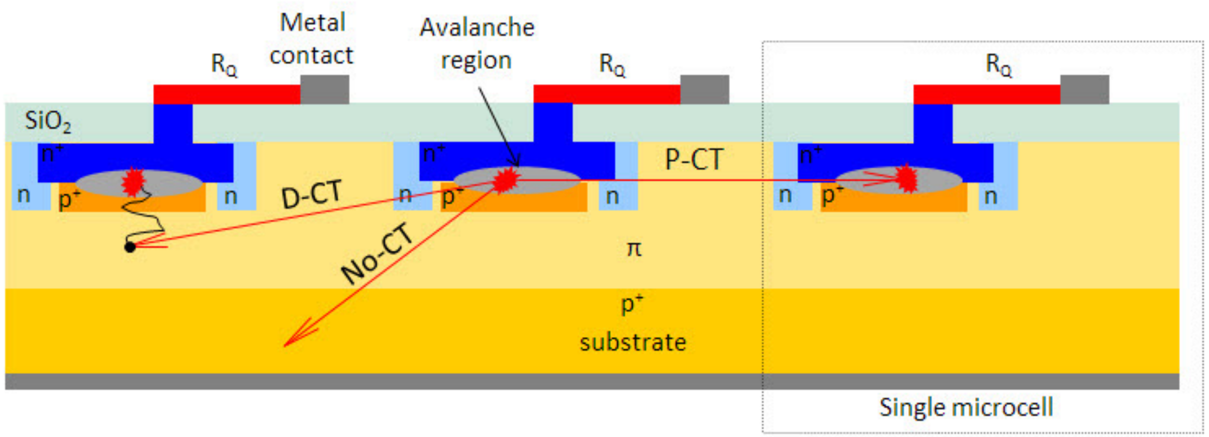

Hamamatsu

Solid state photodetector

Pixelated – cross-talk can become relevant

Compact, lower voltage and more resistant than PMTs

Calibration

Camera

- Dedicated calibration “runs” to measure quantities.
- Also, measure timing precision of the camera
- Pedestal = can be dark, or measured under ambient NSB (Night Sky Background) conditions.

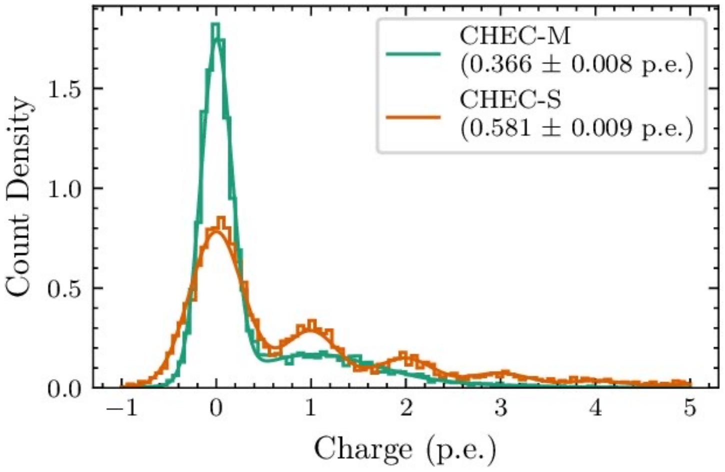

Watson & Zorn ICRC(2019)

$$A^{\mathrm{HG}} = \frac{\mathrm{ADC}^{\mathrm{HG}} - P^{\mathrm{HG}}}{\gamma_{\mathrm{e}}^{\mathrm{ADC}}} \times \mathrm{FF}$$

$$A^{\mathrm{LG}} = \frac{\mathrm{ADC}^{\mathrm{LG}} - P^{\mathrm{LG}}}{\gamma_{\mathrm{e}}^{\mathrm{ADC}}} \times (\mathrm{HG}/\mathrm{LG}) \times \mathrm{FF}$$

- High Gain (HG) and Low Gain (LG) channels per pixel
- P^{HG} = pedestal (baseline) per pixel
- γ_e^{ADC} = gain of the HG channel (ADC counts per photoelectron)
- A^{HG} = amplitude in photoelectrons
- HG/LG = gain ratio
- FF = flat fielding coefficient (flatten relative response over camera)

Calibration

Mirror + Camera

- Overall throughput / efficiency, including mirror reflectivity. Can be done using muons (for example)

$$\frac{d^2N}{dl d\phi} = \alpha \int_{\lambda_1}^{\lambda_2} \frac{\phi(\lambda)}{\lambda^2} \left(1 - \frac{1}{\beta^2 n(\lambda)^2}\right) d\lambda$$

$$I_{pe} = \varepsilon_\mu \frac{1}{2} \alpha I \frac{\omega}{\theta_c} \sin(2\theta_c) D(\rho, \phi)$$

$$D(\rho,\phi) = \begin{cases} 2R\sqrt{1-\left(\frac{\rho}{R}\right)^2 \sin^2\phi} & (\rho > R) \\ R\left[\sqrt{1-\left(\frac{\rho}{R}\right)^2 \sin^2\phi} + \frac{\rho}{R}\cos\phi\right] & (\rho \leq R) \end{cases}$$

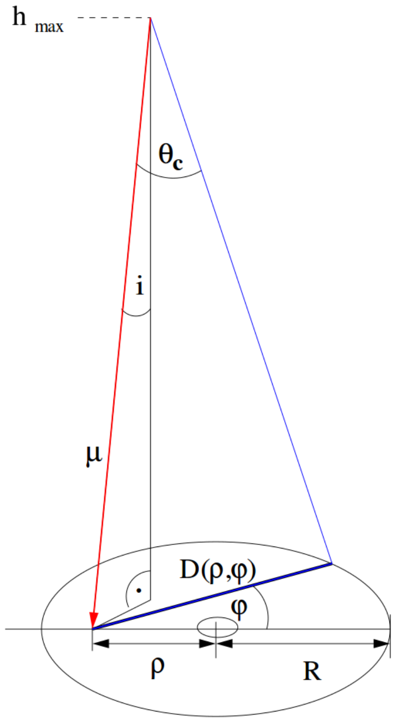

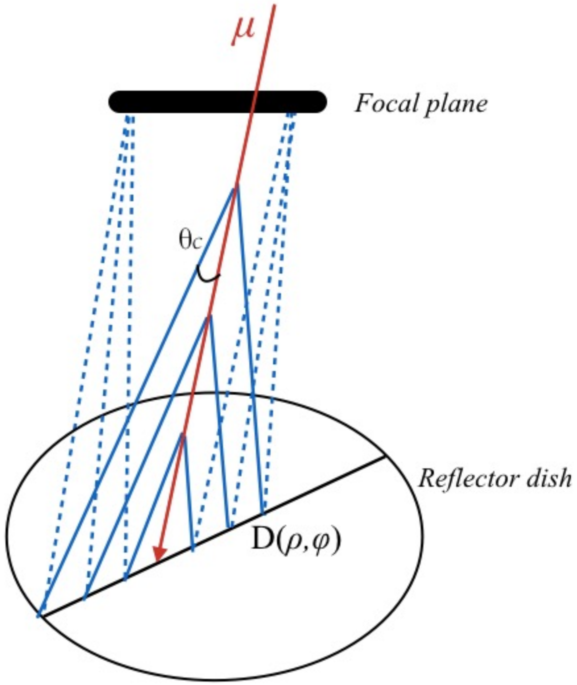

Amount of light produced by a muon and captured by a telescope can be analytically calculated

Comparing this prediction to data enables the optical throughput of the telescope to be evaluated

This can then be monitored over time and used to correct measured images for inefficient photon collection

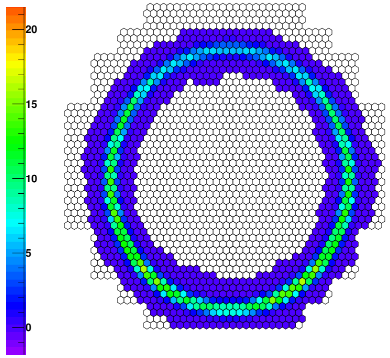

Friedrich-Alexander-Universität
Erlangen-Nürnberg

Erlangen Centre for Astroparticle Physics

Gamma-Ray Astronomy

I – Gamma-ray Production and Detection – part b

Dr Alison Mitchell
Junior Research Group Leader,
FAU Erlangen-Nürnberg

Astroparticle School, Obertrubach-Bärnfels
9th October 2024

Emmy Noether-Programm
DFG Deutsche Forschungsgemeinschaft

Funded by
DFG Deutsche Forschungsgemeinschaft
German Research Foundation

Calibration
Pointing direction

- Where was the telescope *actually* looking?
- Use a bending model to account for telescope structure changes depending on observing direction
- CCD cameras used to take images of LEDs / stars
- Combining the orientation enables reasonable alignment

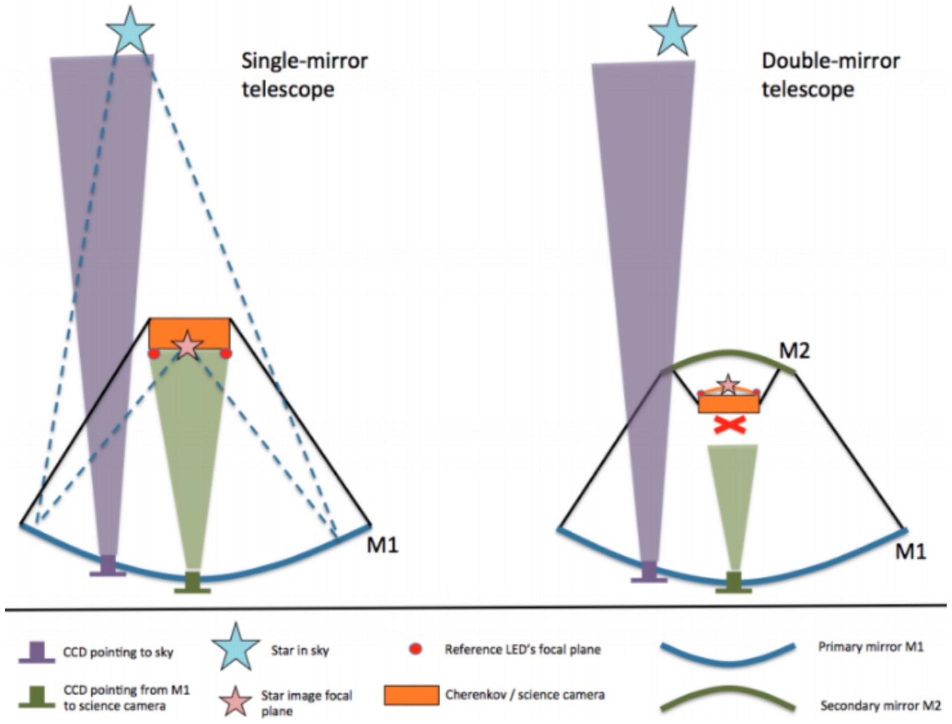

Calibration
Atmosphere

- Atmosphere acts as a part of the detector (calorimeter).
- What was the atmospheric transparency? Were clouds present?
- Level of aerosols / scattering?

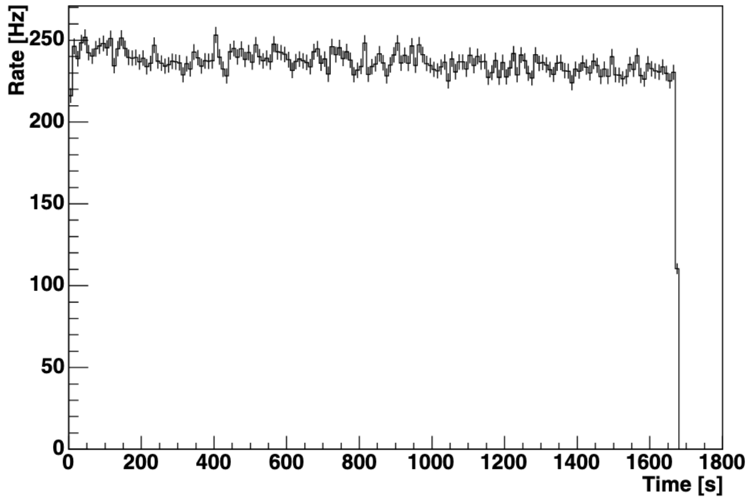

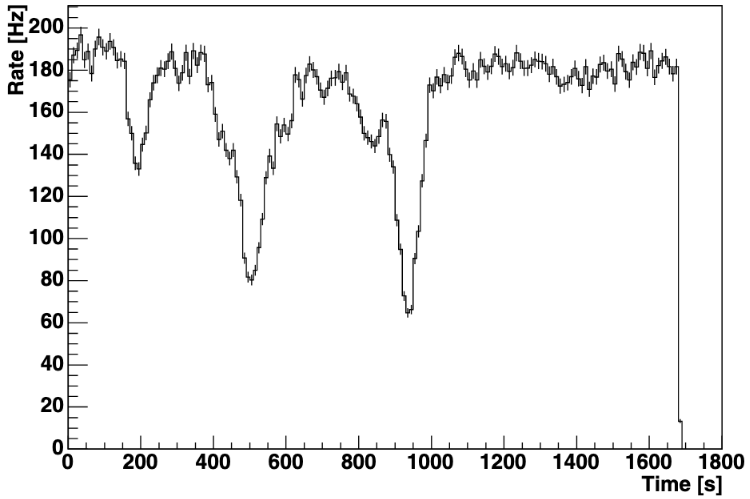

H.E.S.S. collaboration A&A **457**, 899-915 (2006)

Atmospheric Transmission

Refractive index of air is dependent on the altitude above sea level

Cherenkov light is subject to scattering and reduced transmission

The presence of aerosols and clouds additionally impairs transmission.

Aerosol Optical Depth: $T_{aer} = e^{-\int_0^h \alpha(h')dh'}$

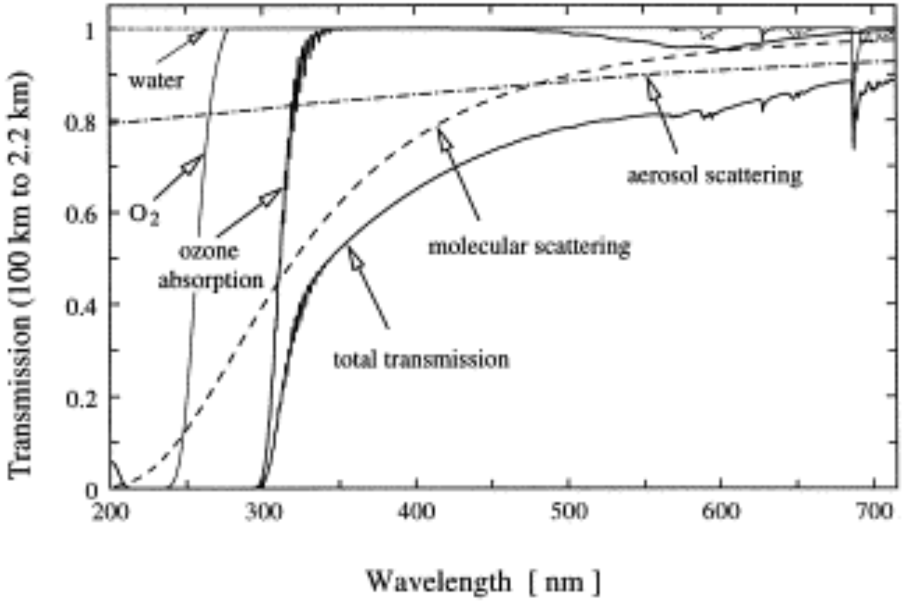

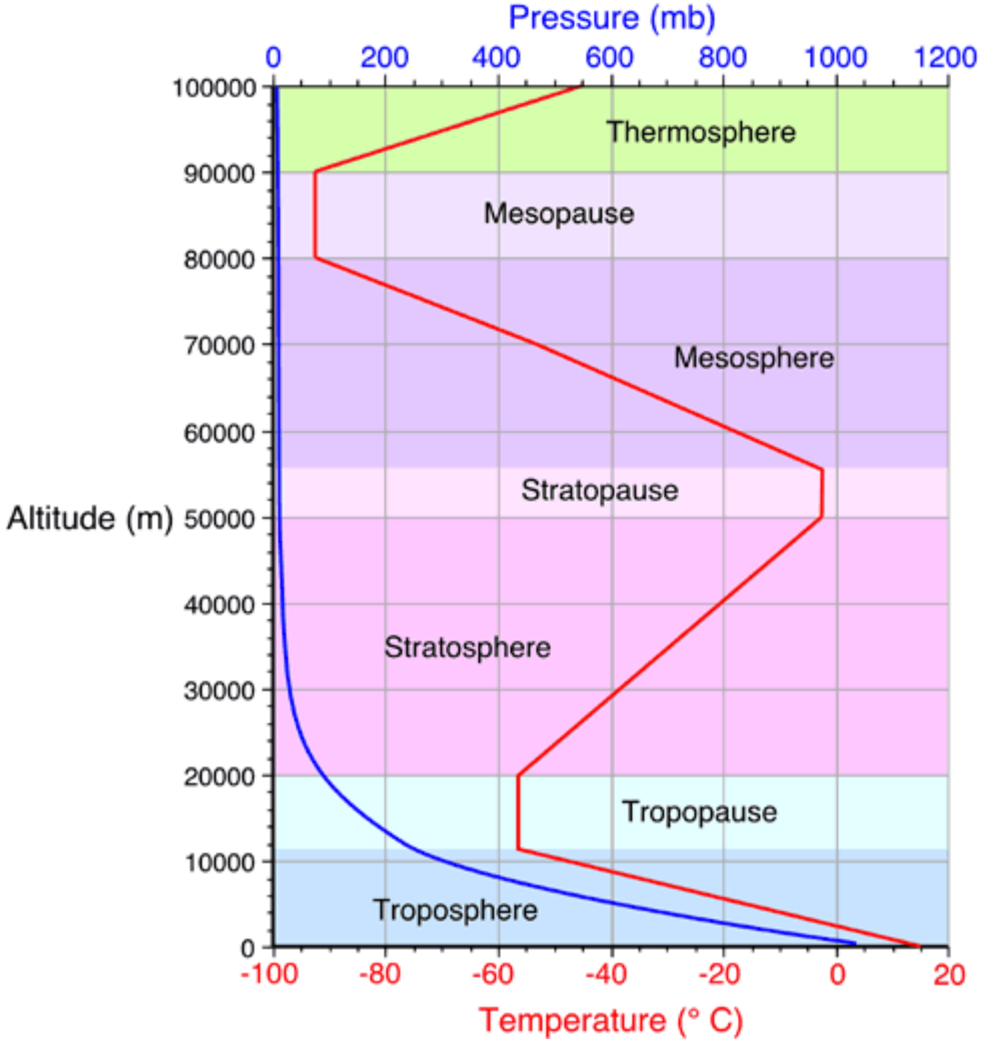

 Bernlöhr Astropart. Phys. **12**, 255-268 (2000)

Data Levels

Common structure between many different experiments to enable using joint tools for analysis
e.g. VODF (very-high-energy open data format) https://vodf.readthedocs.io/en/latest/index.html
Current participants: IACTs (ASTRI, CTAO, FACT, H.E.S.S., MAGIC, VERITAS) WCDs (HAWC, SWGO) Satellites (Fermi-LAT) and Neutrino detectors (IceCube, KM3NeT)

Raw data levels: R0 = device specific, and R1 = common format are not stored.

First level archived is DL0. (Calibration applies at various levels)
DL4 = binned data, e.g. counts maps
DL5 = science products, e.g. flux maps and spectra
DL6 = high-level products, e.g. catalogues

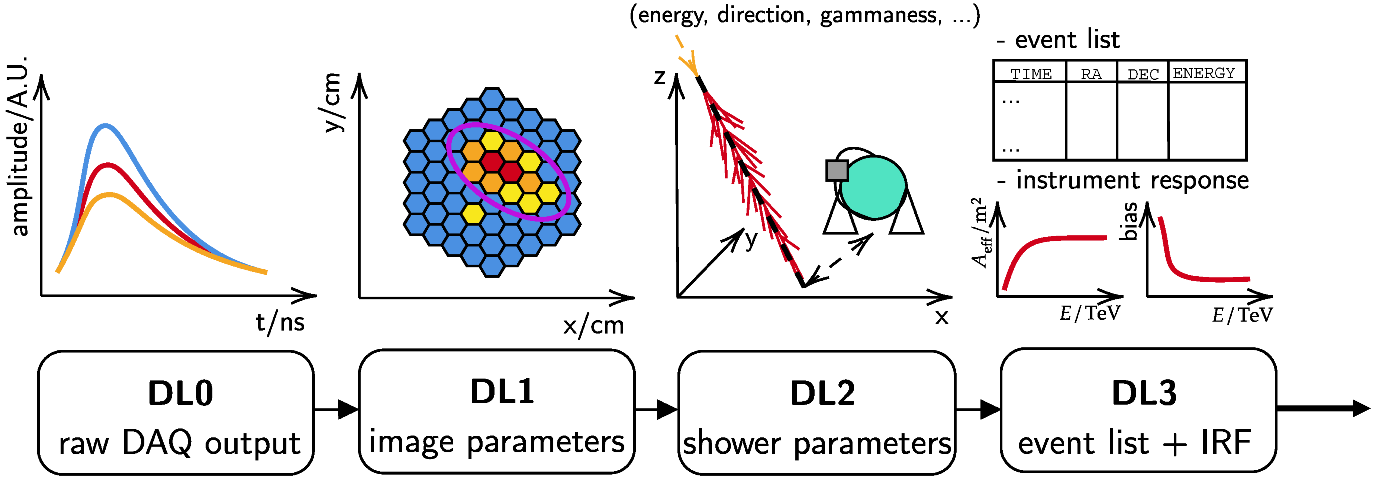

Instrument Response Functions (IRFs)

IRFs describe how the reconstructed event distribution corresponds to the incoming photon distribution

The response is (in general) a function of direction, energy, and time.

Generally factorised into:

Effective area

Point spread function (PSF)

Energy dispersion

and Background rate

2.2 IRF factorisation

Equation 2.2 implies 7-dimensional instrument response functions that in general are computationally unmanageable. Simplifications can be achieved by making further assumptions, and in existing Imaging Air Cherenkov Telescope (IACT) experiments the IRF is generally factorised as follows:

$$R_i(\hat{\alpha}, \hat{\delta}, \hat{E}|\alpha, \delta, E, t) = \mathrm{A}_i(\alpha, \delta, E, t) \times \mathrm{PSF}_i(\hat{\alpha}, \hat{\delta}|\alpha, \delta, E, t) \times \mathrm{D}_i(\hat{E}|\alpha, \delta, E, t) \tag{2.3}$$

where $\mathrm{A}_i(\alpha, \delta, E, t)$ is the effective area in units of cm^2, $\mathrm{PSF}_i(\hat{\alpha}, \hat{\delta}|\alpha, \delta, E, t)$ is the point spread function in units of sr^{-1}, with

$$\int d\hat{\Omega}\ \mathrm{PSF}_i(\hat{\alpha}, \hat{\delta}|\alpha, \delta, E, t) = 1 \tag{2.4}$$

and $\mathrm{D}_i(\hat{E}|\alpha, \delta, E, t)$ is the energy dispersion in units of TeV^{-1}, with

$$\int d\hat{E}\, \mathrm{D}_i(\hat{E}|\alpha, \delta, E, t) = 1 \tag{2.5}$$

Effective area

The effective area is a measure of the detection probability, given the area over which events of a certain energy are collected by the detector.

It is obtained from Monte Carlo via:

$$A_{eff} = \frac{N_\gamma}{N_\gamma^{MC}} A_{MC}$$

where N_γ is the number of gamma-ray events triggering the detector and passing selection cuts.

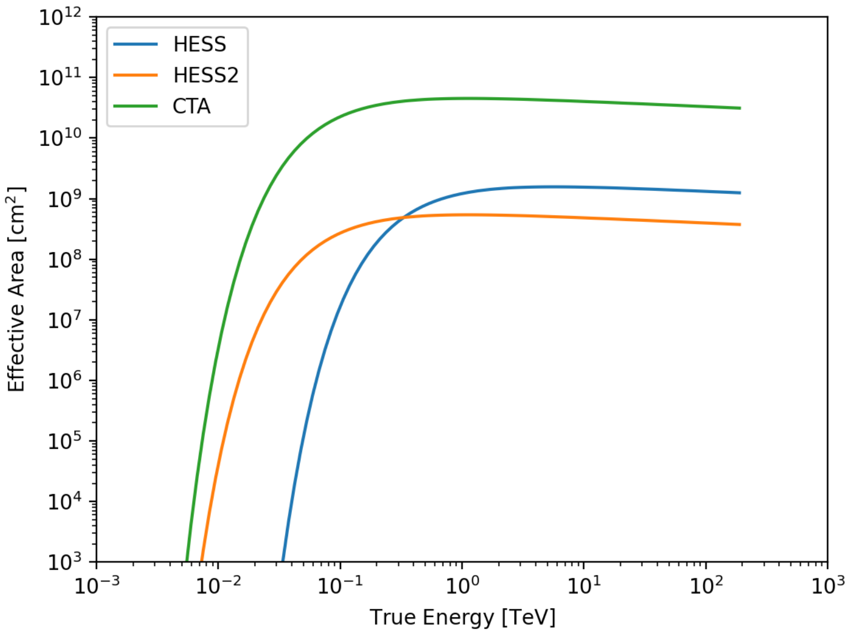

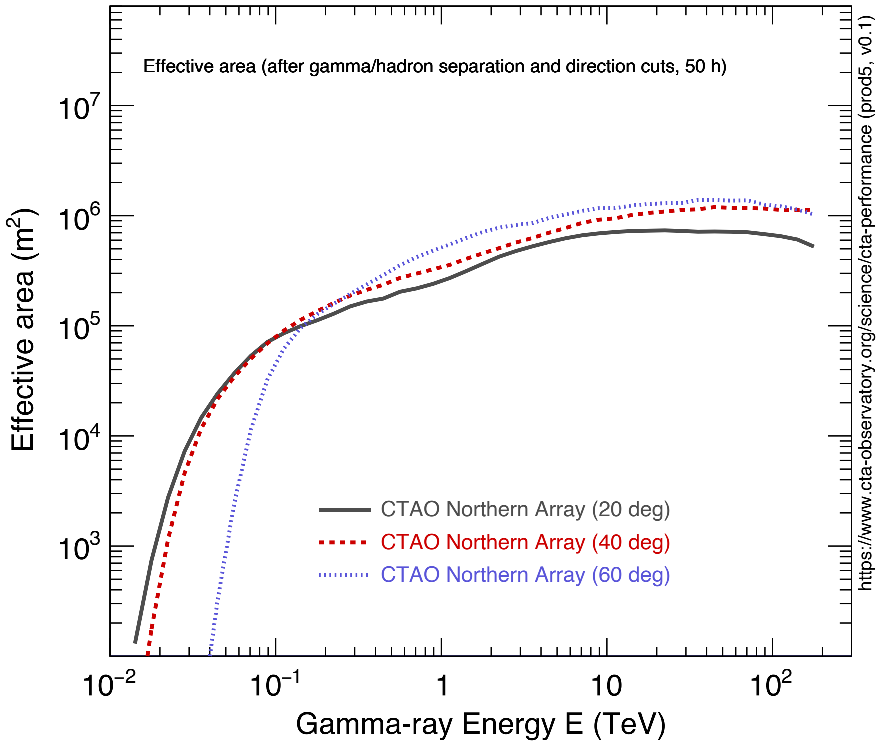

At higher zenith angles, the energy threshold increases, but the effective area at high energies also increases.

Point spread function

The point spread function provides the probability density of the angular separations between the true and reconstructed directions.

i.e. for each true gamma-ray direction, what is the probability that the event is assigned a certain reconstructed direction?

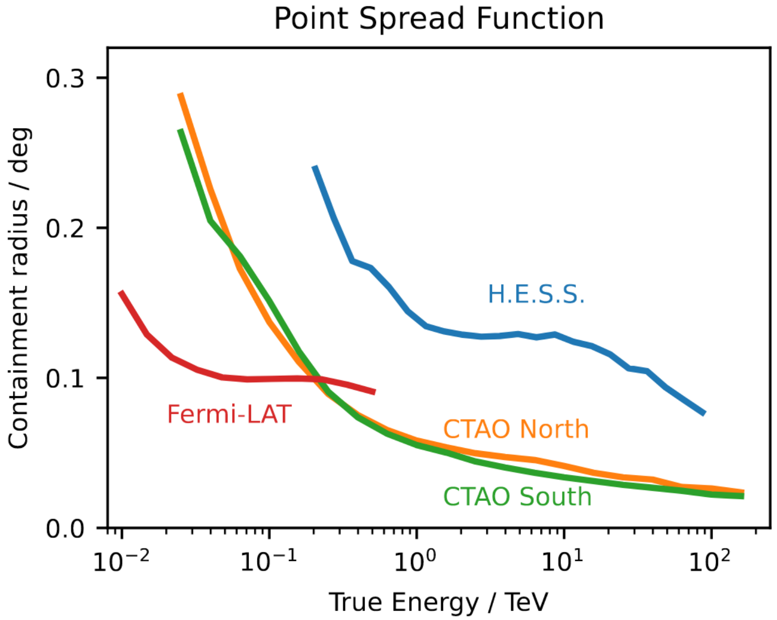

Using a model of the PSF, the 68% and 95% containment radii can be evaluated as a function of energy and offset angle.

Assuming a radially symmetric PSF, typical parameterisations are either using a triple Gaussian:

$$dP/d\Omega(r, S, \sigma_1, A_2, \sigma_2, A_3, \sigma_3) = \frac{S}{\pi}\left[\exp\left(-\frac{r^2}{2\sigma_1^2}\right) + A_2 \exp\left(-\frac{r^2}{2\sigma_2^2}\right) + A_3 \exp\left(-\frac{r^2}{2\sigma_3^2}\right)\right]$$

Or a King function:

$$dP/d\Omega(r, \sigma, \gamma) = \frac{1}{2\pi\sigma^2}\left(1 - \frac{1}{\gamma}\right)\left(1 + \frac{r^2}{2\gamma\sigma^2}\right)^{-\gamma}$$

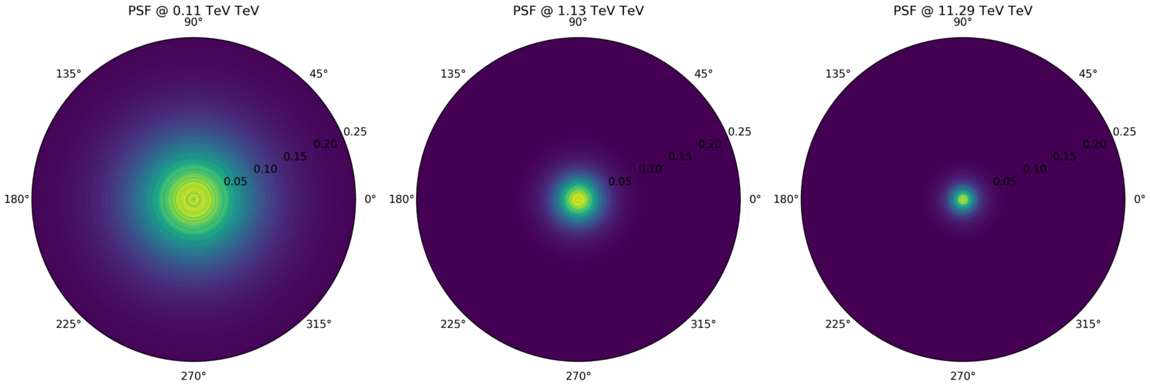

Energy dispersion

The energy dispersion matrix represents the probability density of the energy migration: $\mu = \frac{E}{E_{true}}$

i.e. for a given true gamma-ray energy, how likely is it that the energy is reconstructed to a particular value?

Also established based on Monte Carlo

Distribution of: $\frac{E_{reco} - E_{true}}{E_{true}}$

Mean = energy bias

68% containment radius = energy resolution

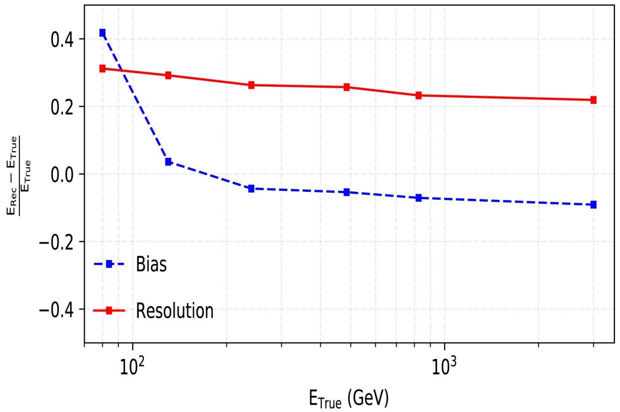

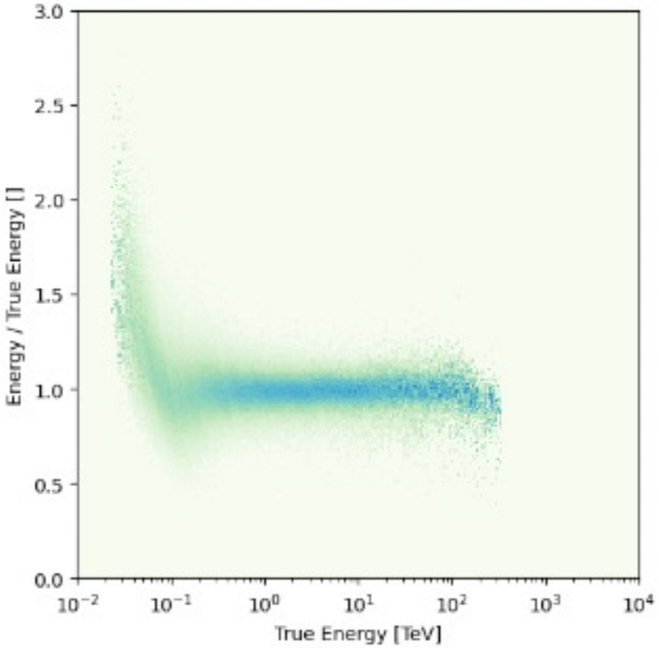

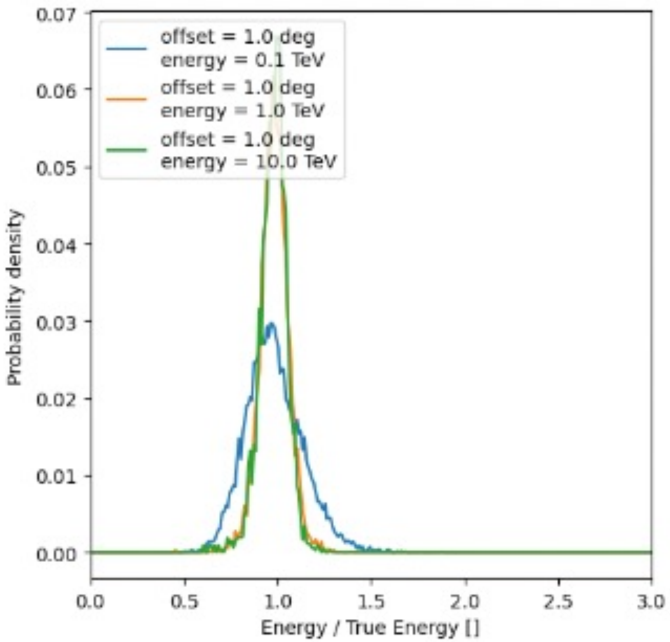

e.g. MACE -- Borwankar et al. Astroparticle Physics 159 (2024) 102960

Background Rate

Expected background rate – how many background events do we expect to mis-classify as signal, as a function of energy and direction?

Can be verified by observing “empty” regions of the sky → i.e. only background events should survive.

Note: there will always be a so-called “irreducible” background of protor events for which the EAS resembles that of a gamma-ray, with a large fraction of the energy being transferred into

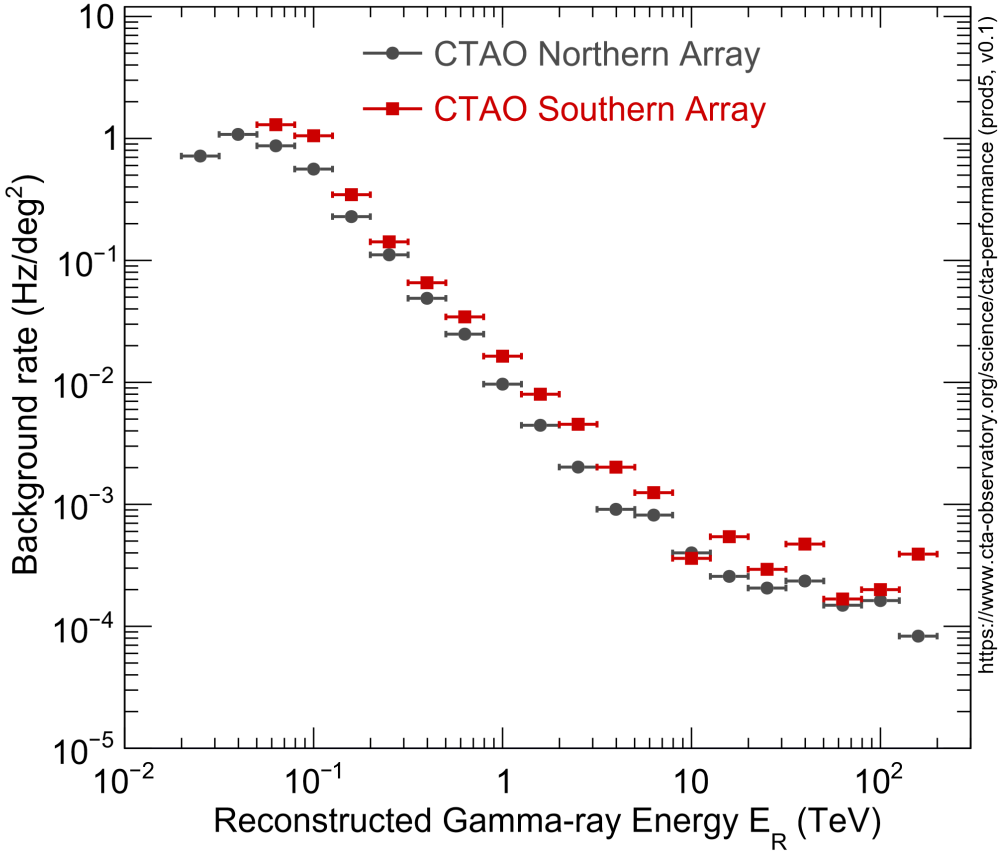

Sensitivity curves

Sensitivity curves are generally evaluated for a specific exposure and assuming a specific source spectrum.

Criteria per energy bin include:
— a minimum of 10 gamma-ray events
— a minimum significance of 5 sigma
— a maximum background systematic of 10%

Which criterion dominates at which energy is indicated on the curve

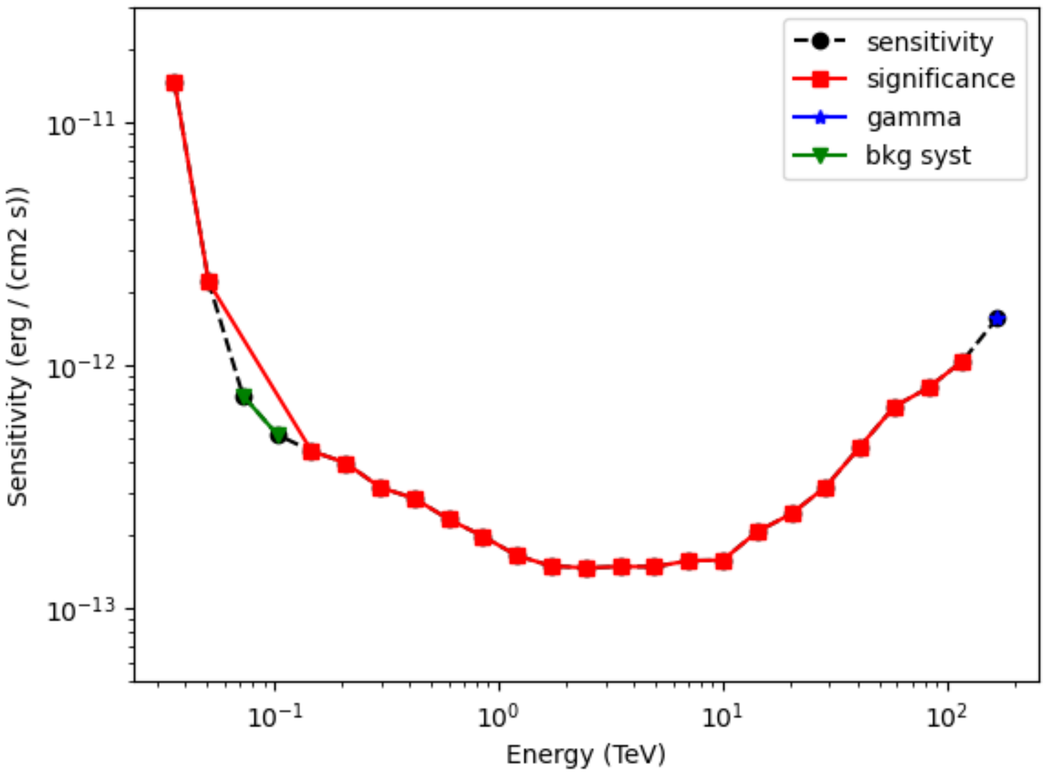

Background systematics tend to dominate at lower energies

Gamma-ray counts tend to dominate at high energies

How to calculate the significance?

Background estimation

Significance is estimated by comparing the number of gamma-ray counts within an On region to the number of counts in a nearby Off region.

The difference in exposures / acceptance between the two is accounted for by the factor alpha

The relative acceptance of a camera drops with angular distance

Hence, IACT observations are usually taken offset from the target

Ring Background → extract Off from a region of equal offset arou target On region

Reflected Background → extract Off from a region of equal offset around the observation position

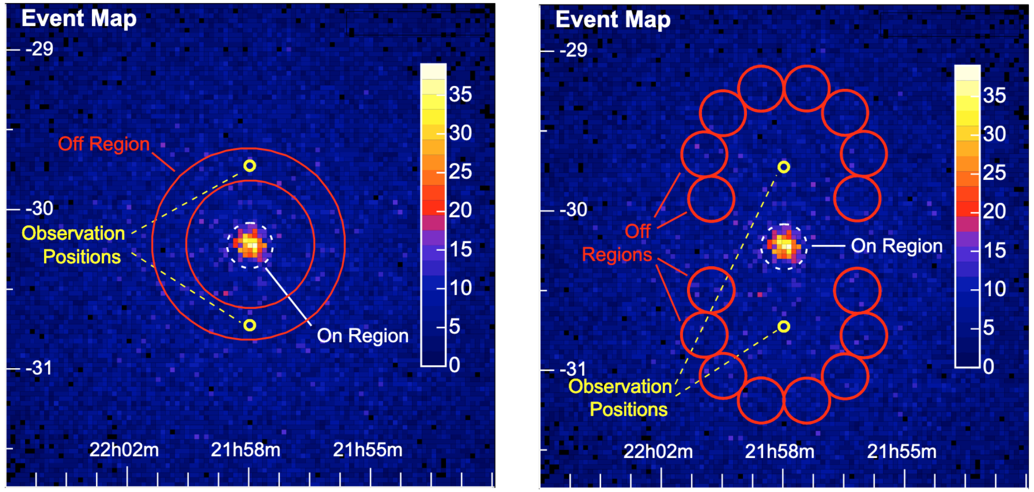

Berge et al, A&A **466** (2007) 1219-1229

$$S = \sqrt{-2\ln\lambda} = \sqrt{2}\left(N_{\mathrm{on}}\ln\left[\frac{1+\alpha}{\alpha}\left(\frac{N_{\mathrm{on}}}{N_{\mathrm{on}}+N_{\mathrm{off}}}\right)\right] + N_{\mathrm{off}}\ln\left[(1+\alpha)\left(\frac{N_{\mathrm{off}}}{N_{\mathrm{on}}+N_{\mathrm{off}}}\right)\right]\right)^{1/2}$$

Li & Ma, ApJ **272** (1983) 317-324

Can also use a background template based on off / empty sky data (matching observations or averaging over many)

Gammapy (γπ) and 3D analysis approaches

γπ A **Python** package for **gamma-ray** astronomy

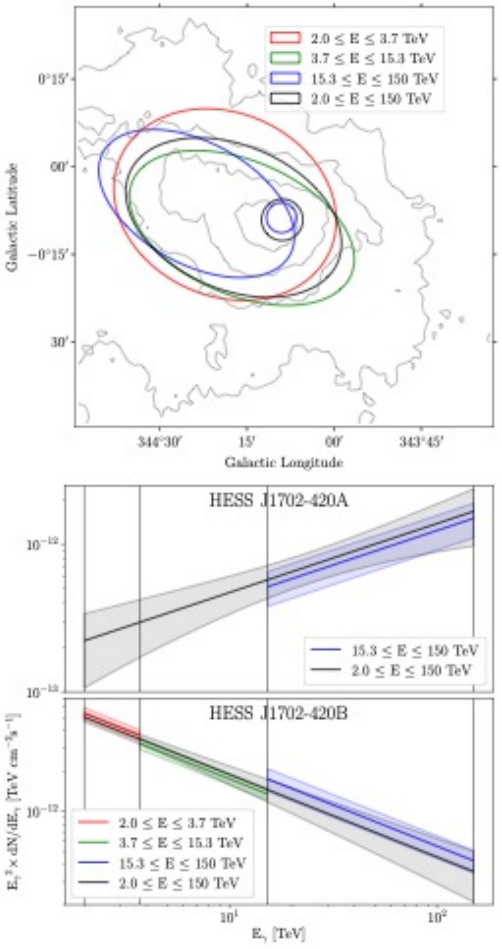

HESS Collaboration A&A **653** (2021) A152

3D analysis fitting:

→ enabling multiple components to be simultaneously fit in spatial and energy dimensions

Especially powerful for studies of complex regions or sources with complex morphology

Examples: HESS J1702-420, HESS J1809-193...   https://gammapy.org/

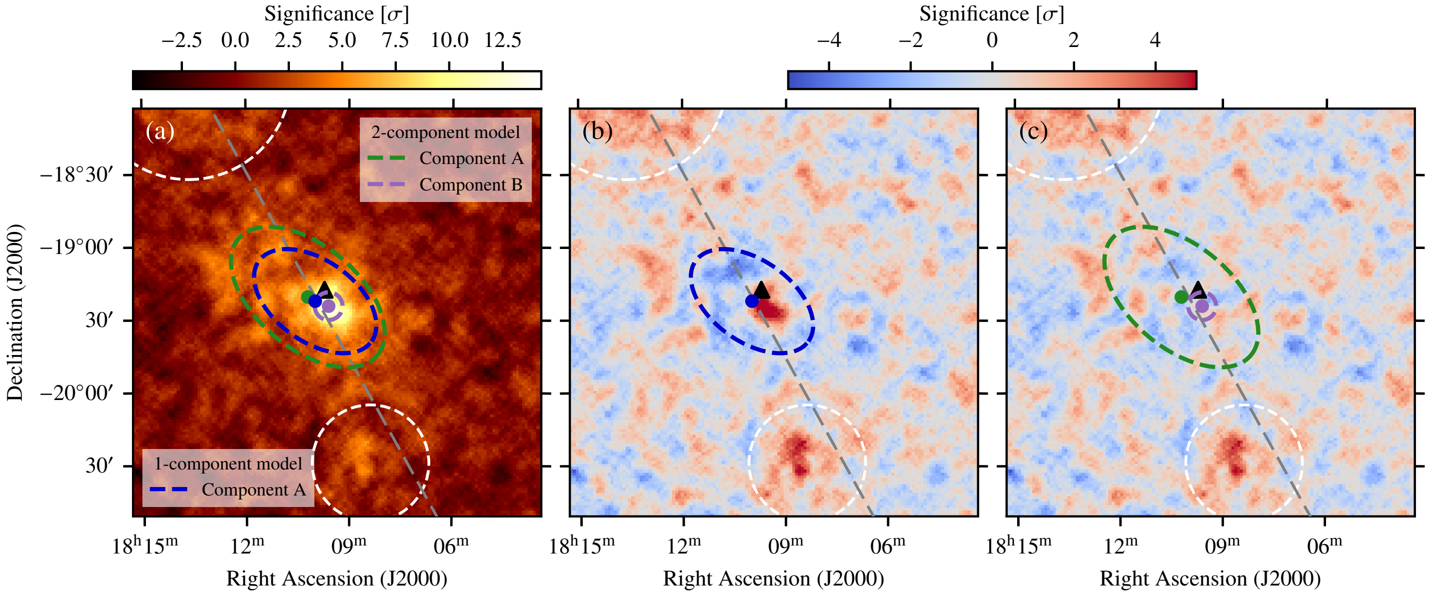

HESS Collaboration A&A **672** (2023) A103

Gammapy (γπ) and 3D analysis approaches

Morphological models:

Gaussian, Generalised Gaussian, Disk, Point, Template, Shell

→ Can be asymmetric / elliptical
→ Caution: containment radii!

Asked ChatGPT to summarise:

Here's an updated table including the containment percentages for **5 sigma** in 1D, 2D, and 3D Gaussian distributions:

Sigma	1D Containment (%)	2D Containment (%)	3D Containment (%)
1σ	68.27%	39.35%	19.87%
2σ	95.45%	86.47%	73.80%
3σ	99.73%	98.89%	97.07%
4σ	99.9937%	99.99%	99.88%
5σ	99.99994%	99.9999%	99.9987%

$$\phi(r) = N \times exp\left[-\left(\frac{r}{r_{eff}}\right)^{(1/\eta)}\right]$$

$$N = \frac{1}{2\pi\sqrt{(1-e^2)}r_0^2\eta\Gamma(2\eta)}$$

$$r_{rmeff}(\mathrm{lon}, \mathrm{lat}) = \sqrt{(r_M \sin(\Delta\phi))^2 + (r_m \cos(\Delta\phi))^2}$$

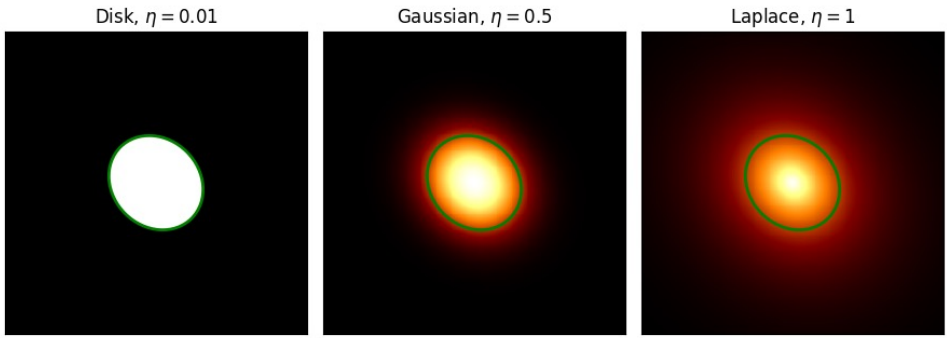

Gammapy (γπ) and 3D analysis approaches

Spectral models:

Power Law, Broken Power Law, Log Parabola, Exponential Cut-off Power Law

Spectral Model	Equation	Parameters
Power Law	$F(E) = N_0 \left(\frac{E}{E_0}\right)^{-\Gamma}$	N_0: normalization, E_0: reference energy, Γ: photon index (spectral slope)
Log Parabola	$F(E) = N_0 \left(\frac{E}{E_0}\right)^{-(\alpha+\beta \log(E/E_0))}$	N_0: normalization, E_0: reference energy, α: slope, β: curvature
Broken Power Law	$F(E) = \begin{cases} N_0 \left(\frac{E}{E_b}\right)^{-\Gamma_1} & \text{for } E < E_b \\ N_0 \left(\frac{E}{E_b}\right)^{-\Gamma_2} & \text{for } E \geq E_b \end{cases}$	N_0: normalization, E_b: break energy, Γ_1: photon index before the break, Γ_2: photon index after the break
Power Law with Exponential Cutoff	$F(E) = N_0 \left(\frac{E}{E_0}\right)^{-\Gamma} \exp\left(-\frac{E}{E_{\text{cut}}}\right)$	N_0: normalization, E_0: reference energy, Γ: photon index, E_{cut}: cutoff energy

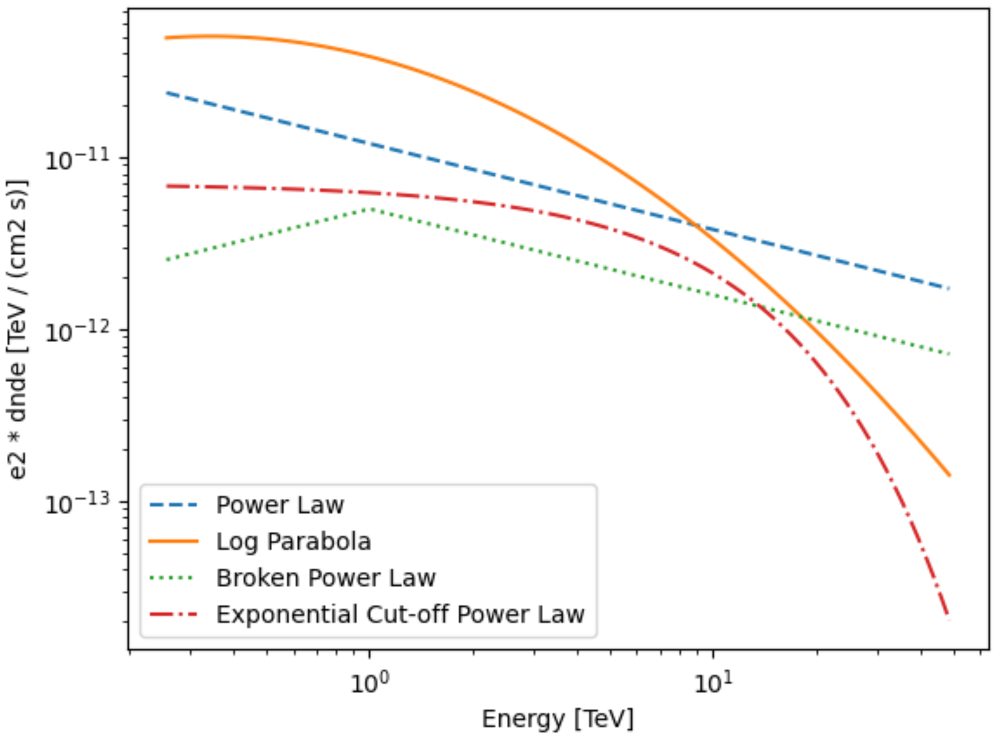

3D analysis = fitting of spatial and spectral models simultaneously to fully describe source components

Multi-instrument joint analyses

Common formats enable data from multiple instruments to be analysed simultaneously (GADF: gamma-astro-data-formats)

e.g. Multi-instrument fit to the Crab nebula spectrum: calibration source for VHE gamma-rays

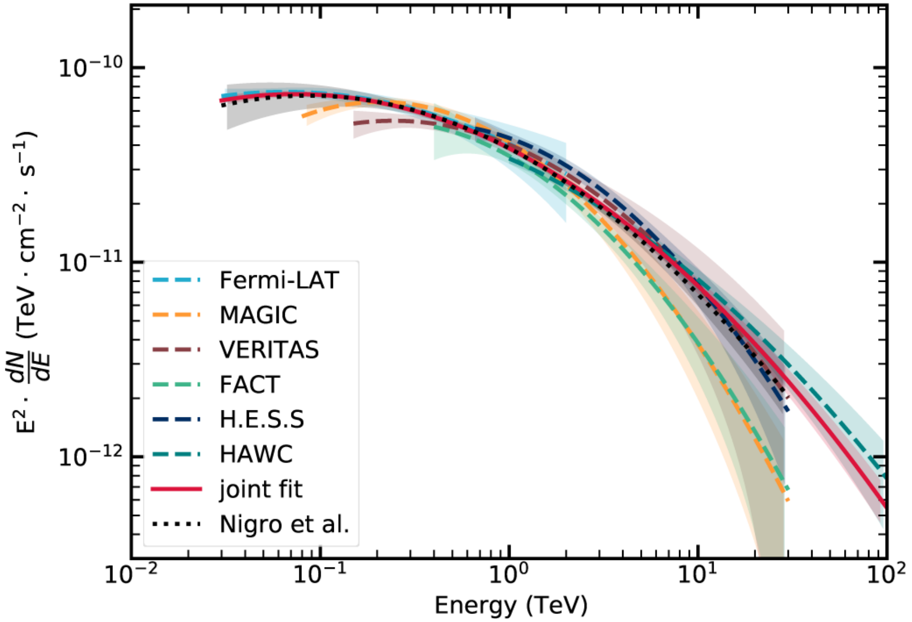

Nigro et al A&A **625** (2019) A10
HAWC collaboration A&A **667** (2022) A36

Simultaneous 3D fitting of data from multiple instruments
e.g. Fermi-LAT and H.E.S.S. for HESS J1813-178
H.E.S.S. collaboration A&A **686** (2024) A149

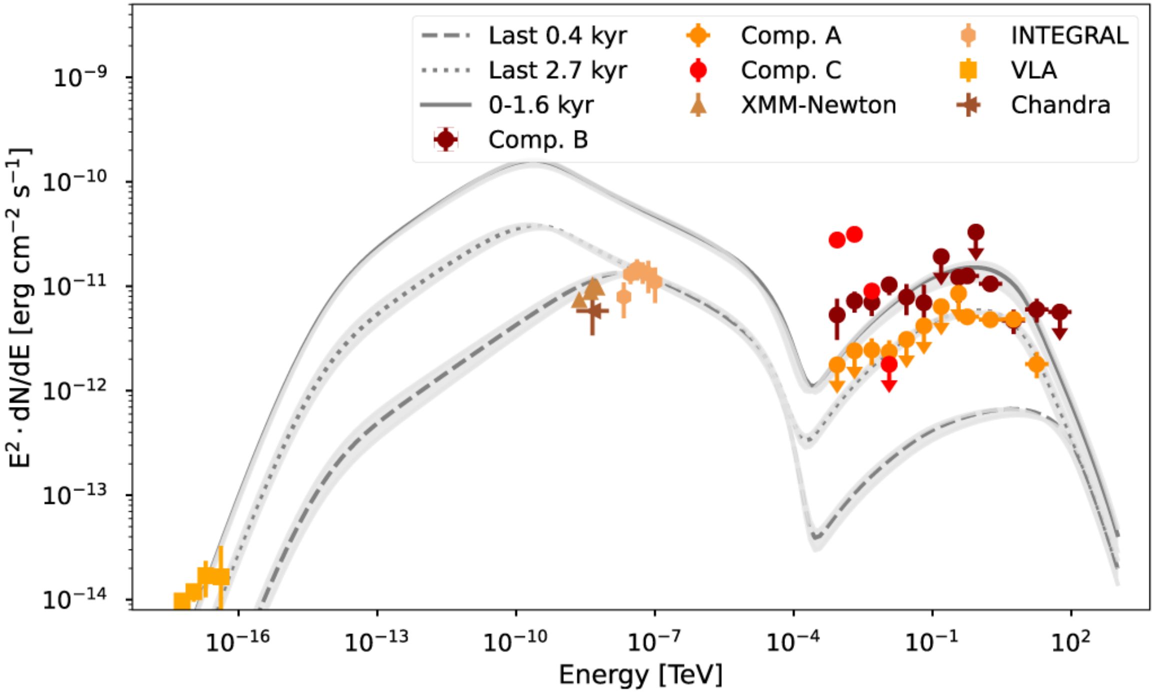

Complementary Facilities

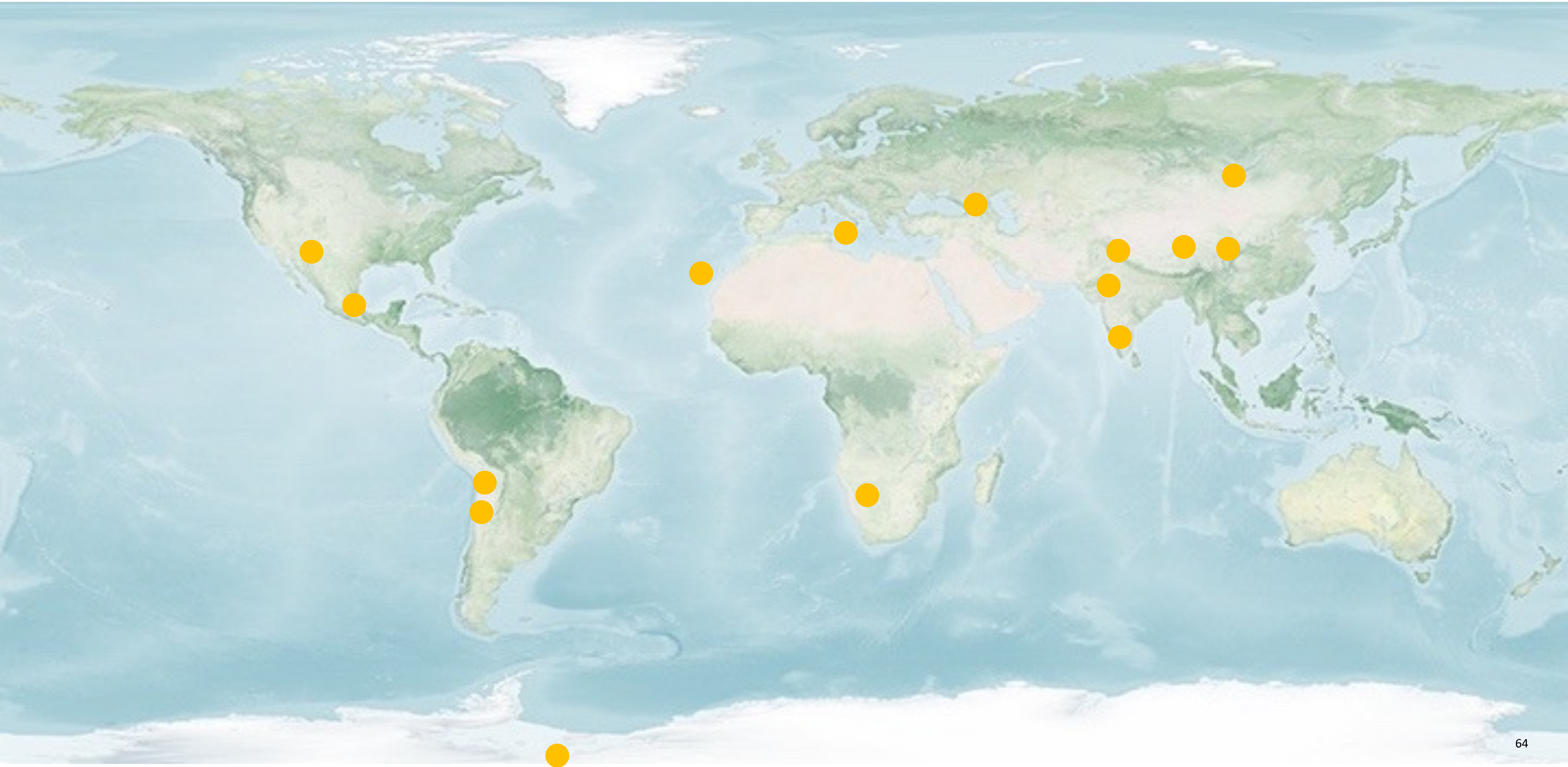

Complementary Facilities

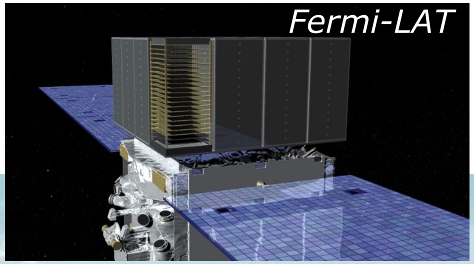

Complementary Facilities

Different techniques → different performance

IACTs

WCDs

Satellite

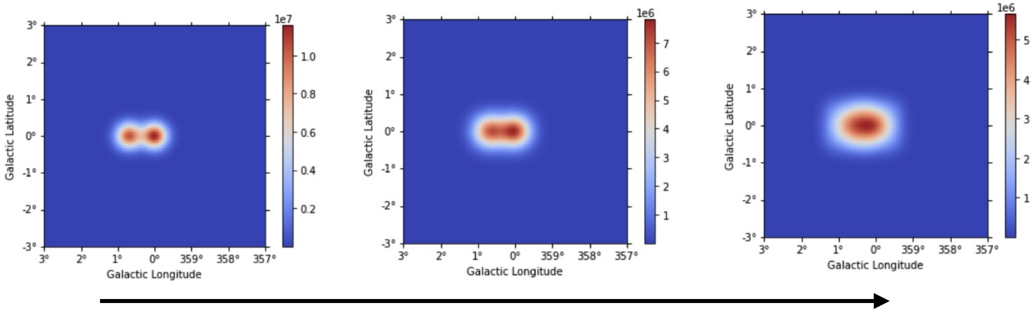

Angular resolution deteriorating

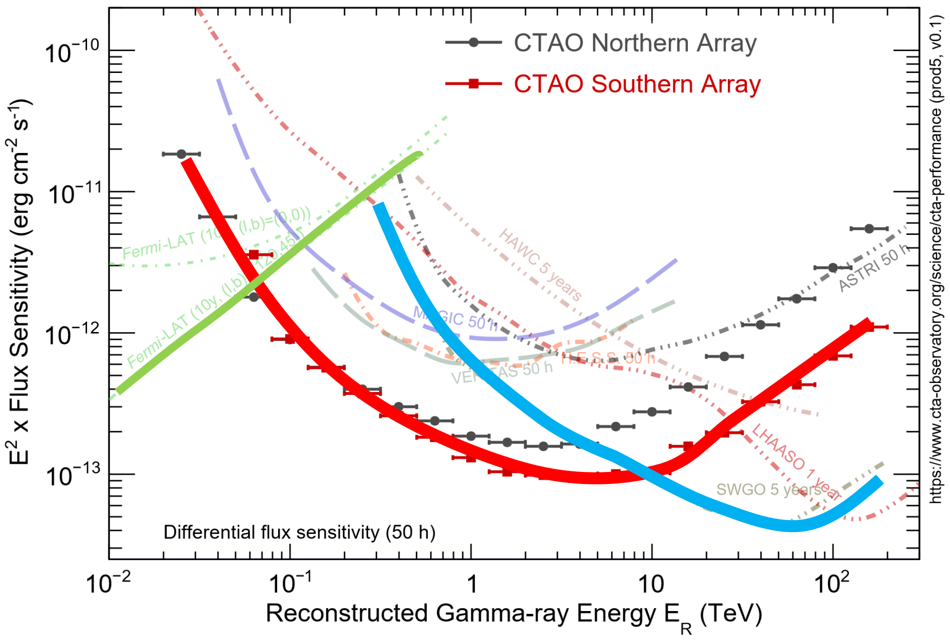

Cross-over energy between instruments depends on exposure

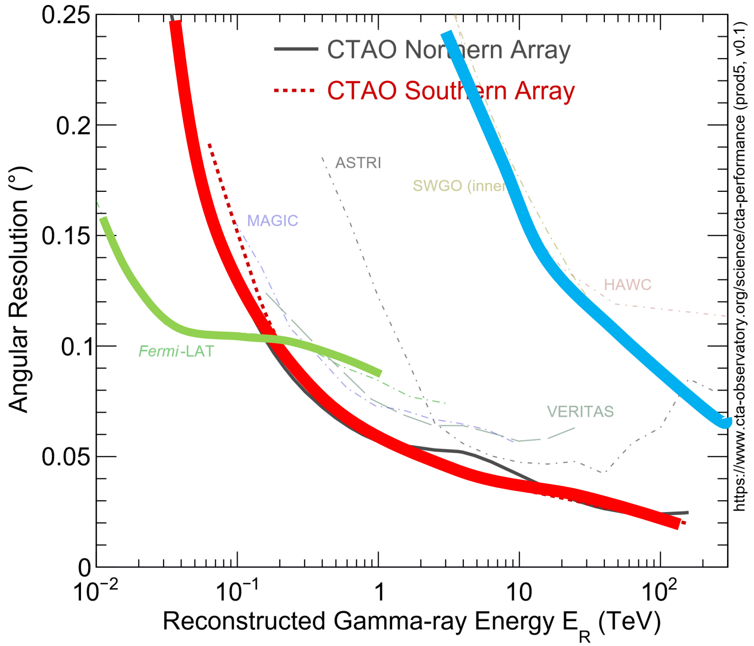

https://www.cta-observatory.org/science/ctao-performance/ , E. de Oña Wilhelmi+

Observations of transients

ToO = Target of Opportunity

The universe is dynamic
→ many interesting targets are short duration events

The sensitivity as a function of time is hence of high importance.

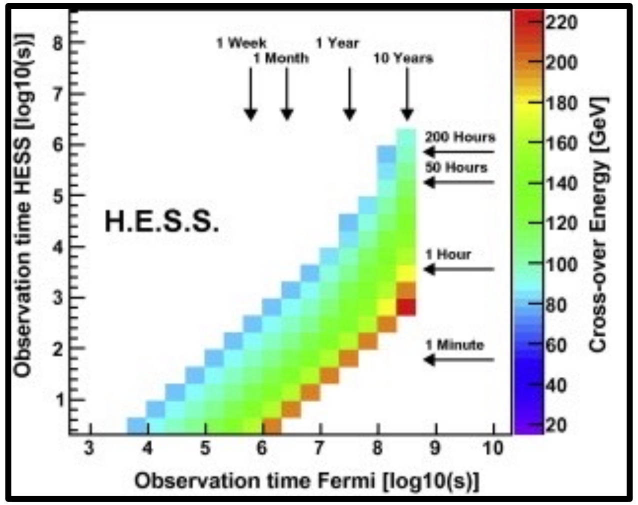

Funk & Hinton, Astropart Phys 43 (348-355), 2013

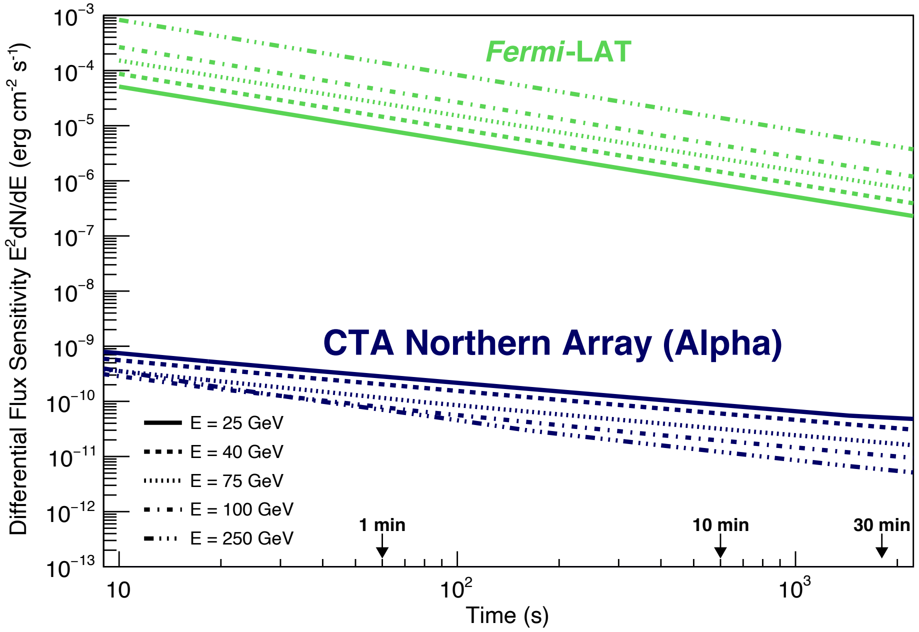

Need sky-scanning instruments to issue alerts and inform e.g. IACTs where to point.

However, short time-scale sensitivity of IACTs far out-performs the Fermi-LAT

Observability

Using the location of a facility based on the ground, we can consider the observability based on which parts of the sky rise >30º altitude

Relative observability showing which parts of the sky receive the most exposure

Plots are shown in galactic coordinates for LST-1 on La Palma and H.E.S.S. in Namibia

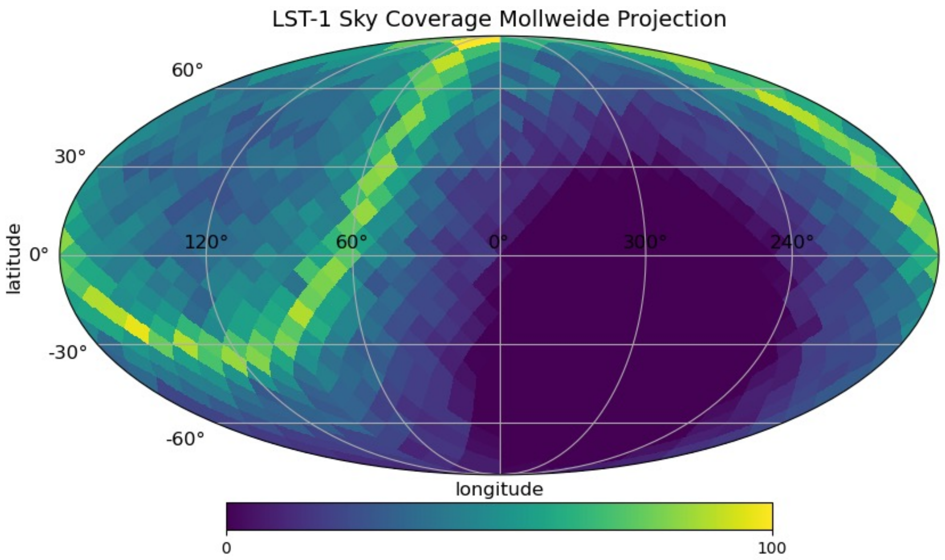

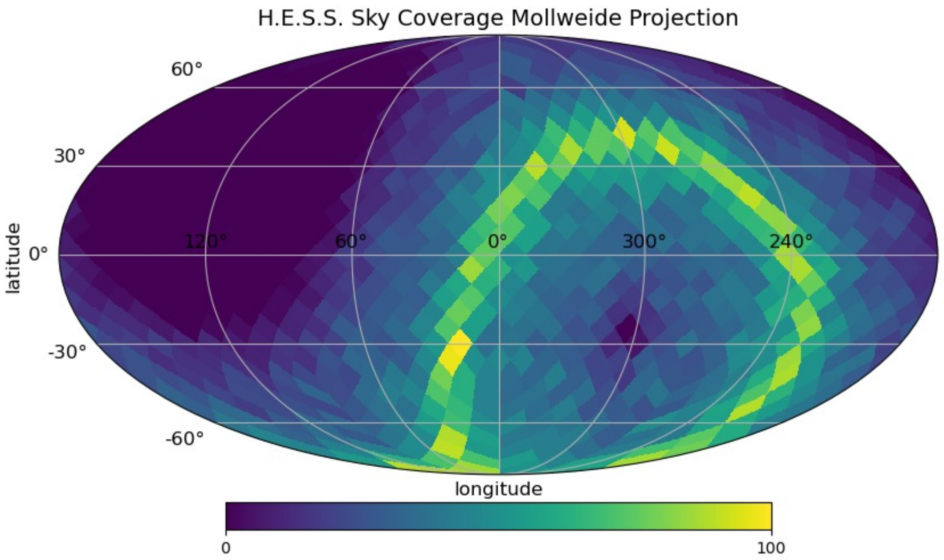

Single source observability

Depends on altitude / zenith angle

IACTs – cannot observe during daytime or under bright moonlight

WCDs – can (In principle) observe continuously, also during daytime

Consider the Crab nebula above the HESS site over the course of a year:

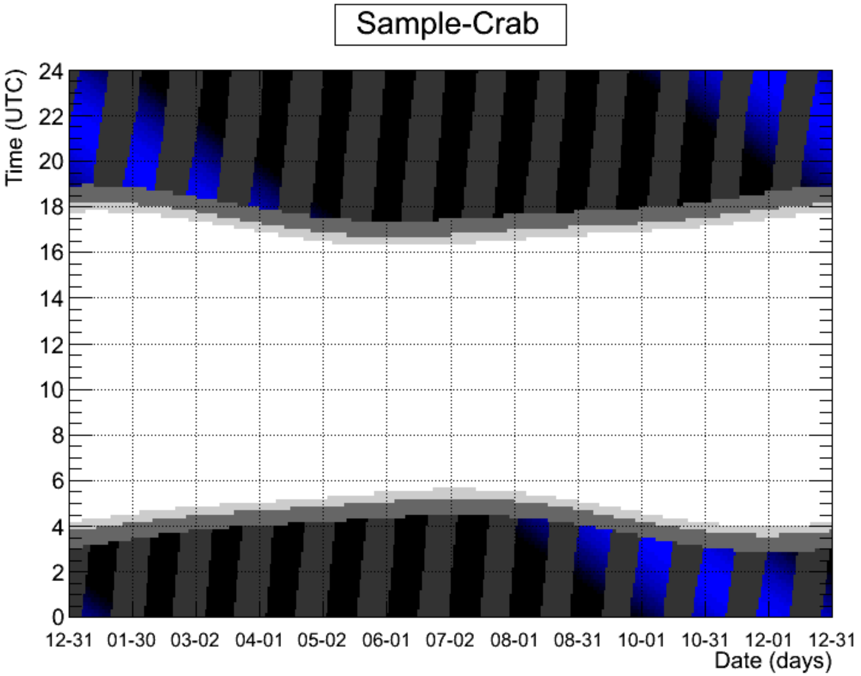

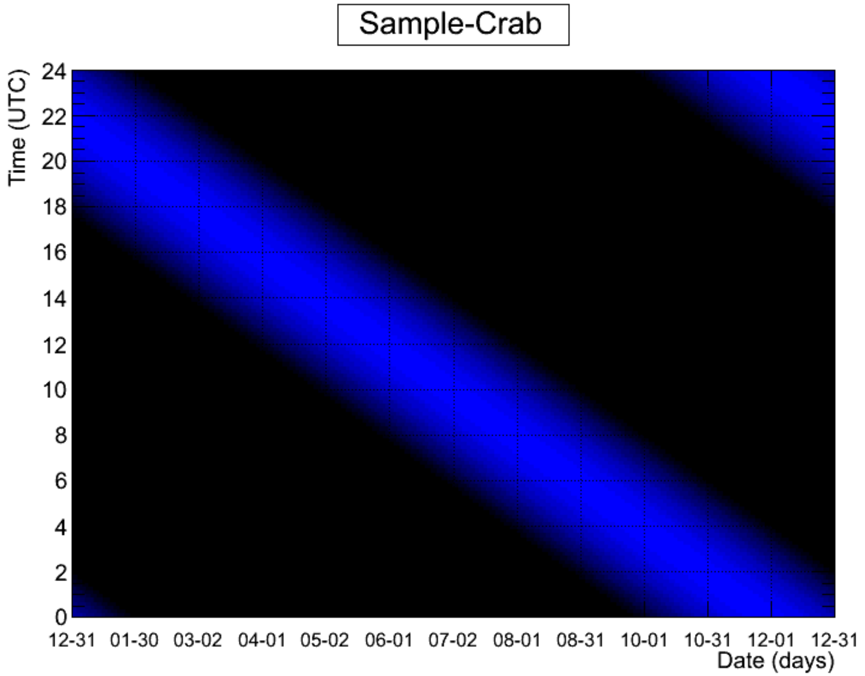

Visibility

Consider a single night:

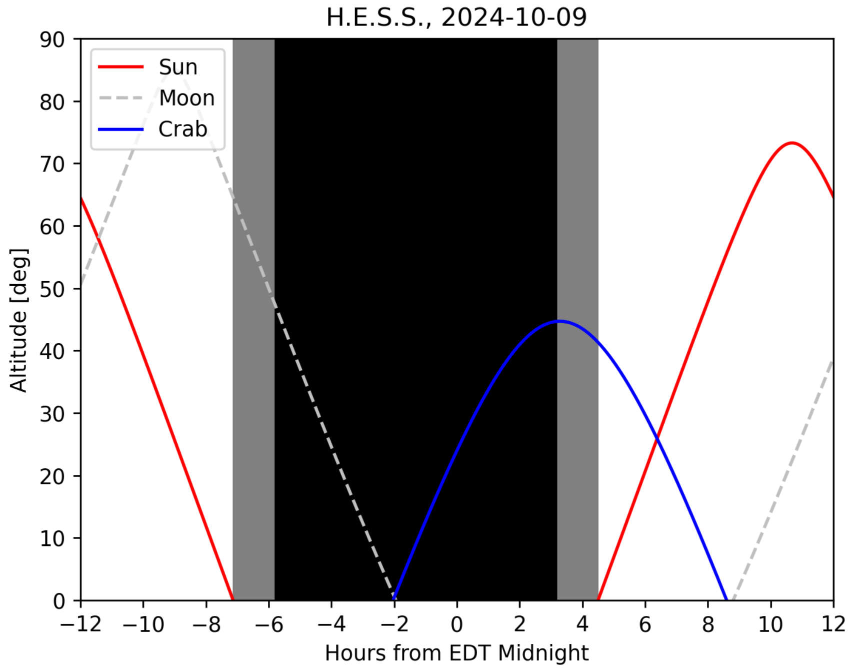

•Altitude above horizon for objects of interest

•White = daylight, sun above horizon;

•grey = twilight, sun below horizon;

•dark = astronomical darkness, sun < -18°

A single source over the year:

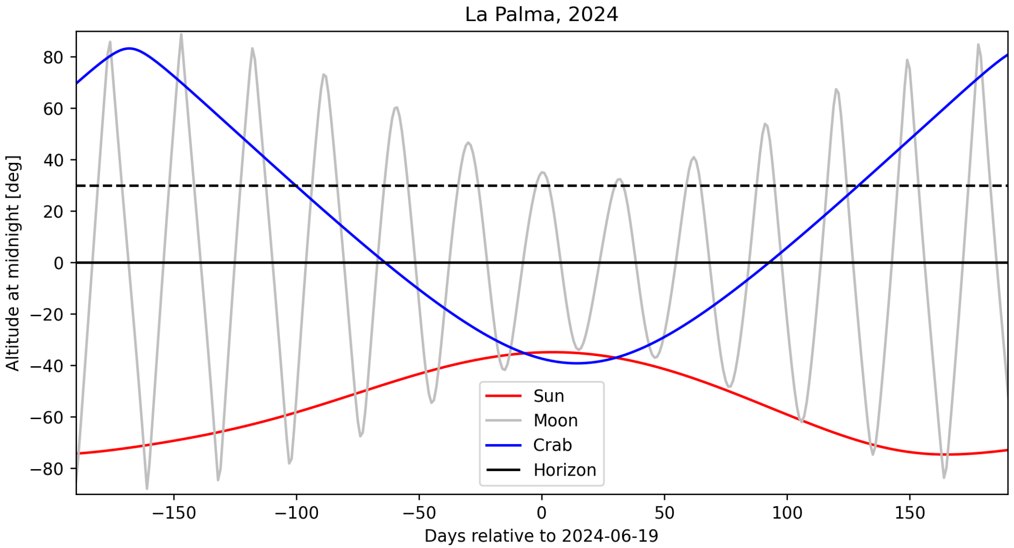

IACTs: Night Sky Background

Night Sky Background (NSB) is comprised of ambient star light, zodiacal light, moonlight and any other additional background optical light sources (including anthropogenic).

This presents challenging observing conditions for sensitive IACTs

Yet a strong motivation → much more observing time available

This can be critical in the case of transient events

Astronomical twilight: sun more than 18° below the horizon
Nautical twilight: sun more than 12° below the horizon
Civil twilight: sun more than 6° below the horizon

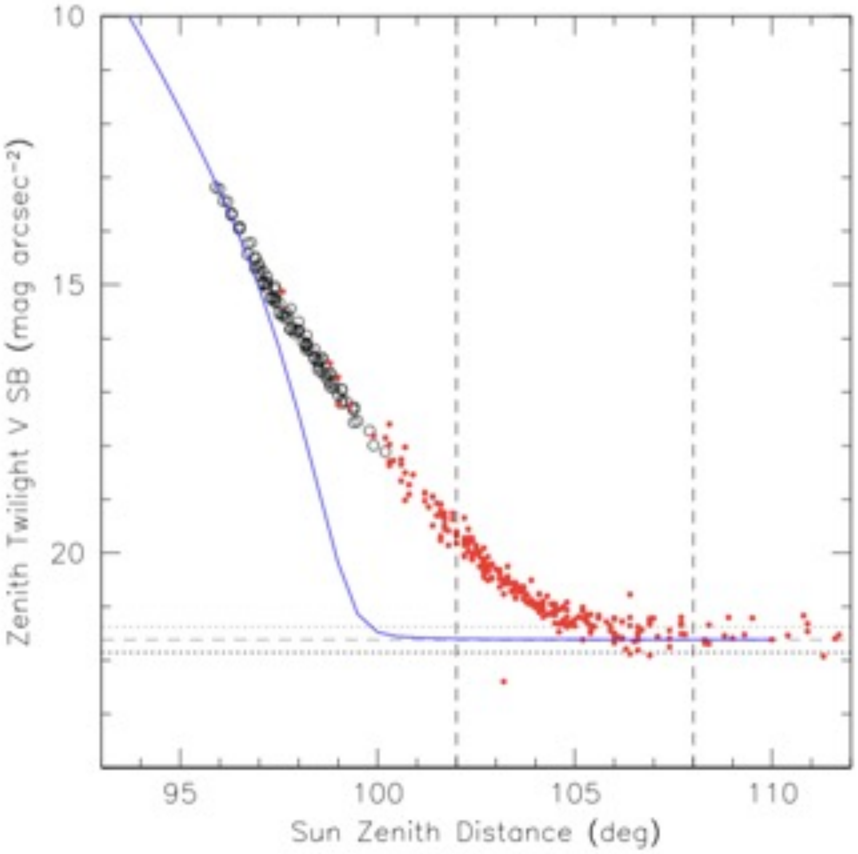

IACTs: Pointing Strategy

Two main categories of pointing strategy:

“Wobble” pointing – taken at an angular offset to the target,
e.g. ±θ in Declination and ±θ/cos(dec) in Right Ascension.
Combined exposure across “wobbles” gives the total On target exposure.

Grid pointing – tiling of pointing positions to cover a specific area of sky

Exposure per pointing position is relevant

Further types:

Drift-scan pointing – telescopes observe at a fixed altitude and azimuth, letting the sky pass through the field-of-view (closest to WCD)

Divergent pointing – telescopes in an array are directed slightly wider than parallel, to cover a larger region of sky instantaneously.

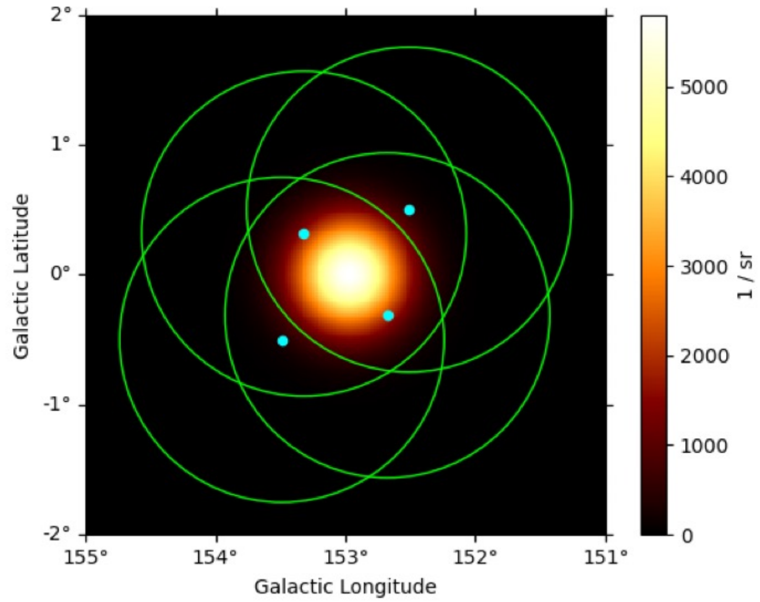

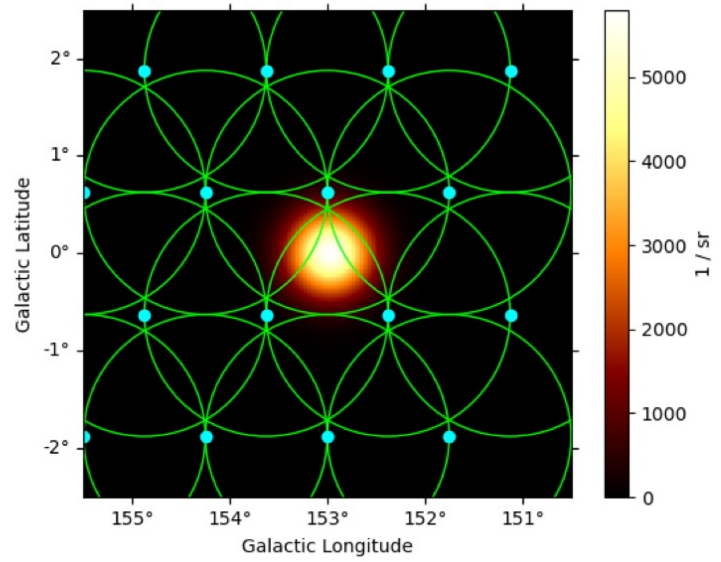

Development of VHE gamma-ray astronomy

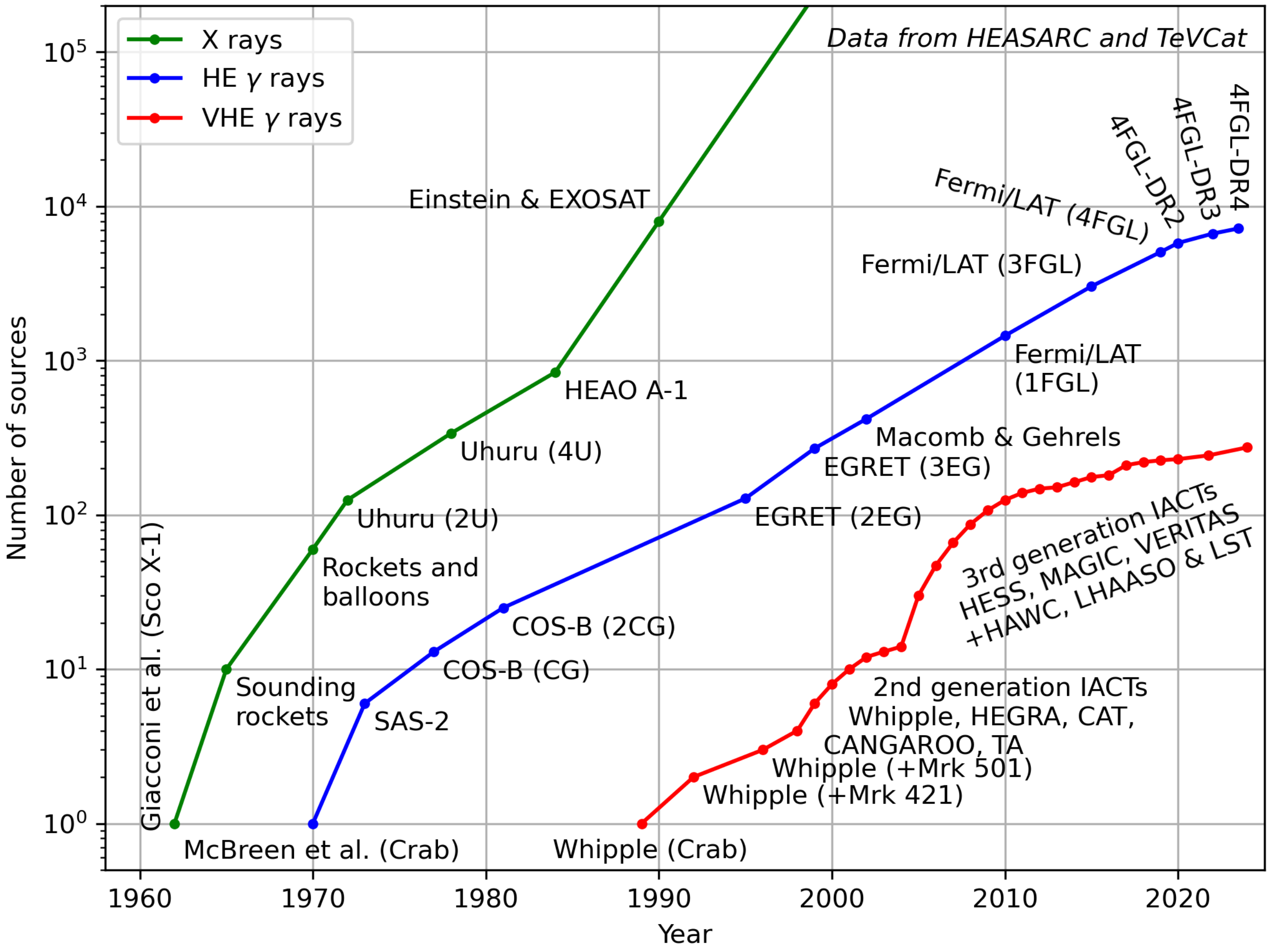

Credit: S. Fegan (2024)

Future for IACTs

Current generation IACTs continue to make discoveries

→ New source classes at TeV energies

First alert from a CTA telescope:
LST detects flaring activity from BL Lacertae (Atel 14783, 2021)

<u>Forthcoming IACT facilities:</u>

→ CTA-North La Palma, Spain
→ CTA-South Paranal, Chile
→ ASTRI mini-array Tenerife,

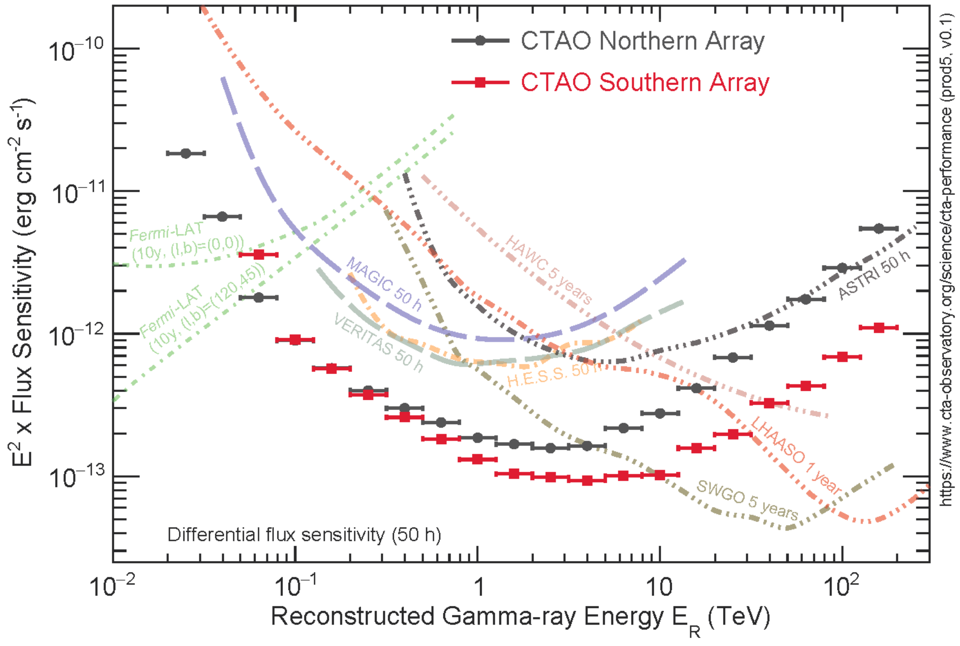

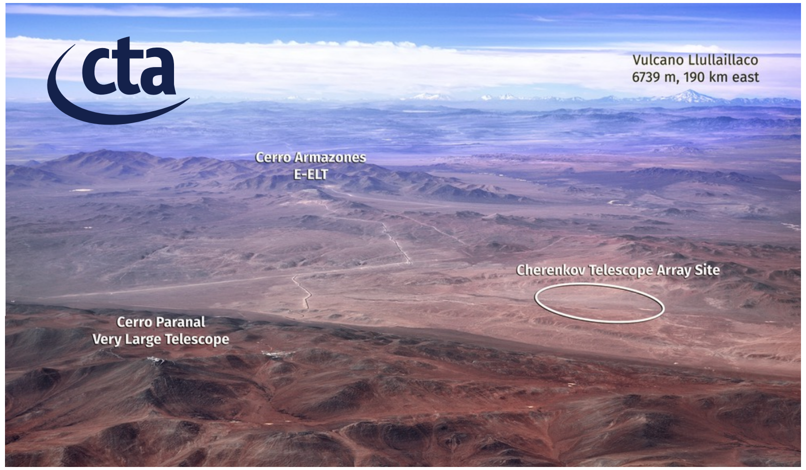

Strengths of IACTs:

→ Good angular and energy resolution

→ Reaction and sensitivity to transient phenomena

Cherenkov Telescope Array

https://www.cta-observatory.org/

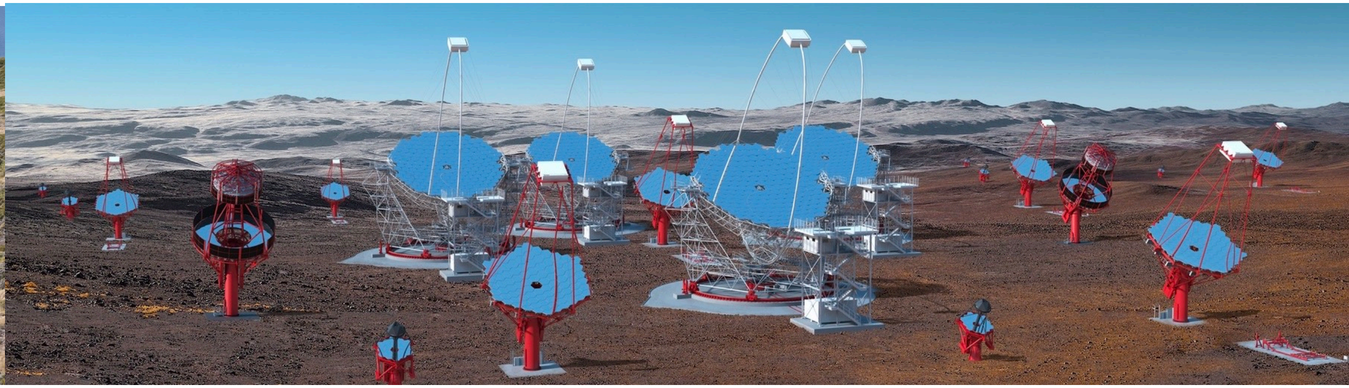

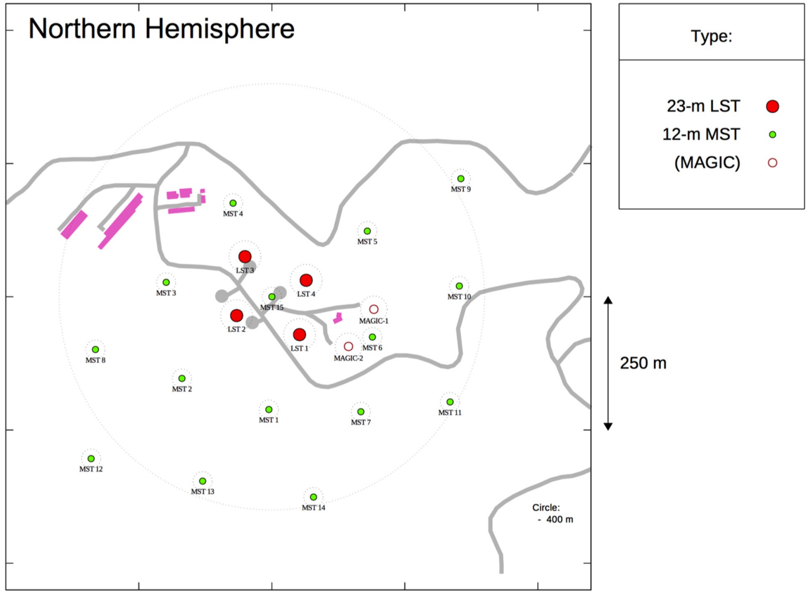

4 LS4 LSTs, 15 MSTs

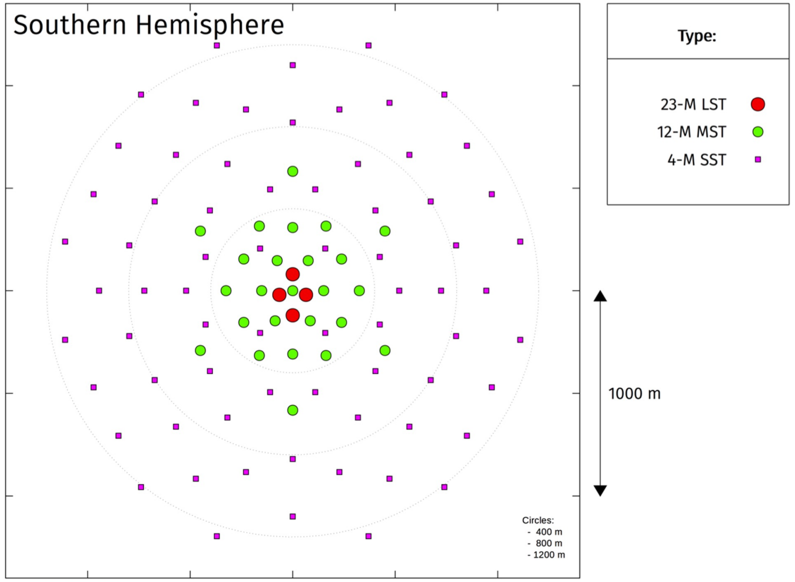

4 LSTs, 25 MSTs, 70 SSTs

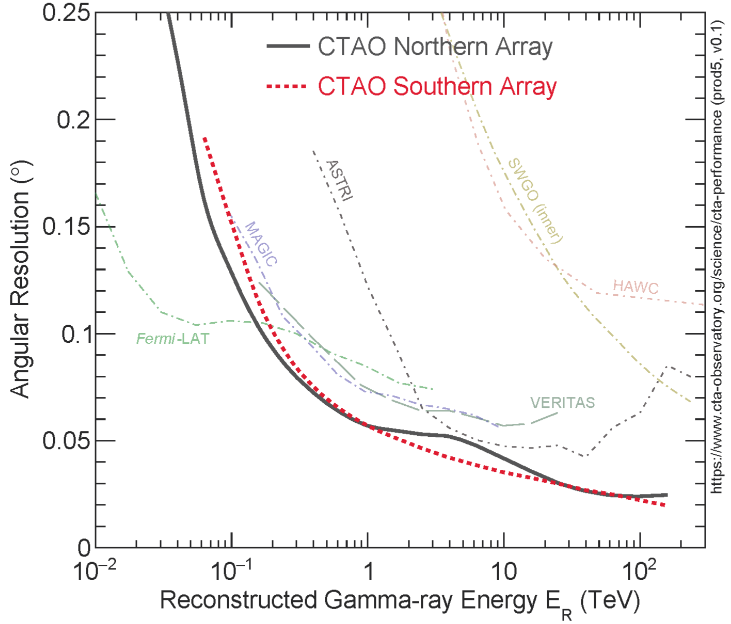

Southern Wide-field Gamma-ray Observatory

https://www.swgo.org/

- Ground-based water Cherenkov detectors are well suited to the highest energies and full sky surveys.
- Current facilities are mainly based in the North
- Future → observe the Southern sky

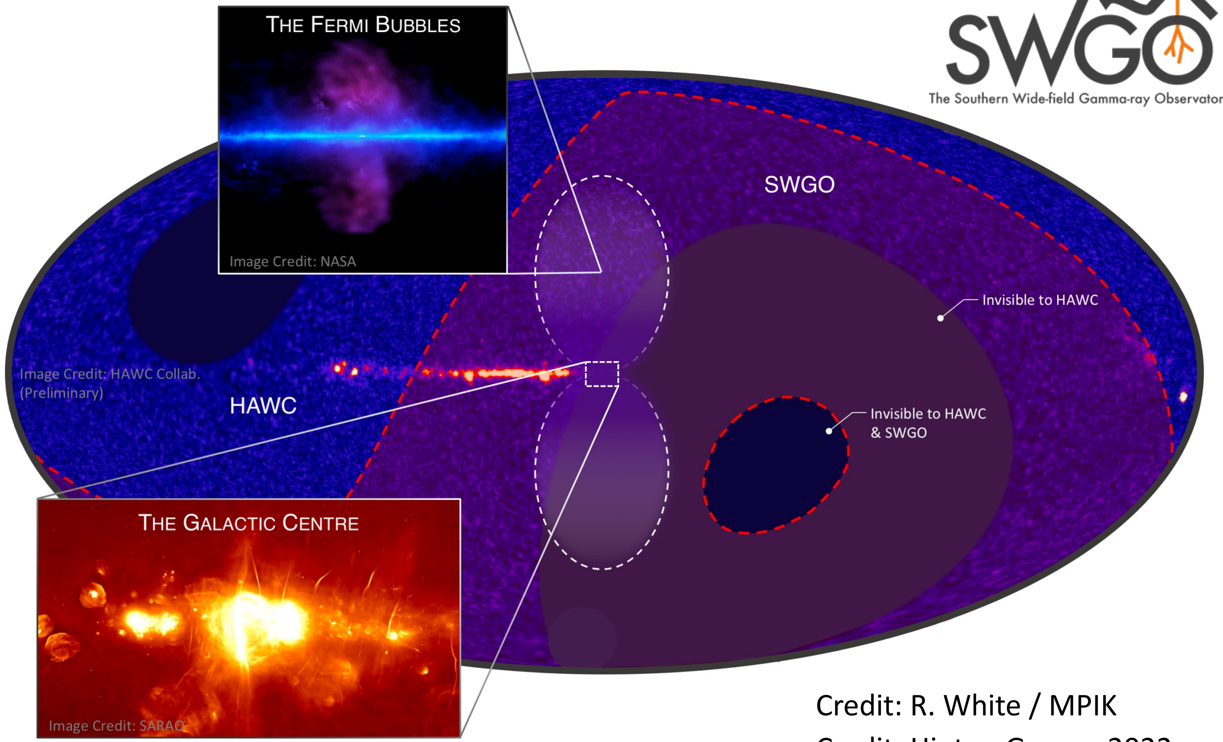

Credit: R. White / MPIK
Credit: Hinton Gamma2022

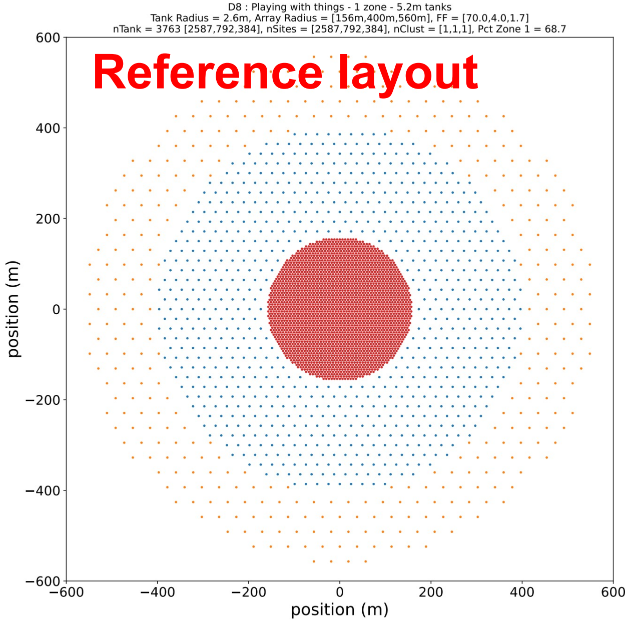

The Shortlisted sites are (in alphabetic order):

***Argentina*: <u>Alto Tocomar</u>** ; 24°12’16.22“ S, 66°30’29.71” W (4800 m.a.s.l)

***Chile* : <u>Pampa La Bola</u>** ; 22°56’41.30“ S, 67°40’39.09” W (4770 m.a.s.l)

***Peru* : <u>Imata</u>** ; 15°50′40.4” S, 71°03′56.7” W (4500 m.a.s.l)

Location:
Pampa La Bola, Chile

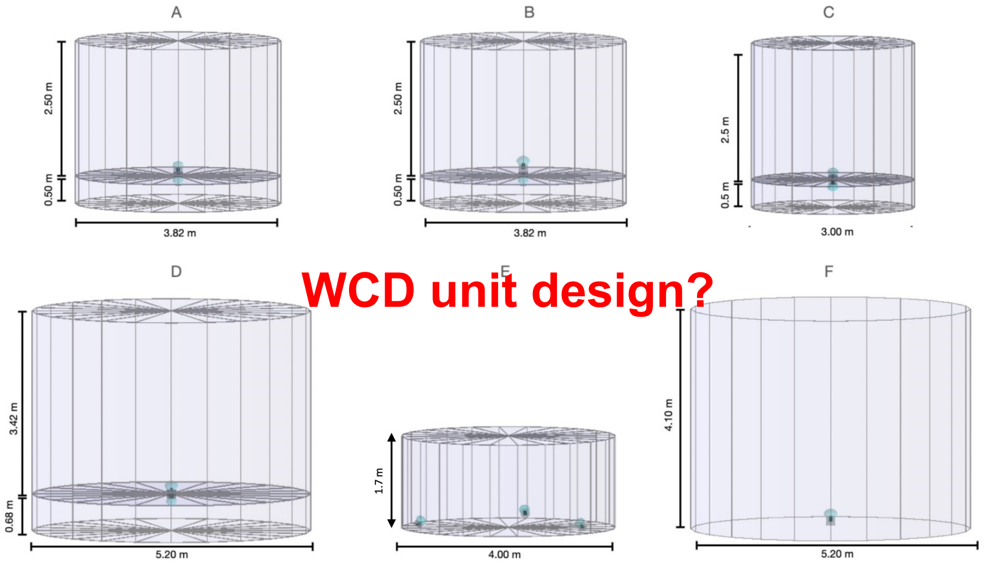

WCD unit design?